Mechanistic Insights into Conventional T and CAR T cell Activation Induced Cell Death and Allogeneic Responses

By

MICHAEL KA-KIT SHENG
DISSERTATION

Submitted in partial satisfaction of the requirements for the degree of

DOCTOR OF PHILOSOPHY

in

Immunology

in the

OFFICE OF GRADUATE STUDIES

of the

UNIVERSITY OF CALIFORNIA

DAVIS

Approved:

William J. Murphy, Chair

Stephen J. McSorley

Joseph M. Tuscano

Committee in Charge

2025

Dedication

謹以此論文獻給我永遠懷念的祖父母：

外祖父母（周何玉麗 和 周道德）

以及

祖父母（盛崇華 和 周秀霞）

您們的精神長存我心，伴我左右，

在我追逐夢想、仰望星辰的旅途中，賦予我無限力量。

若沒有您們的一切，我無法走到今天。

Acknowledgements

Wow! This has been one heck of a journey, filled with plenty of highs and lows, laughs and sorrows, and trials and tribulations; but unquestionably, it has been an incredibly rewarding ride full of academic learning and scholarly pursuit. If someone told me a decade ago, post-undergraduate studies, that I would eventually receive my PhD, I would have laughed and told them they were crazy or that they had lost the plot. It is therefore, a huge and honest testament to the amazing and supportive people around me – mentors, friends and family – that I can conclude this intellectual leg of my journey and call myself 'Doctor.'

First off, I want to thank Dr. Tammy Bui, an exemplary dentist who is also an enormously kind and good friend. In 2019, while hanging out at a speech called Angel's Share in Greenwich Village, NYC, I expressed to her the possibility of returning to school for a PhD. However, having been out of college for several years, I conceded that I felt I could no longer fall back into the grind of perpetual reading and studying. Ever the persistent friend, she strongly encouraged me to never let go of my dreams and reminded me that, "You're never too old to further your education." That night was the genesis of my PhD journey – so thank you Tammy, Dr. Bui, for being that positive force to motivate me to look past my insecurities.

I am extremely grateful to Dr. William Murphy for being a strong mentor during these past four years, for helping me cultivate my mind and grow as an independent scientist, and for encouraging me to always think critically and ask astute questions about my own data. Thank you for running journal club, which was extremely insightful and ingrained in me the values of meticulousness, scientific rigor, and rational

skepticism, all principles that contributed to me becoming more detail-oriented and acutely aware of the expansive scientific literature. In addition, thank you for sending me to conferences to further my education and learn from other stand-out scientists in the field of cancer immunotherapy.

Additionally, thank you to my dissertation committee members – Dr. Stephen McSorley and Dr. Joseph Tuscano – for being supportive and helpful. In conjunction, thank you Dr. Robert Canter, Dr. Arta Monjazeb, and Dr. Anthony Zamora, for their supplementary insights and guidance as well.

I want to express my sincere thanks to Dr. Logan Vick and Dr. Craig Collins for taking their time to train me during the beginning of my lab tenure. Additionally, thank you to Wahed Firoz and Ryan Nielsen for all the help you provided in my experiments. To the four of you, thank you for being wonderful friends and supportive lab mates throughout my PhD.

Furthermore, I am especially thankful to Kelly Loi, who originally started as a high school student working in our lab as part of the CIRM SPARK program and eventually volunteered her weekends during her school year to help run experiments as an unpaid intern. I am so thankful for your contributions and unwavering dedication and wish you nothing but the best in your undergraduate studies!

I want to acknowledge the invaluable contributions of all the adjunct staff at the UC Davis Institute of Regenerative Cures – Justin Graham, John Joyce, Heather Boyle, Dallon Martin, and Jonathan van Dyke. Your routine maintenance of core facilities is instrumental to the success of all labs here and we can never thank you enough.

A big thanks to the GGI program for providing a scientifically rigorous curriculum and building a strong sense of community. I want to especially thank my cohort mates – Alvin Lam, Aryana Razmara, Arthur Flores, Clarisa Martinez, Kayla Thomas, Nicolle Sweeney, Marshall Lammers, Sharon Sanghar, Stephanie Henson – for being great friends throughout the past few years. I will always fondly remember our classes, study sessions, fun get-togethers, and overall, our shared camaraderie.

Thank you to my Regeneron family, especially Dr. Aynur Hermann, Dr. Erica Ullman, and Dr. Ken-wing Lee, for inspiring me and teaching me about work professionalism and scientific rigor during my early adult years. You were instrumental in my personal path in pursuing a PhD and I am grateful for your continued support.

A special thanks to my earlier science mentors in high school and college – Dr. Theo Dreher (Oregon State University), Dr. Donal Manahan (University of Southern California), and Dr. Scott Applebaum (University of Southern California) – for inspiring me as a teenager to pursue a career in science.

Last, and most importantly, thank my so much to my wonderful and loving family. They are truly the most incredible people in my life, and I could never have accomplished my PhD without their undying support for over 30 years. To my mom, Shirley – thank you for teaching me to always trust my heart and instincts. To my dad, Kai – thank you for showing me the value of hard work and strength in the face of adversity. And to my big brother, William – thank you for always being honest and keeping me humble and self-determined throughout the years.

TABLE OF CONTENTS

Mechanistic Insights into Conventional T and CAR T cell Activation Induced Cell Death and Allogeneic Responses

CHAPTER 1: T Cell Immunology and the Preclinical Foundations of CAR T Cells

CHAPTER 2: PD-1 Restrains Interferon-Gamma Mediated Activation-Induced Cell Death that Limits T cell Engraftment and Efficacy

CHAPTER 3: Evidence of Allogeneic-Directed Anti-Tumor Effects by CAR T cells in Preclinical Modeling

CHAPTER 4: Final Thoughts

Dissertation Abstract

T cell adoptive therapies, including chimeric antigen receptor (CAR) T cells, have revolutionized the treatment of cancer, particularly hematological malignancies, yet there are still many poorly understood cellular mechanisms regulating T cell efficacy, persistence and preclinical modeling that negatively impact translational success. My dissertation explores the molecular drivers of conventional T and CAR T cell activation, focusing on the roles of activation-induced cell death (AICD) and unintended allogeneic responses that may confound efficacy data.

In Chapter 1, I introduce foundational studies that laid the groundwork for our current understanding of T cell biology and signaling, and examine how researchers have leveraged those findings to develop CAR T cells. I further review the current CAR T cell preclinical pipeline, highlighting how advances in CAR construct design, manufacturing optimization, application of preclinical models and development of next-generation platforms, are being integrated to improve CAR T cell therapeutic efficacy and clinical translation.

Building on the theme of translational immunobiology, Chapter 2 explores the paradoxical role of PD-1 signaling in conventional and CAR T cells. While there is currently a strong interest in combining checkpoint inhibition with CAR T cell therapy, clinical results have been mixed with multiple studies reporting equivocal or negative data. PD-1 is typically viewed as an inhibitory receptor attenuating T cell activity, although my work demonstrates that during strong T cell receptor or CAR stimulation, PD-1 engagement actually protects T cells from AICD by decreasing interferon-gamma (IFN-γ) production, leading to less CD95 (Fas) expression and subsequently less

apoptosis. Disruption of PD-1 signaling in T cells enhances early activation and cytokine production but compromises long-term cell survival and persistence. These findings highlight a dual role for PD-1 in modulating activation and longevity, with significant implications for optimizing immune checkpoint blockade administration in the context of adoptive T cell therapy.

In Chapter 3, I demonstrate that both non-transduced (NT) and CAR T cells can mount potent cytotoxic responses against an antigen-negative Raji tumor line possibly due to endogenous T-cell receptor (TCR)-mediated alloreactivity. These responses are characterized by increased expression of T cell activation markers, such as CD25, CD69, HLA-DR and PD-1, increased expression of the proliferation marker Ki67, and elevated production of cytokines. These results demonstrate a key limitation in preclinical modeling where the use of certain tumor cell lines can artificially inflate efficacy results due possibly to unintended TCR-mediated reactivity.

Together, these studies provide novel insights into how CAR T cells are shaped by their activation status – the fine balance between increased effector function at the cost of survival – and the importance of performing preclinical modeling with systems that avoid false-positive outcomes and recapitulate clinical conditions.

CHAPTER 1: T Cell Immunology and the Preclinical Foundations of CAR T Cells

Michael K. Sheng[1], William J. Murphy[1*]

1. Department of Dermatology, University of California Davis School of Medicine, Davis, Sacramento, CA, USA

***Corresponding Author:**

Dr. William J. Murphy, Distinguished Professor, Department of Dermatology, School of Medicine, University of California, Davis, Sacramento, CA 95817, USA,

Phone: (916) 703-9397, E-mail: wmjmurphy@health.ucdavis.edu

Abstract

T cells are integral to an effective immune response, mediating diverse roles such as direct killing of infected or cancerous cells, cytokine secretion to activate and recruit other immune populations, and the formation of immunological memory to protect against repeat antigen exposure. Using intracellular signaling motifs from conventional T cell receptors, chimeric antigen receptor (CAR) T cells can be engineered to recognize specific antigens in an MHC-independent manner. CAR T cell therapy has profoundly transformed the cancer treatment landscape, achieving unprecedented clinical success in patients with hematological malignancies. However, challenges such as cytokine release syndrome, neurotoxicity, antigen escape, and limited efficacy in solid tumors remain, underscoring the need for a robust preclinical development pipeline to design novel CAR T cell products and generate clinically meaningful data. This review provides a comprehensive overview of the key stages in CAR T cell therapy development, from CAR construct design and manufacturing optimization to *in vitro* and *in vivo* functionality assessment. We discuss how factors like T cell subset composition, and cytokine choice and expansion duration during manufacturing influence CAR T cell phenotype, persistence, and anti-tumor efficacy. *In vitro* assays offer valuable mechanistic insights but fail to model dynamic immune cell interactions, trafficking, and complex tumor microenvironments. In contrast, *in vivo* models allow for more complex physiological evaluation but are limited by species differences and ethical constraints. Next-generation platforms such as patient-derived tumor organoids and organ- or multi-organ-on-a-chip microfluidics are emerging as powerful tools to model CAR T cell therapy within physiologically relevant contexts such as immune cell trafficking, tumor

architecture and heterogeneity, and the tumor microenvironment. Additionally, computational approaches are being increasingly used to develop novel CAR designs and predict patient responses. By integrating traditional experimental approaches with innovative technologies, the field is poised to improve translational success by generating more clinically predictive data and accelerating the development of safer and more effective CAR T cell therapies.

Introduction

A Brief History of T cell Biology

In a seminal 1961 study, Jacques Miller demonstrated that neonatal thymectomy caused mice to be highly susceptible to infection, proving that the thymus is essential for the development of an effective immune response.[1] Subsequent studies revealed that while removal of the bursa of Fabricius in chickens ablated antibody production but did not impair allograft rejection, thymectomy in mice prevented both allograft rejection and delayed-type hypersensitivity, while only partially reducing antibody responses.[2–4] Collectively, these findings established a functional distinction between lymphocytes derived from the thymus (T cells) that mediate cellular immunity, and those from the bursa (B cells) that produce antibodies. To clarify the thymus's role in lymphocytic development, Miller showed in 1967 that while thymectomy did not prevent the formation and pool of precursor lymphocytes, it was critical for their maturation into immunocompetent cells capable of mounting antigen-specific responses against sheep erythrocytes, causing them to undergo robust proliferation.[5]

Over the ensuing decades, researchers made significant advances in uncovering the molecular mechanisms regulating T cell biology and signaling. In 1974, Rolf Zinkernagel and Peter Doherty demonstrated that cytotoxic T cells from k-haplotype (CBA/H) mice immunized with lymphocytic choriomeningitis virus (LCMV) could only kill infected target cells sharing the same MHC haplotype, and not those expressing b or d haplotypes.[6] This landmark discovery laid the foundation for the concept of MHC restriction in T cell responses.

In the following decade, considerable progress was made in identifying the actual T cell receptor responsible for this MHC restriction. In 1982, Jim Allison and colleagues identified a monoclonal antibody that recognized a unique surface glycoprotein molecule on a clonal T cell tumor, providing the first evidence that a clonotypic T cell receptor (TCR) exists.[7] In a pivotal moment in early 1984, Tak Mak and Mark Davis, along with their colleagues independently cloned the cDNAs encoding the β chain of the human and mouse TCRs respectively.[8,9] Within the year, both groups (along with several others) would clone the α chain.[10–13]

Subsequent studies further delineated the molecular process of T cell activation. In 1986, Alain Townsend and colleagues demonstrated that cytotoxic T cells could recognize short influenza-derived peptides presented on MHC class I molecules and eliminate infected target cells. In 1987, Carl June and colleagues identified CD28 as a crucial co-stimulatory receptor by showing that CD28 engagement enhanced T cell activation and proliferation but only in the context of concurrent protein kinase C or anti-CD3 stimulation, establishing the second important signal in T cell activation.[14]

In the 1990s and early 2000s, immunologists further illuminated the importance of cytokine signaling on T cells, now known as signal 3. Matthew Mescher and colleagues demonstrated that inflammatory cytokines, such as IL-12 and type I interferons, are critical for naïve T cell priming and allow for full clonal expansion and acquisition of effector function.[15,16] Furthermore, in murine models, IL-12 alone was sufficient to comparably replace adjuvant use during peptide immunization, driving equivalent T cell expansion, effector function, and memory formation.[17]

Collectively, these key findings have established our current three signal model of T cell activation, a fundamental dogma in immunology. Signal 1 involves TCR recognition of peptide-MHC complexes; signal 2 involves co-stimulatory receptor binding to respective ligands (i.e., CD28 binding to CD80/CD86); signal 3 involves cytokine receptor signaling. Activation through these three modules results in the clonal expansion, differentiation, and robust effector function of T cells.

The Development and Rise of CAR T cell Therapy

Unlike T cells that are MHC-restricted in activation, in chimeric antigen receptor (CAR) T cell therapy, T cells are taken from a patient and genetically modified to express an artificial receptor – known as a 'CAR' – enabling them to recognize tumor-associated antigens (TAA) and mount a specific and potent and cytotoxic response. In the past decade, CAR T cell therapy has dramatically enhanced the cancer immunotherapy landscape, providing not only a highly efficacious alternative to conventional cancer treatments but also creating a biological blueprint that can potentially be harnessed to treat other uncurable diseases

Clinical trials, such as ELIANA/ENSIGN, ELARA and ZUMA-1, have demonstrated the potent efficacy of CAR T cells in achieving remission and significantly improving overall survival (OS) in relapsed or refractory (R/R) B-cell acute lymphoblastic leukemia (B-ALL) and R/R diffuse large B-cell lymphoma (DLBCL).[18–20] In a direct comparative study, CAR T cell therapy outperformed chemotherapy in terms of remission and OS in patients with R/R B-ALL.[21] Furthermore, several matching-adjusted indirect comparison studies have associated CAR T cell therapies with improved OS,

reduced risk of death, and fewer hospitalizations when compared to historical standard-of-care.[22,23] These findings support CAR T cell therapy not only as a viable treatment option but in certain contexts as a superior alternative to conventional treatments.

Despite clinical success, CAR T cell therapy still faces significant hurdles, including variable patient responses, cytokine release syndrome (CRS), neurotoxicity, tumor heterogeneity, antigen escape, and limited efficacy in solid tumors.[24] Addressing these issues requires a comprehensive preclinical pipeline including rational CAR design, optimized manufacturing, and robust *in vitro* and *in vivo* experimental modeling. These stages are essential for refining product candidates, generating clinically relevant data, and improving the predictive value of preclinical findings. This review examines key aspects of the CAR T cell preclinical pipeline, highlighting current strategies, limitations, and emerging innovations aimed at advancing the next generation of CAR T cell therapies.

CAR T cell Design

As of August 2025, the FDA has approved seven CAR T cell therapies (Table 1). While they all target hematological malignancies, five target the antigen CD19 and two target BCMA. Despite differences in antigen targeted, these therapies share a similar underlying CAR structure.

At its core, a CAR consists of four components: the antigen-binding single-chain variable fragment (scFv), the hinge region, the transmembrane domain, and intracellular signaling domains.[25] The extracellular scFv, composed of the variable heavy (VH) and variable light (VL) regions of a monoclonal antibody connected by a flexible linker, allows for MHC-unrestricted antigen specificity. Immediately downstream is the hinge region, which provides structural flexibility and stability, allowing the scFv to effectively bind to its target antigen. The transmembrane domain anchors the CAR to the T cell membrane.

The intracellular portion of the CAR contains signaling motifs derived from T cell activation proteins such as CD3ζ, CD28, 4-1BB, ICOS, OX40, and other co-stimulatory molecules. These domains enable the CAR T cells to become activated and exert effector functions upon antigen cross-linking. First-generation CARs incorporate only a single CD3z intracellular domain while second and third generation CARs add an additional one or two intracellular signaling domains (i.e., CD28, 4-1BB etc.) respectively, enhancing T cell survival, proliferation, and persistence.[26–28] Additionally, fourth generation CARs, such as armored and T-cell redirected towards universal cytokine killing (TRUCK) CARs, in addition to intracellular signaling domains, include transgenes – such as cytokines, monoclonal antibodies, enzymes, transcription factors,

and other immunomodulatory proteins – to improve CAR T cell function and survival in immunosuppressive tumor microenvironments (TMEs).[29,30] To build upon this concept, more recently researchers have developed fifth-generation CARs, which add signaling domains from cytokine receptors to activate of the JAK-STAT pathway and further promote T cell proliferation, survival, and memory formation.[31]

Currently, all FDA-approved CAR T cell products utilize a second-generation CAR although third- and fourth-generation CAR T cells are actively being tested in clinical trials with promising preliminary results.[32,33] However, While unique CAR designs form the molecular basis for improving CAR T cell function, therapeutic efficacy of the final CAR T cell product is also dependent on how these cells are manufactured.

CAR T cell Manufacturing

CAR T cell manufacturing is increasingly recognized as a crucial determinant for the quality and therapeutic efficacy of the final CAR T cell product. While all current FDA-approved CAR T therapies to date are autologous, to primarily mitigate the risk of graft-versus-host disease (GvHD), significant research is being conducted to develop off-the-shelf allogeneic CAR T cells.[34]

Starting Populations of T cell Subsets

Following blood collection, researchers perform leukapheresis to obtain PBMCs, which can later be processed by magnetic bead sorting or other purification methods to yield an enriched T cell population. A considerable effort has gone into identifying the ideal starting T cell populations to maximize CAR T cell efficacy, especially considering the variability in baseline percentages of CD4+ and CD8+ T cells amongst patients. While CD8+ T cells are classically seen as the primary mediators of cytotoxicity, studies have shown that CAR T cells derived solely from purified CD8+ T cells are hypofunctional and less efficacious as they require strong cytokine signaling and co-stimulatory interactions (i.e., from CD40L-CD40 and CD70-CD27) from CD4+ helper T cells to fully exert their anti-tumor capabilities.[35] Moreover, CD4+ CAR T cells themselves can be cytotoxic and have been identified as the key cell type contributing to long-term disease control in treated patients with chronic lymphocytic leukemia (CLL).[36]

Multiple studies have identified a 1:1 ratio of CD4+:CD8+ T cells to be best for maximizing anti-tumor efficacy.[35,37] This notion is supported by clinical data

demonstrating an association of a CD4+:CD8+ ratio higher than 1.12 with increased risk of treatment failure at three and six months.[38] Due to this, lisocabtagene maraleucel, unlike other products that start with bulk T cell populations, is manufactured by separately generating CD4+ and CD8+ CAR T cells before combining them at a 1:1 ratio for infusion.[39]

In addition to CD4+/CD8+ composition, the differentiation status of the starting T cell population, particularly the CD8+ subset, can significantly impact CAR T cell therapeutic outcome. Surface markers such as CD62L, CCR7, CD45RA, and CD45RO, can classify T cells into distinct subsets: naïve (T_N, CD62L+CCR7+CD45RA+CD45RO-), stem cell memory (T_{SCM}, CD62L+CCR7+CD45RA+CD45RO+), central memory (T_{CM} ,CD62L+CCR7+CD45RA-CD45RO+), effector memory (T_{EM} ,CD62L-CCR7-CD45RA-CD45RO+), and effector (T_{EFF} ,CD62L-CCR7-CD45RA+CD45RO-).[40] CAR T cells derived from T_N, T_{SCM}, and T_{CM} populations tend to persist longer and demonstrate stronger anti-tumor responses.[37,41] Despite this, enrichment less differentiated subsets is not yet adopted in standard manufacturing protocols.

Ex Vivo Expansion: Cytokines Effects

Follow population selection, T cells are activated typically with anti-CD3/CD28 antibodies coated on magnetic beads or embedded in nanomatrices, although alternative methods of activation, such as phytohemagglutinin, have been explored.[42–44] After 24 to 48 hours of activation, T cells are transduced with lentiviral or retroviral vectors encoding the CAR construct and at 72 hours, activation reagents are removed,

and CAR T cells are expanded *ex vivo* in culture media containing cytokines for one to two weeks prior to formulation and infusion.[44]

Historically, IL-2 has been the primary cytokine used during *ex vivo* expansion as it enables robust T cell proliferation and is used in the manufacturing of both tisagenlecleucel and axicabtagene ciloleucel.[45] However, sustained high doses of IL-2 during expansion has been linked with increased CAR T cell exhaustion and regulatory T cell (T_{reg}) induction, which could impair CAR T cell efficacy.[45] Furthermore, prolonged IL-2 signaling can drive terminal differentiation of CAR T cells into T_{EM} or T_{EFF} phenotypes, resulting in a reduced frequency of early memory subsets (T_{SCM} or T_{CM}) and decreased long term persistence and tumor control.[46]

To address these limitations, some protocols instead use a combination of IL-7 and IL-15 for *ex vivo* expansion, which better maintains less differentiated CAR T cell phenotypes, resulting in greater persistence and sustained anti-tumor efficacy.[47,48] IL-21 has been shown to further enrich for less differentiated CAR T cells while increasing both expansion and transduction efficiency during manufacturing.[49]

Ex Vivo Expansion: Culture Duration and Phenotypic Impact

In addition to cytokines, the length of *ex vivo* expansion greatly influences the phenotype and functional quality of the CAR T cell product. Standard manufacturing protocols typically include an expansion period of one to two weeks, during which a heterogeneous mixture of $CD4^+$ and $CD8^+$ T cells proliferates.[44] Within this population, cells exhibit varying degrees of differentiation, spanning from less differentiated (T_{SCM}, T_{CM}) to more differentiated (T_{EM}, T_{EFF}) subsets. Longer culture times tend to drive CAR

T cells towards terminal differentiation and exhaustion, potentially compromising persistence and therapeutic efficacy. Conversely, shorter expansion times help preserve stem-like and early memory phenotypes and is correlated with improved persistence and clinical outcomes. Studies have shown that CAR T cells harvested earlier, 3 or 5 days, into the expansion phase are not only less differentiated but also demonstrate enhanced anti-tumor activity even at lower doses.[50,51] Supporting this, a phase I trial utilizing a next-day manufacturing protocol found that CAR T cells frozen 24 hours after transduction displayed less exhaustion and differentiation, and possessed greater efficacy at low doses in patients with relapsed/refractory B-ALL.[52]

In Vitro Characterization of CAR T cell Efficacy

Following successful generation and expansion, CAR T cells are typically first evaluated in 2D *in vitro* assays to assess their phenotype, functionality, and persistence. Standard assays involve co-incubating CAR T cells with either bead- or plate-bound antigen(s) or immortalized antigen-expressing cell lines for 24 to 72 hours hours.[53] This setup can be performed in single or repeated rounds of restimulation with antigenic targets to evaluate the durability of CAR T cell responses and the effects of prolonged activation on phenotype. Repeated stimulations may better model clinical scenarios where tumor cells are not immediately eliminated but require prolonged immune control.

After co-culture, CAR T cell *in vitro* characterization focuses on four key parameters: 1) phenotypic analysis (activation, exhaustion, and memory markers), 2) secretory profiling (cytokines, cytotoxic granules, and chemokines), 3) proliferative capacity, and 4) cytotoxic function.

Phenotypic Analysis

CAR engagement with antigen results in robust T cell activation, which can be evaluated by upregulated surface expression of activation markers such as CD25, CD69, CD71, and HLA-DR.[54] Conversely, increased expression of inhibitory receptors such as PD-1, LAG-3, TIGIT, TIM-3, and 2B4, may indicate emerging or greater T cell exhaustion, which is associated with poorer clinical outcome.[55–58] These markers can be measured either by flow cytometry or qPCR. Additionally, flow cytometry enables assessment of memory subset differentiation using delineation markers such as CD62L,

CCR7, CD45RA, and CD45RO (as previously discussed), allowing for monitoring of the phenotypic shift towards progressive terminal differentiation following antigen exposure.

Secretory Profiling

Supernatants collected from co-cultures can be analyzed for cytokines, cytotoxic granules, and chemokines, using enzyme-linked immunosorbent assay (ELISA), cytokine bead arrays (CBA), or high-throughput multiplex platforms such as Luminex, Meso Scale Discovery (MSD), or single-cell secretome technologies.[59,60] The secretion of key inflammatory cytokines, including IL-2, IFN-γ, and TNF, and cytotoxic granules, including granzyme B and perforin, is indicative of functional CAR T cell activation and cytolytic potential.[61,62] However, while elevated cytokine secretion may indicate potent effector function, it may also correlate clinically with an increased risk of cytokine release syndrome (CRS), immune effector cell-associated neurotoxicity syndrome (ICANS), or tumor lysis syndrome (TLS).[63] In addition, chemokines such as CCL19, MIP-1α, and SDF-1α may indicate the potential of CAR T cells to recruit other immune populations, especially innate immune cells.[64]

Proliferative Capacity

The ability of CAR T cells to expand upon antigen encounter is a critical indicator of therapeutic efficacy. Clinically, greater in vivo CAR T cell expansion has been associated with complete responders, while limited expansion is more often observed in non-responders or partial responders.[65] *In vitro*, proliferative capacity can be assessed directly by counting total cell numbers post-stimulation or by [^{3}H]-thymidine

incorporation assays. Alternatively, flow cytometry approaches can also be used, including detection of proliferation markers, such as Ki-67, or BrdU incorporation, as well as tracking dye dilution methods using CFSE or CellTrace Violet.[66]

Cytotoxic Function

Cytotoxicity can be measured both directly and indirectly. Direct methods include quantifying target cell death by flow cytometry using viability dyes (i.e., propidium iodide, 7-AAD) or apoptosis markers (i.e., annexin V) to distinguish between live, apoptotic, and dead target cells, or by engineering target cells to express fluorescent proteins (i.e., GFP) or luciferase, then monitoring the loss of these signals over time as an indicator of cell death.[67] Indirect methods include impedance-based killing assays (e.g., xCELLigence) or measuring the release of intracellular contents such as ATP, lactate dehydrogenase (LDH), or chromium-51 from lysed cells.[67] These assays provide multiple functional readouts to evaluate the ability of CAR T cells to kill antigen-expressing tumor target cells.

Limitations of Preclinical In Vitro Assessment

While *in vitro* assays serve as a useful first pass in evaluating CAR T cell effector function and proliferative capacity upon antigen encounter, they fall short in replicating complex *in vivo* physiological conditions. Standard co-culture assays create an artificial environment where CAR T cells are placed in close immediate proximity with tumor cells overexpressing the targeted antigen. In reality, CAR T cells must circulate

systemically, traffic to the tumor site, and infiltrate the TME, where its functionality is influenced by immunological and metabolic barriers.

In solid tumors, antigen expression may not be restricted to malignant cells and are often expressed at varying levels on normal tissues, increasing the risk of on-target, off-tumor (OTOT) toxicity, a phenomenon observed in multiple clinical trials.[68] Additionally, while tumor cell lines used in co-culture assays typically express uniformly high levels of antigen, patient tumors are generally far more heterogeneous, and may exhibit low antigen density, which can reduce CAR T cell activation and cytotoxicity.[69]

A major limitation of *in vitro* modeling is the absence of an immunosuppressive TME. *In vivo*, CAR T cells must contend with the presence of regulatory T (T_{reg}) cells, myeloid-derived suppressor cells (MDSCs), and M2-polarized tumor-associated macrophages (TAMs).[70–73] These cells secrete immunosuppressive cytokines like TGF-β and IL-10, express inhibitory ligands, and interfere with T cell homing, all of which collectively impair CAR T cell function in the TME and are rarely accounted for in standard *in vitro* assays.[74,75] Conversely, by releasing pro-inflammatory cytokines and chemokines, CAR T cells can also recruit other immune and stromal populations to the TME.[76] This is particularly true for fourth-generation CAR T cells, which are engineered to secrete immunomodulatory factors that enhance not only their own anti-tumor capabilities but also that of neighboring immune cells.[77]

Furthermore, *in vitro* assays typically fail to replicate other critical features of the TME, such as hypoxia, acidic pH, nutrient depletion, and abnormal vasculature (i.e. fibrotic stromal barriers), all factors that impact CAR T cell trafficking, persistence, metabolism, and overall effector function.[78,79]

To improve the translational relevance of 2D in vitro assays, future studies should consider incorporating stromal, endothelial, and immunosuppressive immune cells, introducing physical barriers to mimic tumor vasculature, and simulating hostile conditions (i.e., hypoxia, low pH, and nutrient scarcity). While *in vitro* models are important for early-stage CAR T cell evaluation, their inability to recapitulate the complexities of human physiology and the TME limits their translational value and underscores the need for complementary *in vivo* modeling.

In Vivo Characterization of CAR T cell Efficacy

In vivo models provide an essential platform for evaluating CAR T cell efficacy, persistence, trafficking, and safety in physiologically relevant context. These models typically involve engrafting either human (xenogeneic) or murine (syngeneic) tumor cells into mice and subsequently treating them with CAR T cells. Unlike *in vitro* assays, during *in vivo* modeling, CAR T cells circulate, traffic to tumor sites, and interact with the tumor microenvironment (TME).

Xenogeneic Mouse Modeling

Xenogeneic models typically involve implanting human tumor cell lines or patient-derived xenografts (PDXs) into severely immunodeficient mice such as NSG, NOG, or NRG strains.[80,81] These mice lack functional T, B, and NK cells, and exhibit deficiencies in their macrophage and dendritic cell compartments, allowing for engraftment of both human tumor cells and human CAR T cells.[82] PDXs, generated from clinical tumor samples grown and passaged in immunodeficient mice, may improve translational relevance by modeling tumor heterogeneity although they are limited logistically by availability (depending on the tumor), long establishment times, and high costs. Repeated passaging also selects for dominant fast-growing subclones thereby reducing tumor heterogeneity over time.[83] In addition, the human TME in PDXs is progressively replaced with murine extracellular matrix and stromal cells limiting its ability to faithfully model the human TME.[84]

Hematological tumors are typically injected intravenously while solid tumors can be implanted subcutaneously, orthotopically, or intravenously, depending on the cancer

type and the experimental objectives. After a period of engraftment, CAR T cells are then administered intravenously, and anti-tumor efficacy is monitored primarily through survival analysis over time. To better mirror the clinical process, lymphodepleting regimes, such as radiation and chemotherapy (i.e., cyclophosphamide/fludarabine), may be administered beforehand to enhance CAR T cell engraftment. This preconditioning, however, can lead to altered tumor metabolism and premature tumor clearance, complicating interpretation of CAR T cell eficacy.[85] Furthermore, since immunodeficient mice lack other functional immune populations and interactions between then and CAR T cells, the effects of lymphodepletion in this context may not be physiologically representative.[86] Tumor burden can be assessed via caliper measurements (solid tumors), flow cytometry, MRI, or bioluminescent/fluorescent imaging using tumor cells engineered to express luciferase or fluorescent proteins.[87,88] These imaging techniques are especially valuable for tracking disease progression in disseminated or metastatic cancer models.

Additionally, CAR T cell persistence and memory phenotype can be evaluated by collecting and processing blood, lymphoid tissues (although lymph nodes are absent in most immunodeficient strains), tumor-infiltrated organs, and tumors themselves and analyzing via flow cytometry or immunohistochemistry. Cytokine and chemokine secretion profiles can also be evaluated by serum analysis. While immunodeficient mouse models provide valuable insight into CAR T cell efficacy and persistence *in vivo*, they ultimately lack a functional immune system and therefore cannot accurately model the spectrum of CAR T cell interactions with other immune cell types. Furthermore, while functional myeloid-derived suppressor cells (MDSCs) and tumor-associated

macrophages (TAMs) have been detected in NSG mice, their impact on human CAR T cells may be minimized due to species incompatibility.[89]

To better model these human immune interactions, humanized mouse models can be generated by engrafting human PBMCs or hematopoietic stem cells into immunodeficient mice. To promote engraftment and support development of human immune lineages, these mice are often engineered to express additional human components such as cytokines (i.e., NSG-SGM3), MHC molecules, or phagocytosis-inhibiting receptors like SIRPα (i.e., MISTRG mice). Despite these advances, however, cross-species incompatibilities remain. Human CAR T cells cannot fully interact with mouse cytokines, vasculature, or stroma, and additionally, humanized mice develop graft-versus-host disease (GvHD), limiting experimental windows.[90] Furthermore, while human cytokines such as TNF and IL-1α/β can signal through murine receptors, xenogeneic models are inconsistent and unreliable for evaluating systemic toxicities with mixed reports showing that they observe systemic toxicities in some cases and not in others.[91–94] To address these limitations, syngeneic mouse models are often used in conjunction or as an alternative platform to assess CAR T cell activity in the context of a fully functional species-compatible immune system.

Syngeneic Mouse Modeling

In syngeneic models, murine tumor cell lines are implanted into immunocompetent mice, typically C57BL/6 or BALB/c strains, which are then treated with mouse-derived CAR T cells. These models offer one distinct advantage over xenogeneic ones by

enabling the evaluation of CAR T cell function in the context of a fully intact immune system. This includes interactions and crosstalk with endogenous T cells, innate immune cells, stromal components, and tumor vasculature, all of which can modulate CAR T cell efficacy, expansion, and persistence.[95,96]

Additionally, while lymphodepleting regimens can be applied in xenogeneic models, their use in syngeneic ones provide greater physiological relevance owing to an intact immune system.[97] Furthermore, since cytokine-receptor signaling is maintained in a mouse-to-mouse context, systemic toxicities, including CRS or immune-mediated organ damage, can be more accurately modeled than in immunodeficient or humanized mice. Toxicity assessments include histopathological analysis, complete blood counts, and serum chemistry testing (e.g., ALT, AST) to monitor organ function and hematological changes.[98]

However, translating syngeneic models to humans is limited by reliance on murine CAR T cells and tumor antigens, which may not accurately reflect the functionality of human CAR T cells. Additionally, mouse tumor cell lines are often more immunogenic than patient tumors, which may cause overestimation of CAR T cell potency.[99] Therefore, while syngeneic models are important to study immune dynamics and safety profiles, their results should be evaluated together with xenogeneic and humanized models for a more comprehensive preclinical evaluation.

Limitations of In Vivo Models

While *in vivo* models have significantly advanced the preclinical evaluation of CAR T cells, mouse biology does not fully capture human physiology particularly in

terms of immune cell trafficking, cytokine signaling, and systemic toxicity. Toxicities observed in mice do not always translate to humans, especially since disease states must often be artificially induced. Furthermore, neither tumor cell lines nor PDXs fully capture the heterogeneity, TME, and complexity of human patient tumors, limiting the ability of these models to simulate mechanisms of tumor resistance such as antigen loss or immune escape.[100]

To address these limitations, alternative animal models have been explored. Canines, for example, are genetically and histologically similar to humans and share comparable inherited disease patterns and microbiome compositions.[101] Furthermore, their cancers arise spontaneously in immunocompetent hosts, leading to tumor heterogeneity that more closely resembles human disease.[102] Non-human primates, which are even more genetically similar with humans, have been shown to recapitulate key CAR T cell-associated toxicities such as cytokine release syndrome (CRS) and neurotoxicity with high fidelity.[103] However, both canine and non-human primate models are limited by high costs, logistical challenges, and ethical constraints.

Future Directions

In 2013, European states adopted EU Directive 2010/63/EU strengthening ethical reviews of all animal studies. Furthermore, the European Parliament passed a resolution in 2021 calling for a plan to phase out all animal testing by 2035. In the United States, the FDA Modernization Act 2.0 was signed into law in 2022 removing the federal mandate for animal testing in drug approvals. More recently, the SPARE Act was introduced to Congress in March 2025 proposing to ban animal use in all federally funded research facilities, and the NIH announced in July 2025 that it would no longer fund research exclusively relying on animal models. With the research community moving towards replacing *in vivo* models, it is necessary to develop advanced *in vitro* techniques that faithfully replicate complex *in vivo* biology.

Patient-derived tumor organoids (PDTOs) are derived from stem or progenitor cells of a patient's tumor, embedded in an 3D extracellular matrix and differentiated into organ-like tissues that largely preserve the histological and molecular heterogeneity of the original tumor. While PDTOs do not yet fully recapitulate the tumor microenvironment (TME) or CAR T cell trafficking dynamics within the human body, they represent a 3D spatial model to study CAR T cell efficacy in a heterogeneous tumor. Multiple studies have demonstrated the strong predictive ability of PDTOs for immunotherapy outcomes.[104,105] Notably, a recent study successfully generated glioblastoma PDTOs that accurately mirrored patient responses to CAR T cell therapy, both treatment efficacy and potential neurotoxicity, in a simultaneous, side-by-side comparison.[106]

To better simulate immune cell trafficking and the TME, organ-on-a-chip (OOC) and multi-organs-on-a-chip (MOC) platforms have been developed that use microfluidic technologies to create interconnected microchannels mimicking vasculature, enabling the flow of immune cells through tissue-like structures that incorporate organ-specific tissues along with stromal cells, endothelial cells, immune cells, and components of the extracellular matrix.[107] Along with their ability to evaluate CAR T cell efficacy in complex, physiologically relevant environments, these systems have been shown to successfully replicate interactions between CAR T and other cell types, such as M2-like TAMs impairing CAR T cell cytotoxicity.[108] Researchers have also engineered these platforms to emulate TME-associated stresses such as hypoxia and acidic pH, allowing for predictive assessment of CAR T cell function under adverse environmental conditions.[109,110]

Complementing both established and innovative techniques is *in silico* modeling and machine learning (ML), which are transforming CAR T cell development. These computational tools can simulate molecular interactions and predict CAR-to-antigen binding interfaces at the atomic level, enabling the development of CAR constructs that avoid steric hindrance and improve target engagement.[111,112] ML algorithms can further integrate large datasets, including single-cell RNA sequencing (scRNA-seq), spatial transcriptomics, proteomics, metabolomics, and link them to patient outcomes and uncover key cellular mechanisms, signaling networks, and predictive biomarkers influencing CAR T cell efficacy. In one study, deep learning models accurately predicted over 90% of clinical outcomes in mantle cell lymphoma patients.[113] When computational approaches are integrated with experimental data, they can yield personalized,

mechanistically predictive insights that improve translational success without reliance on animal models.

Conclusions

In conclusion, T cells play an instrumental part of an effective immune response, clonally expanding in the presence of antigenic peptides presented onto MHC, and mediating immunity through cytotoxic effector function, orchestrating immune cell recruitment via cytokines and chemokines, and generating long-lasting immunological memory. Advances in the molecular understanding of basic T cell biology have allowed researchers to leverage the signaling motifs of classical T cell activation receptors to engineer CAR T cells that can mediate MHC-unrestricted cell-mediated cytotoxicity. However, CAR T cells still face significant clinical challenges, especially pertaining to differences in patient responses, systemic toxicities, tumor heterogeneity, antigen escape, and limited efficacy in solid tumors. A thorough understanding of the preclinical pipeline – including CAR design, manufacturing optimizing, and experimental modeling – is essential for developing next-generation CAR T cell therapies. Refining the CAR construct and manufacturing process, applying current preclinical models while acknowledging their limitations, and incorporating innovative technologies to uncover novel mechanistic insights will enable generation of more clinically meaningful data and improve the translational success of future CAR T cell therapies.

References

1. Miller, J. IMMUNOLOGICAL FUNCTION OF THE THYMUS. *The Lancet* **278**, 748–749 (1961).

2. Cooper, M. D., Peterson, R. D. A. & Good, R. A. Delineation of the Thymic and Bursal Lymphoid Systems in the Chicken. *Nature* **205**, 143–146 (1965).

3. Cooper, M. D., Peterson, R. D. A., South, M. A. & Good, R. A. THE FUNCTIONS OF THE THYMUS SYSTEM AND THE BURSA SYSTEM IN THE CHICKEN. *J. Exp. Med.* **123**, 75–102 (1966).

4. Miller, J. F. A. P., Mitchell, G. F. & Weiss, N. S. Cellular Basis of the Immunological Defects in Thymectomized Mice. *Nature* **214**, 992–997 (1967).

5. Miller, J. F. A. P. & Mitchell, G. F. The Thymus and the Precursors of Antigen Reactive Cells. *Nature* **216**, 659–663 (1967).

6. Zinkernagel, R. M. & Doherty, P. C. Restriction of in vitro T cell-mediated cytotoxicity in lymphocytic choriomeningitis within a syngeneic or semiallogeneic system. *Nature* **248**, 701–702 (1974).

7. Allison, J. P., McIntyre, B. W. & Bloch, D. Tumor-specific antigen of murine T-lymphoma defined with monoclonal antibody. *J. Immunol. Baltim. Md 1950* **129**, 2293–2300 (1982).

8. Hedrick, S. M., Cohen, D. I., Nielsen, E. A. & Davis, M. M. Isolation of cDNA clones encoding T cell-specific membrane-associated proteins. *Nature* **308**, 149–153 (1984).

9. Yanagi, Y. *et al.* A human T cell-specific cDNA clone encodes a protein having extensive homology to immunoglobulin chains. *Nature* **308**, 145–149 (1984).

10. Saito, H. *et al.* A third rearranged and expressed gene in a clone of cytotoxic T lymphocytes. *Nature* **312**, 36–40 (1984).

11. Sim, G. K. *et al.* Primary structure of human T-cell receptor a-chain. (1984).

12. Chien, Y. *et al.* A third type of murine T-cell receptor gene. *Nature* **312**, 31–35 (1984).

13. Yanagi, Y., Chan, A., Chin, B., Minden, M. & Mak, T. W. Analysis of cDNA clones specific for human T cells and the alpha and beta chains of the T-cell receptor heterodimer from a human T-cell line. *Proc. Natl. Acad. Sci.* **82**, 3430–3434 (1985).

14. June, C. H., Gillespie, M. M. & Thompson, C. B. T-Cell Proliferation Involving the CD28 Pathway Is Associated with Cyclosporine-Resistant Interleukin 2 Gene Expression. *MOL CELL BIOL*.

15. Curtsinger, J. M. *et al.* Inflammatory Cytokines Provide a Third Signal for Activation of Naive CD4+ and CD8+ T Cells. *J. Immunol.* **162**, 3256–3262 (1999).

16. Curtsinger, J. M., Valenzuela, J. O., Agarwal, P., Lins, D. & Mescher, M. F. Cutting Edge: Type I IFNs Provide a Third Signal to CD8 T Cells to Stimulate Clonal Expansion and Differentiation. *J. Immunol.* **174**, 4465–4469 (2005).

17. Schmidt, C. S. & Mescher, M. F. Adjuvant Effect of IL-12: Conversion of Peptide Antigen Administration from Tolerizing to Immunizing for CD8+ T Cells In Vivo. *J. Immunol.* **163**, 2561–2567 (1999).

18. Neelapu, S. S. *et al.* Axicabtagene Ciloleucel CAR T-Cell Therapy in Refractory Large B-Cell Lymphoma. *N. Engl. J. Med.* **377**, 2531–2544 (2017).

19. Maude, S. L. *et al.* Tisagenlecleucel in Children and Young Adults with B-Cell Lymphoblastic Leukemia. *N. Engl. J. Med.* **378**, 439–448 (2018).

20. Fowler, N. H. *et al.* Tisagenlecleucel in adult relapsed or refractory follicular lymphoma: the phase 2 ELARA trial. *Nat. Med.* **28**, 325–332 (2022).

21. Wei, G. *et al.* CD19 targeted CAR-T therapy versus chemotherapy in re-induction treatment of refractory/relapsed acute lymphoblastic leukemia: results of a case-controlled study. *Ann. Hematol.* **97**, 781–789 (2018).

22. V. Stackelberg, A. *et al.* Tisagenlecleucel vs. historical standard of care in children and young adult patients with relapsed/refractory B-cell precursor acute lymphoblastic leukemia. *Leukemia* **37**, 2346–2355 (2023).

23. Kordbacheh, T. *et al.* A Real-World Comparison of CAR T-Cell Therapy Versus a Historical Standard-of-Care Approach for Relapsed-Refractory Large B-Cell Lymphoma in Ontario, Canada. *Blood* **144**, 5134–5134 (2024).

24. Majzner, R. G. & Mackall, C. L. Clinical lessons learned from the first leg of the CAR T cell journey. *Nat. Med.* **25**, 1341–1355 (2019).

25. Zhang, C., Liu, J., Zhong, J. F. & Zhang, X. Engineering CAR-T cells. *Biomark. Res.* **5**, 22 (2017).

26. Irving', E. A. The Cytoplasmic Domain of the T Cell Receptor 6 Chain Is Sufficient to Couple to Receptor-Associated Signal Transduction Pathways.

27. Krause, A. *et al.* Antigen-dependent CD28 Signaling Selectively Enhances Survival and Proliferation in Genetically Modified Activated Human Primary T Lymphocytes. *J. Exp. Med.* **188**, 619–626 (1998).

28. Maher, J., Brentjens, R. J., Gunset, G., Rivière, I. & Sadelain, M. Human T-lymphocyte cytotoxicity and proliferation directed by a single chimeric TCRζ /CD28 receptor. *Nat. Biotechnol.* **20**, 70–75 (2002).

29. Chmielewski, M. & Abken, H. TRUCKS, the fourth-generation CAR T cells: Current developments and clinical translation. *Adv. CELL GENE Ther.* **3**, (2020).

30. Tang, L., Pan, S., Wei, X., Xu, X. & Wei, Q. Arming CAR-T cells with cytokines and more: Innovations in the fourth-generation CAR-T development. *Mol. Ther.* **31**, 3146–3162 (2023).

31. Kagoya, Y. *et al.* A novel chimeric antigen receptor containing a JAK–STAT signaling domain mediates superior antitumor effects. *Nat. Med.* **24**, 352–359 (2018).

32. Derigs, P. *et al.* Third-generation anti-CD19 CAR T cells for relapsed/refractory chronic lymphocytic leukemia: a phase 1/2 study. *Leukemia* **38**, 2419–2428 (2024).

33. Steffin, D. *et al.* Interleukin-15-armoured GPC3 CAR T cells for patients with solid cancers. *Nature* **637**, 940–946 (2025).

34. Li, Y.-R., Zhu, Y., Fang, Y., Lyu, Z. & Yang, L. Emerging trends in clinical allogeneic CAR cell therapy. *Med* 100677 (2025) doi:10.1016/j.medj.2025.100677.

35. Lee, S. Y. *et al.* $CD8^+$ chimeric antigen receptor T cells manufactured in absence of $CD4^+$ cells exhibit hypofunctional phenotype. *J. Immunother. Cancer* **11**, e007803 (2023).

36. Melenhorst, J. J. *et al.* Decade-long leukaemia remissions with persistence of CD4+ CAR T cells. *Nature* **602**, 503–509 (2022).

37. Sommermeyer, D. *et al.* Chimeric antigen receptor-modified T cells derived from defined CD8+ and CD4+ subsets confer superior antitumor reactivity in vivo. *Leukemia* **30**, 492–500 (2016).

38. Galli, E. *et al.* The CD4/CD8 ratio of infused CD19-CAR-T is a prognostic factor for efficacy and toxicity. *Br. J. Haematol.* **203**, 564–570 (2023).

39. Abramson, J. S. *et al.* Lisocabtagene maraleucel for patients with relapsed or refractory large B-cell lymphomas (TRANSCEND NHL 001): a multicentre seamless design study. *The Lancet* **396**, 839–852 (2020).

40. Golubovskaya, V. & Wu, L. Different Subsets of T Cells, Memory, Effector Functions, and CAR-T Immunotherapy. *Cancers* **8**, 36 (2016).

41. Arcangeli, S. *et al.* CAR T cell manufacturing from naive/stem memory T lymphocytes enhances antitumor responses while curtailing cytokine release syndrome. *J. Clin. Invest.* **132**, e150807 (2022).

42. Wang, X. & Rivière, I. Clinical manufacturing of CAR T cells: foundation of a promising therapy. *Mol. Ther. - Oncolytics* **3**, 16015 (2016).

43. Gulden, G. *et al.* CAR-T Cells with Phytohemagglutinin (PHA) Provide Anti-Cancer Capacity with Better Proliferation, Rejuvenated Effector Memory, and Reduced Exhausted T Cell Frequencies. *Vaccines* **11**, 313 (2023).

44. Ayala Ceja, M., Khericha, M., Harris, C. M., Puig-Saus, C. & Chen, Y. Y. CAR-T cell manufacturing: Major process parameters and next-generation strategies. *J. Exp. Med.* **221**, e20230903 (2024).

45. Watanabe, N., Mo, F. & McKenna, M. K. Impact of Manufacturing Procedures on CAR T Cell Functionality. *Front. Immunol.* **13**, 876339 (2022).

46. Kaartinen, T. *et al.* Low interleukin-2 concentration favors generation of early memory T cells over effector phenotypes during chimeric antigen receptor T-cell expansion. *Cytotherapy* **19**, 689–702 (2017).

47. Xu, Y. *et al.* Closely related T-memory stem cells correlate with in vivo expansion of CAR.CD19-T cells and are preserved by IL-7 and IL-15. *Blood* **123**, 3750–3759 (2014).

48. Zhou, J. *et al.* Chimeric antigen receptor T (CAR-T) cells expanded with IL-7/IL-15 mediate superior antitumor effects. *Protein Cell* **10**, 764–769 (2019).

49. Du, L. *et al.* IL-21 Optimizes the CAR-T Cell Preparation Through Improving Lentivirus Mediated Transfection Efficiency of T Cells and Enhancing CAR-T Cell Cytotoxic Activities. *Front. Mol. Biosci.* **8**, 675179 (2021).

50. Ghassemi, S. *et al.* Reducing *Ex Vivo* Culture Improves the Antileukemic Activity of Chimeric Antigen Receptor (CAR) T Cells. *Cancer Immunol. Res.* **6**, 1100–1109 (2018).

51. Cadinanos-Garai, A. *et al.* High-dimensional temporal mapping of CAR T cells reveals phenotypic and functional remodeling during manufacturing. *Mol. Ther.* **33**, 2291–2309 (2025).

52. Dias, J., Garcia, J., Agliardi, G. & Roddie, C. CAR-T cell manufacturing landscape—Lessons from the past decade and considerations for early clinical development. *Mol. Ther. - Methods Clin. Dev.* **32**, 101250 (2024).

53. Si, X., Xiao, L., Brown, C. E. & Wang, D. Preclinical Evaluation of CAR T Cell Function: In Vitro and In Vivo Models. *Int. J. Mol. Sci.* **23**, 3154 (2022).

54. Caruso, A. *et al.* Flow cytometric analysis of activation markers on stimulated T cells and their correlation with cell proliferation. *Cytometry* **27**, 71–76 (1997).

55. Wherry, E. J. & Kurachi, M. Molecular and cellular insights into T cell exhaustion. *Nat. Rev. Immunol.* **15**, 486–499 (2015).

56. Anderson, A. C., Joller, N. & Kuchroo, V. K. Lag-3, Tim-3, and TIGIT: Co-inhibitory Receptors with Specialized Functions in Immune Regulation. *Immunity* **44**, 989–1004 (2016).

57. Fraietta, J. A. *et al.* Determinants of response and resistance to CD19 chimeric antigen receptor (CAR) T cell therapy of chronic lymphocytic leukemia. *Nat. Med.* **24**, 563–571 (2018).

58. Ledergor, G. *et al.* CD4+ CAR T-cell exhaustion associated with early relapse of multiple myeloma after BCMA CAR T-cell therapy. *Blood Adv.* **8**, 3562–3575 (2024).

59. Xue, Q. *et al.* Single-cell multiplexed cytokine profiling of CD19 CAR-T cells reveals a diverse landscape of polyfunctional antigen-specific response. *J. Immunother. Cancer* **5**, 85 (2017).

60. Platchek, M., Lu, Q., Tran, H. & Xie, W. Comparative Analysis of Multiple Immunoassays for Cytokine Profiling in Drug Discovery. *SLAS Discov.* **25**, 1197–1213 (2020).

61. Xue, Q. *et al.* Single-cell multiplexed cytokine profiling of CD19 CAR-T cells reveals a diverse landscape of polyfunctional antigen-specific response. *J. Immunother. Cancer* **5**, 85 (2017).

62. Lemoine, J., Ruella, M. & Houot, R. Overcoming Intrinsic Resistance of Cancer Cells to CAR T-Cell Killing. *Clin. Cancer Res.* **27**, 6298–6306 (2021).

63. Zhang, Y. *et al.* Exploring CAR-T Cell Therapy Side Effects: Mechanisms and Management Strategies. *J. Clin. Med.* **12**, 6124 (2023).

64. Lei, W. *et al.* Safety and feasibility of anti-CD19 CAR T cells expressing inducible IL-7 and CCL19 in patients with relapsed or refractory large B-cell lymphoma. *Cell Discov.* **10**, 5 (2024).

65. Mueller, K. T. *et al.* Cellular kinetics of CTL019 in relapsed/refractory B-cell acute lymphoblastic leukemia and chronic lymphocytic leukemia. *Blood* **130**, 2317–2325 (2017).

66. Lašťovička, J., Rataj, M. & Bartůňková, J. Assessment of lymphocyte proliferation for diagnostic purpose: Comparison of CFSE staining, Ki-67 expression and 3H-thymidine incorporation. *Hum. Immunol.* **77**, 1215–1222 (2016).

67. Kiesgen, S., Messinger, J. C., Chintala, N. K., Tano, Z. & Adusumilli, P. S. Comparative analysis of assays to measure CAR T-cell-mediated cytotoxicity. *Nat. Protoc.* **16**, 1331–1342 (2021).

68. Flugel, C. L. *et al.* Overcoming on-target, off-tumour toxicity of CAR T cell therapy for solid tumours. *Nat. Rev. Clin. Oncol.* **20**, 49–62 (2023).

69. Zhang, B., Wu, J., Jiang, H. & Zhou, M. Strategies to Overcome Antigen Heterogeneity in CAR-T Cell Therapy. *Cells* **14**, 320 (2025).

70. Burga, R. A. *et al.* Liver myeloid-derived suppressor cells expand in response to liver metastases in mice and inhibit the anti-tumor efficacy of anti-CEA CAR-T. *Cancer Immunol. Immunother.* **64**, 817–829 (2015).

71. Cervantes, E. V. *et al.* MDSC Suppression of CAR T Cells Can be Reduced By Targeted Signaling Disruption. *Blood* **134**, 4438–4438 (2019).

72. Sun, Y. *et al.* Depletion of Tregs from CD4⁺ CAR -T cells enhances the tumoricidal effect of CD8⁺ CAR -T cells in anti- CD19 CAR -T therapy. *FEBS J.* **292**, 1904–1919 (2025).

73. Zhao, L. *et al.* The transition between M1 and M2 macrophage phenotypes is associated with the disease status following CD19 CAR-T therapy for B cell lymphoma/leukemia. *Cell Death Dis.* **16**, 275 (2025).

74. Groth, C. *et al.* Immunosuppression mediated by myeloid-derived suppressor cells (MDSCs) during tumour progression. *Br. J. Cancer* **120**, 16–25 (2019).

75. Yamaguchi, Y. *et al.* PD-L1 blockade restores CAR T cell activity through IFN-γ-regulation of CD163+ M2 macrophages. *J. Immunother. Cancer* **10**, e004400 (2022).

76. Adachi, K. *et al.* IL-7 and CCL19 expression in CAR-T cells improves immune cell infiltration and CAR-T cell survival in the tumor. *Nat. Biotechnol.* **36**, 346–351 (2018).

77. Hawkins, E. R., D'Souza, R. R. & Klampatsa, A. Armored CAR T-Cells: The Next Chapter in T-Cell Cancer Immunotherapy. *Biol. Targets Ther.* **Volume 15**, 95–105 (2021).

78. Jiang, H., Hegde, S. & DeNardo, D. G. Tumor-associated fibrosis as a regulator of tumor immunity and response to immunotherapy. *Cancer Immunol. Immunother.* **66**, 1037–1048 (2017).

79. Tiwari, A., Trivedi, R. & Lin, S.-Y. Tumor microenvironment: barrier or opportunity towards effective cancer therapy. *J. Biomed. Sci.* **29**, 83 (2022).

80. Ito, M. *et al.* NOD/SCID/γcnull mouse: an excellent recipient mouse model for engraftment of human cells. *Blood* **100**, 3175–3182 (2002).

81. Walsh, N. C. *et al.* Humanized Mouse Models of Clinical Disease. *Annu. Rev. Pathol. Mech. Dis.* **12**, 187–215 (2017).

82. Shultz, L. D. *et al.* Human Cancer Growth and Therapy in Immunodeficient Mouse Models. *Cold Spring Harb. Protoc.* **2014**, pdb.top073585 (2014).

83. Liu, Y. *et al.* Patient-derived xenograft models in cancer therapy: technologies and applications. *Signal Transduct. Target. Ther.* **8**, 160 (2023).

84. Blomme, A. *et al.* Murine stroma adopts a human-like metabolic phenotype in the PDX model of colorectal cancer and liver metastases. *Oncogene* **37**, 1237–1250 (2018).

85. Xia, Z. *et al.* Preclinical evaluation of cyclophosphamide and fludarabine combined with CD19 CAR-T in the treatment of B-cell hematologic malignancies *in vivo*. *Oncol. Res.* **32**, 1109–1118 (2024).

86. Lickefett, B. *et al.* Lymphodepletion – an essential but undervalued part of the chimeric antigen receptor T-cell therapy cycle. *Front. Immunol.* **14**, 1303935 (2023).

87. Puaux, A.-L. *et al.* A Comparison of Imaging Techniques to Monitor Tumor Growth and Cancer Progression in Living Animals. *Int. J. Mol. Imaging* **2011**, 1–12 (2011).

88. Vermeer, M. H., Moins-Teisserenc, H., Bagot, M., Quaglino, P. & Whittaker, S. Flow cytometry for the assessment of blood tumour burden in cutaneous T-cell lymphoma: towards a standardized approach. *Br. J. Dermatol.* **187**, 21–28 (2022).

89. Long, A. H. *et al.* Reduction of MDSCs with All-trans Retinoic Acid Improves CAR Therapy Efficacy for Sarcomas. *Cancer Immunol. Res.* **4**, 869–880 (2016).

90. King, M. A. *et al.* Human peripheral blood leucocyte non-obese diabetic-severe combined immunodeficiency interleukin-2 receptor gamma chain gene mouse model of xenogeneic graft- *versus* -host-like disease and the role of host major histocompatibility complex. *Clin. Exp. Immunol.* **157**, 104–118 (2009).

91. Libert, C., Brouckaert, P., Shaw, A. & Fiers, W. Induction of interleukin 6 by human and murine recombinant interleukin 1 in mice. *Eur. J. Immunol.* **20**, 691–694 (1990).

92. Wen, H. *et al.* Preclinical safety evaluation of chimeric antigen receptor-modified T cells against CD19 in NSG mice. *Ann. Transl. Med.* **7**, 735–735 (2019).

93. Garcia-Beltran, W. F. *et al.* Innate Immune Reconstitution in Humanized Bone Marrow-Liver-Thymus (HuBLT) Mice Governs Adaptive Cellular Immune Function and Responses to HIV-1 Infection. *Front. Immunol.* **12**, 667393 (2021).

94. Jamali, A. *et al.* Early induction of cytokine release syndrome by rapidly generated CAR T cells in preclinical models. *EMBO Mol. Med.* **16**, 784–804 (2024).

95. Rodriguez-Garcia, A. *et al.* CAR-T cell-mediated depletion of immunosuppressive tumor-associated macrophages promotes endogenous antitumor immunity and augments adoptive immunotherapy. *Nat. Commun.* **12**, 877 (2021).

96. Rosen, R. S., Yang, J. H., Peña, J. S., Schloss, R. & Yarmush, M. L. An in vitro model of the macrophage-endothelial interface to characterize CAR T-cell induced cytokine storm. *Sci. Rep.* **13**, 18835 (2023).

97. Lickefett, B. *et al.* Lymphodepletion – an essential but undervalued part of the chimeric antigen receptor T-cell therapy cycle. *Front. Immunol.* **14**, 1303935 (2023).

98. Guo, J. *et al.* Preclinical delayed toxicity studies of BCMA CAR T-cell injection in B-NDG mice with multiple myeloma. *Front. Immunol.* **15**, 1435934 (2024).

99. Dranoff, G. Experimental mouse tumour models: what can be learnt about human cancer immunology? *Nat. Rev. Immunol.* **12**, 61–66 (2012).

100. Ruella, M., Korell, F., Porazzi, P. & Maus, M. V. Mechanisms of resistance to chimeric antigen receptor-T cells in haematological malignancies. *Nat. Rev. Drug Discov.* **22**, 976–995 (2023).

101. Santiago-Rodriguez, T. M. Comparative oncology using domesticated dogs and their microbiome. *Front. Vet. Sci.* **11**, 1378551 (2024).

102. Pinho, S. S., Carvalho, S., Cabral, J., Reis, C. A. & Gärtner, F. Canine tumors: a spontaneous animal model of human carcinogenesis. *Transl. Res.* **159**, 165–172 (2012).

103. Taraseviciute, A. *et al.* Chimeric Antigen Receptor T Cell–Mediated Neurotoxicity in Nonhuman Primates. *Cancer Discov.* **8**, 750–763 (2018).

104. Vlachogiannis, G. *et al.* Patient-derived organoids model treatment response of metastatic gastrointestinal cancers. *Science* **359**, 920–926 (2018).

105. Grönholm, M. *et al.* Patient-Derived Organoids for Precision Cancer Immunotherapy. *Cancer Res.* **81**, 3149–3155 (2021).

106. Logun, M. *et al.* Patient-derived glioblastoma organoids as real-time avatars for assessing responses to clinical CAR-T cell therapy. *Cell Stem Cell* **32**, 181-190.e4 (2025).

107. Ngashangva, L. & Martin, S. Organ-on-chip for advancing CAR therapy. *Clin. Transl. Immunol.* **14**, e70024 (2025).

108. Bains, R. S. *et al.* Vascularized tumor-on-a-chip to investigate immunosuppression of CAR-T cells. *Lab. Chip* **25**, 2390–2400 (2025).

109. Ando, Y. *et al.* Evaluating CAR-T Cell Therapy in a Hypoxic 3D Tumor Model. *Adv. Healthc. Mater.* **8**, 1900001 (2019).

110. Bouquerel, C. *et al.* Precise and fast control of the dissolved oxygen level for tumor-on-chip. *Lab. Chip* **22**, 4443–4455 (2022).

111. Mohanty, R., Manoswini, M., Dhal, A. K. & Ganguly, N. In silico analysis of a novel protein in CAR T- cell therapy for the treatment of hematologic cancer through molecular modelling, docking, and dynamics approach. *Comput. Biol. Med.* **151**, 106285 (2022).

112. Lima, A. J. F. *et al.* In silico and in vivo analysis reveal impact of c-Myc tag in FMC63 scFv-CD19 protein interface and CAR-T cell efficacy. *Comput. Struct. Biotechnol. J.* **23**, 2375–2387 (2024).

113. Yan, F. *et al.* Predicting CAR-T Response in Mantle Cell Lymphoma Using Deep Neural Network Models on Single-Cell RNA Sequencing Data. *Blood* **142**, 4377–4377 (2023).

CHAPTER 2: PD-1 Restrains Interferon-Gamma Mediated Activation-Induced Cell Death that Limits T cell Engraftment and Efficacy

Michael K. Sheng,[1] Logan V. Vick,[1] Craig P. Collins,[1] Ryan N. Nielsen,[1] Wahed A. Firoz,[1] Kelly Loi,[1] Lam T. Khuat,[1†] Bruce R. Blazar,[2] Ying Xiong,[3] Zhongyu Zhu,[3] Yanping Xie,[3] Sho Yoshimoto,[4‡], Nicola J. Mason,[4] Robert J. Canter,[5] Joshua F. Meckler,[6] Joseph M. Tuscano,[6] Arta M. Monjazeb,[7] Anthony E. Zamora,[8] William J. Murphy,[1*]

1. Department of Dermatology, University of California Davis School of Medicine, Davis, Sacramento, CA, USA

2. Masonic Cancer Center, Department of Pediatrics, University of Minnesota, Minneapolis, MN, USA

3. Caring Cross, Gaithersburg, MD, USA

4. Department of Pathobiology, School of Veterinary Medicine, University of Pennsylvania, Philadelphia, PA, USA

5. Department of Surgery, University of California Davis School of Medicine, Davis, Sacramento, CA, USA

6. Department of Internal Medicine, University of California Davis School of Medicine, Davis, Sacramento, CA, USA

7. Department of Radiation Oncology, University of California Davis School of Medicine, Davis, Sacramento, CA, USA

8. Department of Medicine, Medical College of Wisconsin, Milwaukee, WI, USA

† Current affiliation: Antibody & Vaccine Group, Centre for Cancer Immunology, School of Cancer Sciences, Faculty of Medicine, Southampton General Hospital, University of Southampton, Southampton, United Kingdom.

‡ Current affiliation: Department of Veterinary Medicine, School of Veterinary Medicine, Azabu University, Sagamihara, Kanagawa 252-0206, Japan

***Corresponding Author:**

Dr. William J. Murphy, Distinguished Professor, Department of Dermatology, School of Medicine, University of California, Davis, Sacramento, CA 95817, USA,

Phone: (916) 703-9397, E-mail: wmjmurphy@health.ucdavis.edu

Abstract

Adoptive T cell therapies, including chimeric antigen receptor (CAR) T cells, are increasingly being applied for cancer and other diseases. Immune checkpoint inhibitors (ICIs), including those targeting the PD-1/PD-L1 axis, focus on enhancing T cell activation and effector functions. However, clinical combination of combined ICI and CAR T cell therapies have yielded mixed results. Activation-induced cell death (AICD) as a potential limiting factor in these responses has not been fully explored. Here, using multiple models, we show that during strong T cell receptor (TCR) or chimeric antigen receptor (CAR) stimulation, PD-1 signaling protects both conventional and CAR T cells from AICD. This occurs in part by suppressing interferon-gamma (IFN-γ) production and downstream CD95 expression. Using murine, canine, and human T and CAR T cell models, we demonstrate that genetic deletion, signal modulation, or antibody blockade of PD-1 augments early T cell activation and increases IFN-γ production but is followed by increased apoptosis and decreased persistence. Deletion of the IFN-γ receptor in T and CAR T cells reduced AICD, improving engraftment and anti-tumor efficacy. These findings identify a dual role for PD-1 in restraining T cell activation while also preserving survival, with clinical implications for optimizing checkpoint blockade in immunotherapy.

Introduction

T cell checkpoint molecules such as PD-1, upon engagement with its ligands PD-L1 and PD-L2, inhibit T cell activation, leading to impaired cytokine production, proliferation, and effector function[1,2]. Physiologically, these inhibitory receptors are essential for maintaining immune homeostasis by preventing self-antigen recognition, limiting overactivation, and sustaining memory T cell responses following strong or continuous stimulation – such as during acute and chronic viral infections, particularly in aged individuals[3–5]. In chronic disease settings, such as some viral infections and cancers, PD-1 expression remains elevated and is associated with an “exhausted” phenotype characterized by reduced proliferative capabilities and cytokine production[6,7]. Immune checkpoint inhibitor (ICI) approaches targeting the PD-1/PD-L1 axis have been shown to reinvigorate precursor exhausted T cells (T_{pex}) and lower activation thresholds, thereby expanding tumor-specific T cell responses and leading to significantly improved anti-tumor responses against multiple cancer types[8–10].

Activation-induced cell death (AICD) is another essential mechanism for maintaining immune balance where apoptosis is triggered by heightened or prolonged activation[11]. AICD has been observed across various cell types, including lymphocytes[12,13]. In T cells, AICD plays a critical role in limiting excess immune responses by ensuring clonal contraction after antigen clearance and by maintaining peripheral tolerance by eliminating self-reactive cells[12–14]. It is primarily mediated through the upregulation of the death receptor CD95 (Fas) and its ligand CD95L (FasL), both of which are induced on T cells upon activation[15,16]. CD95-CD95L interactions recruit the death-inducing signaling complex (DISC), initiating a caspase cascade that

ultimately results in apoptosis[17]. Interestingly, AICD has been linked to interferon-gamma (IFN-γ) production, which can enhance CD95 expression and sensitize cells to apoptosis[18,19]. ICIs, by rejuvenating and augmenting T cell responses, increase IFN-γ secretion[20–22]. However, while most studies focus on their effects in boosting T cell activation and effector function, little attention has been given to how these therapies may impact AICD and affect long-term persistence of antigen-specific T cells. This is particularly relevant under conditions of strong and/or continuous T cell stimulation, such as during cancer and/or adoptive cell therapies. Notably, lymphopenia following ICI administration has been reported in several clinical trials, raising the possibility that AICD may limit the sustained durability of ICI-augmented T cell responses[23,24].

The success of genetically engineered chimeric antigen receptor (CAR) T cells in certain cancers has generated interest in applying ICIs to further enhance their therapeutic efficacy. However, clinical applications of combined ICI and CAR T cell therapy have surprisingly yielded equivocal or negative results[25–27]. Additionally, several studies have demonstrated that disruption of PD-1 signaling in activated CAR T cells decreases proliferation and compromises long-term persistence[28,29]. To investigate the underlying biology, we examined the impact of PD-1 signal inhibition on T and CAR T cell function using mouse, canine, and human T or CAR T cells. We report that across all systems, PD-1 abrogation via either genetic ablation, signal modulation, or antibody blockade, initially enhanced T and CAR T cell activation, but was subsequently followed by increased AICD and impaired T cell persistence. Using PD-1$^{-/-}$ mouse T cells, a PD-1/CD28 chimeric switch receptor in canine CAR T cells, and PD-1 antibody blockade with mouse T, human T, and human CAR T cells, we observed that increased T cell

activation was consistently followed by greater T and CAR T cell loss compared to controls. ICI noticeably increased IFN-γ production, which correlated with increased AICD. Abrogation of IFN-γ signaling through the removal of IFNGR expression resulted in improved T cell persistence and greater anti-tumor efficacy. These results demonstrate that the PD-1/PD-L1 pathway plays a significant role in T cell maintenance during strong activation, including CAR signaling, by inhibiting IFN-γ production and subsequent CD95 upregulation, thereby preventing AICD. Furthermore, impairing IFN-γ signaling via IFNGR knockout attenuates AICD, resulting in greater T and CAR T cell engraftment and efficacy, representing a promising strategy for improving the effectiveness and therapeutic durability of CAR T cells.

Methods

Tumor Cell Lines and Culture

The wild-type (WT) human Burkitt's lymphoma cell line, Raji (RRID: CVCL_0511), was generously gifted by Caring Cross. The human PD-L1-expressing Raji cell line (Raji/hPD-L1) was purchased from InvivoGen (InvivoGen, Cat. #raji-hpdl1). Luciferase-expressing Raji/hPD-L1 cells (Raji/hPD-L1/ffLuc) were generated by infecting Raji/hPD-L1 cells with GFP and firefly luciferase-expressing virus provided by Caring Cross in the presence of 5 µg/mL polybrene (Millipore, Cat. #TR-1003-G). Subsequently, GFP+ cells were flow sorted and expanded. Raji and Raji/hPD-L1 cells expressing Incucyte Nuclight Green were generated by transducing parental lines with lentivirus encoding for Incucyte Nuclight Green at an MOI of 3 in the presence of 5 µg/mL polybrene. The transduced cells were selected for Nuclight Green expression in media containing 1 µg/mL puromycin (Gibco, Cat. #: A1113803). The K562 cell line (RRID: CVCL_0004) expressing canine CD20, canine PD-L1, GFP, and firefly luciferase (K562/cCD20/cPD-L1/GFP-ffLuc) was generated and provided by the laboratory of Dr. Nicola Mason (University of Pennsylvania School of Veterinary Medicine). Both cell lines were cultured in RF10C media and passaged twice a week to maintain high cell viability (>90%). RF10C media is made of: 90% RPMI 1640 without glutamine (Gibco, Cat. #: 21870084), 10% Nu-Serum (Corning, Cat. #: 355100), 2 mM L-glutamine (Gibco, Cat. #: 25030081), 1x MEM non-essential amino acids (Gibco, Cat. #: 11140050), 1 mM sodium pyruvate (Gibco, Cat. #: 11360070), 1% penicillin/streptomycin (Gibco, Cat. #: 15140122), 1 mM HEPES (Gibco, Cat. #: 15630080). All tumor cell lines were tested to

ensure there was no mycoplasma every 3 months using a MycoStrip kit (InvivoGen, Cat. #: rep-mysnc-100) and evaluated for antigen expression prior to use.

Mice

Wild-type (WT) female C57BL/6J mice (Jackson Laboratory, RRID: IMSR_JAX:000664) and IFNGR1 knockout (IFNGR$^{-/-}$) female mice (Jackson Laboratory, RRID: IMSR_JAX:003288) were purchased from the Jackson Laboratory. PD-1 knockout (PD-1$^{-/-}$) C57BL/6J mice were generously provided by Dr. Bruce Blazar (University of Minnesota Medical School). Male and female NOD.Cg-*Prkdc*^{scid} *Il2rg*^{tm1Wjl}/SzJ (NSG) mice (Jackson Laboratory, RRID: IMSR_JAX:005557) were also purchased from the Jackson Laboratory. Mice were housed in groups of four per cage under specific pathogen-free (SPF) conditions at the University of California, Davis (UC Davis) Institute for Regenerative Cures, an AAALAC-accredited animal facility. Animals were maintained on a 12-hour light/dark cycle with ad libitum access to food (NIH-31 chow) and water. All animal procedures were approved by the UC Davis Institutional Animal Care and Use Committee (IACUC) protocols 20395, 20680, 20707, 22739, and carried out in accordance with institutional guidelines, ethical regulations, and humane endpoints. Group sizes were selected based on previous studies and the principal investigator's guidance.

Mouse Splenocyte In Vitro Studies

Splenocytes harvested from WT, IFNGR$^{-/-}$, PD-1$^{-/-}$ C57BL/6J mice were processed into single-cell suspensions in D-PBS (Gibco, Cat. #: 14190136) + 2% FBS and filtered

through a Falcon 70 µm cell strainer (Corning, Cat. #352350). Afterwards, splenocytes were treated for 5 minutes with 1x RBC lysis buffer (BioLegend, Cat. #: 420302) and washed once with D-PBS and 2% FBS. They were then counted using a Z1 Coulter Particle Counter (Beckman Coulter). They were then resuspended to a concentration of 0.75x10^6 – 1.0x10^6 cells/mL in RF10C media. 200 µL of the single cell suspensions were plated in 96-well round bottom plates (~1.5x10^5 to 2.0x10^5 cells per well) and activated with 0.625 µg/mL concanavalin A (conA). In studies involving the addition of mouse IFNγ, 100 ng/mL of mouse IFNγ (Miltenyi, Cat. #: 130-105-785) were concurrently added to select wells with conA. After 72 hours of activation, splenocytes were counted using a hemocytometer and trypan blue exclusion. Cells were incubated with Near-IR (780) viability dye (Invitrogen, Cat. #: L34976), Fc blocked with a 1:20 of TruStain FcX anti-mouse CD16/32 (BioLegend, Cat. #: 101320), surface stained (APC anti-mouse CD45 [BioLegend, Cat. # 103112], BV785 anti-mouse CD3 [BioLegend, Cat. #: 100231], BV711 anti-mouse CD4 [BioLegend, Cat. #: 100549], BV605 anti-mouse CD8 [BioLegend, Cat. #: 100743], PerCP/Cyanine5.5 anti-mouse CD25 [BioLegend, Cat. #: 101912], FITC anti-mouse CD69 [Cat. #: 104506], PE anti-mouse PD-1 [BioLegend, Cat. #: 135206]), intracellular stained as applicable (APC/Cyanine7 anti-mouse IFN-γ [BioLegend, Cat. #: 505850]), incubated with fluorescently labeled annexin V as applicable (Pacific Blue annexin V [BioLegend, Cat. #: 640918] or PE/Dazzle 594 annexin V [BioLegend, Cat. #: 640956]) and analyzed by flow cytometry.

Mouse Splenocyte In Vivo Allogeneic Adoptive Transfer Studies

WT and PD-1$^{-/-}$ bone marrow chimeras were generated by adoptive transfer of 2.5x10^7 bone marrow cells isolated from C57BL/6J WT or PD-1$^{-/-}$ mice into lethally irradiated C57BL/6J WT recipient mice. Recipients were subjected to a split-dose total body irradiation regimen (2 × 650 cGy) prior to transplantation. Allogeneic adoptive transfer experiments were performed using a C57BL/6J (H-2^{b}) into NSG (H-2^{g7}) model. NSG recipients received a sublethal total body irradiation (TBI) conditioning regimen of 200–300 cGy prior to intravenous injection (i.v.) of donor cells. Donor cells were harvested from the spleens and lymph nodes of C57BL/6J mice, mechanically processed into single-cell suspensions. 10x10^6 donor cells were transferred intravenously into preconditioned recipients. PD-1 blockade was performed using an anti-mouse PD-1 monoclonal antibody (clone 29F.1A12, BioXCell, Cat. # BE0273). A loading dose of 500 µg was administered on day 1, followed by maintenance doses of 250 µg twice weekly (e.g. days 4, 7, 11, 14, etc.). At indicated time points, spleens were removed and mechanically processed into single-cell suspensions in D-PBS + 2% FBS, filtered through a Falcon 70 µm cell strainer, treated with 5 mL of 1x RBC lysis buffer, washed once in D-PBS + 2% FBS, and counted using a Z1 Coulter Particle Counter (Beckman Coulter). Cells were incubated with either eFluor 780 viability dye (Invitrogen, Cat. #: 65-0865-14 or Zombie NIR viability dye (BioLegend, Cat. #: 640956), Fc blocked with a 1:20 of TruStain FcX anti-mouse CD16/32, surface stained (APC/Fire 810 anti-mouse CD45 [BioLegend, Cat. #: 103174], BUV563 anti-mouse CD3 [BD Biosciences, Cat. #: 741319], BUV395 anti-mouse CD4 [BD Biosciences, Cat. #: 563790], BUV496 anti-mouse CD8a [BD Biosciences, Cat. #: 750024], R718 anti-mouse CD11b [BD

Biosciences, Cat. #: 567469], PE/Fire 700 anti-mouse CD11c [BioLegend, Cat. #: 161108], BUV615 anti-mouse CD19 [BD Biosciences, Cat. #: 751213], PE/Dazzle 594 anti-mouse CD25 [BioLegend, Cat. #: 101920], BV650 anti-mouse CD69 [BioLegend, Cat. #: 104541], RB744 anti-mouse LAG3 [BD Biosciences, Cat. #: 756907], APC anti-mouse TIGIT [BioLegend, Cat. #: 142106], PE anti-mouse TIM3 [BioLegend, Cat. #: 119704]), intracellular stained as applicable (BV421 anti-mouse Ki67 [BioLegend, Cat. #: 151208]), incubated with fluorescently labeled annexin V as applicable (Pacific Blue annexin V [BioLegend, Cat. #: 640918]) and analyzed by flow cytometry. Cytokine analysis was performed using cytokine bead array (CBA) kits to detect IFN-γ (BD, Cat. #: 558296) and TNF (BD, Cat. #: 558299). Adoptive transfer experiments using PD-1$^{-/-}$ donor cells were conducted under similar conditions. Recipients were conditioned with 200–300 cGy TBI prior to receiving 8 - 10x10^6 WT or PD-1$^{-/-}$ via intravenous injection. At indicated time points, blood and spleen were obtained for immune analysis. Blood was treated twice with 1x RBC lysis buffer, and spleens were processed into single-cell suspensions, filtered through a Falcon 70 μm cell strainer and counted using a Z1 Coulter Particle Counter. Cells were incubated with eFluor 780 viability dye or Zombie NIR viability dye, Fc blocked with a 1:20 of TruStain FcX anti-mouse CD16/32, surface stained (BUV395 anti-mouse CD45 [BD Biosciences, Cat. #: 564279], BUV496 anti-mouse CD3 [BD Biosciences, Cat. #: 741117], BV711 anti-mouse CD4 [BioLegend, Cat. #: 100549], BV605 anti-mouse CD8 [BioLegend, Cat. #: 100743], PerCP/Cyanine5.5 anti-mouse CD25 [BioLegend, Cat. #: 101912], FITC anti-mouse CD69 [Cat. #: 104506] or FITC anti-mouse CD95 [BioLegend, Cat. #: 152606], PerCP-eFluor710 anti-mouse LAG3 [Invitrogen, Cat. #: 46-2239-42], APC anti-mouse TIGIT

[BioLegend, Cat. #: 142106], PE anti-mouse TIM3 [BioLegend, Cat. #: 119704]) incubated with fluorescently labeled annexin V as applicable (Pacific Blue annexin V [BioLegend, Cat. #: 640918]) and analyzed by flow cytometry. ~2.0x10^6 to 5.0x10^6 splenocytes from day 21 were flash frozen and stored at -80°C for qPCR.

Canine PBMC/T cell Isolation

Whole blood was obtained from canine donors from the laboratory of Dr. Robert Rebhun (UC Davis School of Veterinary Medicine) and diluted 1:1 with D-PBS containing 2% FBS. The resulting diluted blood was placed into 50 mL SepMate PBMC isolation tubes (STEMCELL Technologies, Cat. #: 85450) pre-filled with 15 mL of lymphocyte separation media (Corning, Cat. #: 25-072-CV) and centrifuged at 1200 x g for 10 minutes at room temperature with the brake on. The top layer containing the enriched PBMCs was poured into a new 50 mL conical tube and washed once with D-PBS containing 2% FBS. Afterwards, to remove residual red blood cells the purified canine PBMCs were treated with 1x RBC lysis buffer for 5 minutes and washed once with D-PBS and 2% FBS. Canine T cells were isolated as described previously[32].

Canine CAR T cell Generation, Expansion and Validation

Lentiviral vectors encoding a chimeric antigen receptor (CARs) targeting canine CD20, with or without a canine PD-1-CD28 chimeric switch receptor (CSR), as well as canine T cell anti-CD3/anti-CD28 activation beads, were generously provided by the laboratory of Dr. Nicola Mason (University of Pennsylvania School of Veterinary Medicine). Isolated canine T cells were activated, transduced, and validated for CAR transduction

efficiency using previously described methods with lentiviral transduction performed at a multiplicity of infection (MOI) of 10[32]. CSR transduction efficiency was validated using human PD-1 biotinylated antibody (R&D, Cat. #: BAF1086) combined with BV605 streptavidin (BioLegend, Cat. #: 405229). After transduction, canine CAR T cells were cultured and expanded in RF10C media containing 100 IU/mL recombinant human interleukin-2 (rhIL-2, TECIN Teceleukin, Bulk Ro 23-6019, provided by National Cancer Institute). Every 2 days, cells were counted and resuspended to a concentration of 0.5x10^6 in RF10C media until use.

Canine CAR T cell In Vitro Studies

Canine wild-type (WT) cCD20 or cCD20 + PD-1 chimeric switch receptor (CSR) CAR T cells were incubated with irradiated (10,000 cGy) K562/cCD20/cPD-L1/GFP-ffLuc cells at a 1:1 effector:target (E:T) ratio for 72 hours in 3 consecutive stimulations. After the third stimulation, supernatants were collected and ELISA (R&D Systems, Cat. #: CAIF00) was used to quantify the levels of canine IFN-γ produced.

Canine CAR T cell Treatment of Tumor-Bearing Mice

NSG mice were i.v. injected with 2.0x10^7 K562/cCD20/cPD-L1/GFP-ffLuc cells on day 0. On day 10, mice were treated with 3.0x10^6 WT cCD20 or cCD20 + CSR CAR T cells. On indicated time points, spleens and bone marrow were harvested. Spleens and bone marrow were mechanically processed into single-cell suspensions in D-PBS + 2% FBS, filtered through a Falcon 70 μm cell strainer, treated with 5 mL of 1x RBC lysis buffer, washed once in D-PBS + 2% FBS, and counted using a Z1 Coulter Particle

Counter. Cells were then incubated with Zombie NIR viability dye, Fc blocked with a 1:20 of TruStain FcX anti-mouse CD16/32 a, surface stained (APC anti-mouse CD45 [BioLegend, Cat. #: 103112], PE-Cyanine7 anti-canine CD4 [Invitrogen, Cat. #: 25-5040-42], eFluor 450 anti-canine CD8a [Invitrogen, Cat. #: 48-5080-42], PE anti-canine CD25 [Invitrogen, Cat. #: 12-0250-42] and analyzed with flow cytometry. Tumor burden in mice was assessed at indicated timepoints by i.p. injection of 4.5 mg D-luciferin (Revvity, Catalog #: 122799) followed by bioluminescent imaging using the IVIS Lumina III system (PerkinElmer, Cat. #: CLS136334).

Human PBMC/T cell Isolation

Leukocyte reduction chambers containing blood from healthy human donors were procured from (Vitalant) and diluted 1:1 with D-PBS containing 2% FBS. The diluted blood was placed into 50 mL SepMate PBMC isolation tubes pre-filled with 15 mL of lymphocyte separation media and centrifuged at 1200 x g for 10 minutes at room temperature with the brake on. The top layer containing the enriched PBMCs was poured into a new 50 mL conical tube and washed once with D-PBS containing 2% FBS. Afterwards, to remove residual red blood cells the purified human PBMCs were treated with 1x RBC lysis buffer for 5 minutes and washed once with D-PBS and 2% FBS. T cells were subsequently isolated from the enriched PBMCs using a MagniSort human T cell enrichment kit (Invitrogen, Catalog #: 8804-6810-74) and cryopreserved in 90% FBS and 10% DMSO at -80°C for 24 to 72 hours. Isolated T cells were stored in liquid nitrogen for long-term storage until used for CAR T cell generation.

Human PBMC In Vivo Xenogeneic Adoptive Transfer Studies

Xenogeneic adoptive transfer experiments were performed using human PBMCs into an NSG model as previously described[34]. 10.0x10^6 human PBMCs were injected i.v. into NSG recipients on day 0. On days 0, 3, 7, 11 and 14, select mice also received either human IgG isotype control (Invitrogen, Cat. #: 31154) or 500 µg of anti-human PD-1 (pembrolizumab) injected i.p. On indicated timepoints, blood was collected or and/or spleens were harvested. Blood was treated twice with 1x RBC lysis buffer, and spleens were processed into single-cell suspensions in D-PBS + 2% FBS, filtered through a Falcon 70 µm cell strainer, treated once with 1x RBC lysis buffer, and counted using a Z1 Coulter Particle Counter. Cells from spleens and bone marrow were incubated with live/dead aqua viability dye (Invitrogen, Cat #: L34957), Fc blocked with a 1:20 dilution of human TruStain FcX and a 1:20 dilution of TruStain FcX anti-mouse CD16/32, surface stained (BV785 anti-human CD3 [BioLegend, Cat. #: 317330], BV711 anti-human CD4 [BioLegend, Cat. #: 317440], FITC anti-human CD8 [BioLegend, Cat. #: BioLegend, Cat. #: 344704], Alexa647 anti-HLA-DR [BioLegend, Cat. #: 307622], PE anti-human PD-1 [BioLegend, Cat. #: 329906]) and analyzed by flow cytometry. Clinical assessment of acute GVHD was conducted according to previously described methods[50].

Human CAR T cell Generation, Expansion and Validation

Isolated T cells were thawed from liquid nitrogen on day 0 and resuspended in pre-warmed TexMACS GMP medium (Miltenyi Biotec, Cat. #: 170-076-307) and counted. To activate, they were resuspended to a concentration of 1x10^6 cells/mL in TexMACS

containing 200 IU/mL rhIL2 and a 1:20 dilution of MACS GMP T cell TransAct (Miltenyi Biotec, Cat. #: 200-076-204). 1 day post-activation, T cells were transduced with lentivirus encoding a tri-specific CAR recognizing hCD19/hCD20/hCD22 (provided by Caring Cross) at an MOI of 40. On day 3, T cells were collected, centrifuged at 1200 RPM for 5 minutes, and the media decanted. The T cells were then resuspended in pre-warmed TexMACS medium, counted, and subsequently resuspended to a concentration of 0.25x10^6 cells/mL in TexMACS containing 200 IU/mL rhIL2. On days 6, 8, and 10, the T cells were counted and resuspended to a concentration of 0.5x10^6 cells/mL in TexMACS containing 200 IU/mL rhIL2. CAR T cells were validated by primary staining with recombinant human CD19 Fc chimera protein (R&D Systems, Cat. #: 9269-CD-050) and human siglec-2 (CD22) His-tag recombinant protein (Invitrogen, Cat. #: A42609) followed by secondary staining with Alexa Fluor 647 goat anti-human Fc (Jackson ImmunoResearch, Cat. #: 109-606-098) and PE His antibody (Miltenyi, Cat. #: 130-120-718) and analysis by flow cytometry. CAR T cells were used for experiments between days 10 and 12.

Human CAR T cell CRISPR KO and Validation

On day 3 post-T cell activation (as described above), human CAR T cells were collected and resuspended to a concentration of 20x10^6 cells/mL in Buffer R (Thermo Fisher, Cat. #: MPK10096B). CRISPR-Cas9 ribonucleoprotein (RNP) mixtures were prepared per 2.0x10^6 human CAR T cells by incubating 100 pmol of IFNGR1 gRNA (Thermo Fisher, Cat. #: CRISPR748746_SGM) with 12.5 µg of TrueCut Cas9 Protein v2 (Thermo Fisher, Cat. #: A36498) and 50 µL of Buffer R for 20 minutes at room temperature.

Afterwards, 50 µL of each RNP mixture was added to 100 µL of CAR T cells, collected in a 100 µL Neon transfection system pipette and electroporated using a Neon Electroporation System set to the conditions 1600 V/10 ms/3 pulses. After electroporation, the cells were added back to pre-warmed TexMACS medium containing 200 IU/mL rhIL2 and cultured as described above. To validate knockout efficiency, WT and IFNGR1 KO CAR T cells were stained with PE anti-human CD119 (IFN-γ R α chain) antibody (BioLegend, Cat. #: 308704) or PE mouse IgG2b, κ isotype ctrl antibody (BioLegend, Cat. #: 400314) and analyzed with flow cytometry.

Human CAR T In Vitro Studies

In a 96-well round bottom plate, CAR T cells were co-cultured with irradiated (10,000 cGy) Raji WT or Raji/hPD-L1 cells for 72 hours with and without the addition of 20 µg/mL of pembrolizumab at a 1:1 E:T ratio (1.0x10^5 cells of both) in TexMACS GMP medium. Afterwards, supernatants were collected and IFN-γ and IL-2 levels were measured by ELISA (Invitrogen, Cat. #: 88-7316-22; Invitrogen, Cat. #: 88-7025-22). Cells were then incubated with Zombie NIR viability dye, Fc blocked with a 1:20 dilution of human TruStain FcX (BioLegend, Cat. #: 422302), surface stained (anti-human CD22-His + PE anti-His, BV711 anti-human CD3 [BD Biosciences, Cat. #: 563725], BV785 anti-human CD4 [BioLegend, Cat. #: 317442], BUV737 anti-human CD8 [BD Biosciences, Cat. #: 749367], BV421 anti-human CD25 [BioLegend, Cat. #: 302630], BV605 anti-human CD69 [BioLegend, Cat. #: 310938], BV650 anti-human CD95 [BioLegend, Cat. #: 305642], BV510 anti-HLA-DR [BioLegend, Cat. #: 307646]), intracellular stained when applicable (PE/Cyanine7 anti-human Granzyme B

[BioLegend, Cat. #: 372214], PE/Dazzle 594 anti-human Ki67 [BioLegend, Cat. #: 350534], BV605 anti-human CD107a [BioLegend, Cat. #: 328634], APC anti-human IL2 [eBioscience, Cat. #: 17-7029-82], BV421 anti-human IFN-γ [BioLegend, Cat. #: 506538]), incubated with PE-Dazzle 594 annexin V when applicable (BioLegend, Cat. #: 640956) and analyzed by flow cytometry. CAR T cytotoxicity studies were done by plating CAR T cells with either target Raji WT/Nuclight Green or Raji/hPD-L1/Nuclight Green cells at different E:T ratios in a 96-well flat bottom plate. The plate was placed in an Incucyte Live-Cell Analysis System (Sartorius) for 72 hours and analyzed using Incucyte analysis software (Sartorius). For IFN-γ studies, CAR T cells were co-cultured with 100 ng/mL rhIFN-γ for 24 hours in TexMACS. For restimulation experiments with TransAct, a 1:20 dilution TransAct for 3 days is used followed by restimulation, cell counts by trypan blue exclusion, and/or flow cytometry. For flow cytometry, cells were incubated with Zombie NIR viability dye, surface stained (anti-human CD22-His + PE anti-His, BV711 anti-human CD3 [BD Biosciences, Cat. #: 563725], BV785 anti-human CD4 [BioLegend, Cat. #: 317442], BUV737 anti-human CD8 [BD Biosciences, Cat. #: 749367], BV650 anti-human CD95 [BioLegend, Cat. #: 305642]) and incubated with PE-Dazzle 594 annexin V and analyzed by flow cytometry.

Human CAR T cell Treatment of Tumor-Bearing Mice

NSG mice were injected i.v. with 1x10^6 Raji/hPD-1/ffLuc cells on day 0 and 5x10^6 CAR T cells on day 9. On day 9, select mice also received 500 µg of anti-human PD-1 (pembrolizumab) injected i.p. with subsequent doses of 250 µg on days 13 and 17. On indicated timepoints, blood, spleens, and bone marrow were harvested. Blood was

collected in Microtainer Collection Tubes (BD Biosciences, Cat. #: 365967) and spun at 8000 x g for 10 minutes to acquire serum; serum was frozen at -80°C until used. Spleens and bone marrow were mechanically processed into single-cell suspensions in D-PBS + 2% FBS, filtered through a Falcon 70 µm cell strainer, treated with 5 mL of 1x RBC lysis buffer, washed once in D-PBS + 2% FBS, and counted using a Z1 Coulter Particle Counter. ~2.0x10^6 to 5.0x10^6 spleen cells were flash frozen and stored at -80°C for qPCR. For RNA-seq, human CD3+ cells were sorted from splenocytes stained with FITC anti-human CD3 (BioLegend, Cat. #: 300406) on a FACSAria II (BD), flash frozen and stored at -80°C until used. Cells from spleens and bone marrow were incubated with Zombie NIR viability dye, Fc blocked with a 1:20 dilution of human TruStain FcX and a 1:20 dilution of TruStain FcX anti-mouse CD16/32, surface stained (anti-human CD22-His + PE anti-His, BV711 anti-human CD3 [BD Biosciences, Cat. #: 563725], BV785 anti-human CD4 [BioLegend, Cat. #: 317442], BUV737 anti-human CD8 [BD Biosciences, Cat. #: 749367], BV421 anti-human CD25 [BioLegend, Cat. #: 302630], BV605 anti-human CD69 [BioLegend, Cat. #: 310938] or BV605 anti-human LAG3 [BioLegend, Cat. #: 369323], BV650 anti-human CD95 [BioLegend, Cat. #: 305642], BV510 anti-HLA-DR [BioLegend, Cat. #: 307646], BUV395 anti-human TIGIT [BD Biosciences, Cat. #: 747845], BV421 anti-human TIM3 [BioLegend, Cat. #: 345007]), intracellular stained when applicable (PE/Cyanine7 anti-human Granzyme B [BioLegend, Cat. #: 372214], PE/Dazzle 594 anti-human Ki67 [BioLegend, Cat. #: 350534]), incubated with PE-Dazzle 594 annexin V when applicable (BioLegend, Cat. #: 640956) and analyzed by flow cytometry. Serum human IFN-γ, IL-2, and TNF levels were measured in serum samples using cytometric bead array (CBA) kits purchased

from BD Biosciences (BD Biosciences, Cat. #: 558269, 558270, 558273). Tumor burden in mice was assessed at indicated timepoints by i.p. injection of 4.5 mg D-luciferin on indicated timepoints followed by bioluminescent imaging using the IVIS Lumina III system.

Bulk RNA-seq

Snap-frozen, sorted $CD3^+$ T cells were isolated from spleens of tumor-bearing mice treated with CAR T cells, with or without pembrolizumab, and submitted to Novogene for bulk RNA-seq. Total RNA (1 μg per sample) was used for library preparation using the NEBNext Ultra RNA Library Prep Kit for Illumina (NEB, Cat. #: E7770), following the manufacturer's protocol. mRNA was enriched with poly-T magnetic beads and fragmented using divalent cations. First-strand cDNA synthesis was performed using random hexamer primers and M-MuLV Reverse Transcriptase, followed by second-strand synthesis with DNA Polymerase I and RNase H. Libraries were end-repaired, adenylated, ligated with NEBNext adaptors, and size-selected (150–200 bp) using AMPure XP beads (Beckman Coulter). USER enzyme (NEB, Cat. #: M5505L) treatment and PCR amplification were followed by purification and quality assessment via Agilent Bioanalyzer 2100. FASTQ reads were trimmed and quality-filtered using *fastp*, and metrics including Q20, Q30, and GC content were calculated. High-quality paired-end reads were aligned to the reference genome using Spliced Transcripts Alignment to a Reference (STAR) software with default parameters. Genome and annotation files were sourced from NCBI (RRID: SCR_006472), UCSC (RRID: SCR_005780), or Ensembl (RRID: SCR_002344). Downstream analysis was performed using the aligned datasets.

Differential expression analysis between the samples and groups was performed using the DESeq2 (RRID: SCR_000154) R package. P values were also adjusted using the Benjamini–Hochberg method. Genes with an adjusted P value < 0.005 were considered significantly differentially expressed.

qPCR

RNA from flash frozen samples was extracted using a RNeasy Plus Mini Kit (Qiagen, Catalog #: 74136) with cDNA made using iScript RT Supermix (BioRad, Catalog #: 1708840). qPCR was run using SsoAdvanced Universal SYBR Green Supermix (BioRad, Catalog #: 1725270) with primers directed against indicated genes using a BioRad CFX384 system.

Trypan Blue Exclusion

Throughout the experiments, total splenocyte and bone marrow numbers were determined using a Z1 Coulter Particle Counter (Beckman Coulter). For cell counting during *in vitro* experiments, trypan blue exclusion was performed using a 1:1 dilution of cells-to-trypan blue (Gibco, Cat. #: 15250061) and recording total and live cell numbers using a BioRad TC20 automated cell counter (BioRad, Cat. #: 1450102).

Flow Cytometry

For intracellular cytokine or CD107a staining, cells were incubated for 5 hours prior with a 1:1000 dilution of GolgiPlug (BD, Cat. #: 555029) and a 1:1500 dilution of GolgiStop (BD, Cat. #: 554724) prior to surface staining. Viability dye was prepared in D-PBS; all

cells were incubated at room temperature during viability dye staining. Surface antibody dilutions were prepared and washing was performed in staining buffer consisting of D-PBS (Gibco, Cat. #14190-136) and 2% fetal bovine serum (FBS) (Gibco, Cat. #A5256701). Cells were incubated with surface antibodies on ice for 30 minutes per staining step and washed once in staining buffer between each step. For intracellular staining, cells were fixed and permeabilized using Cytofix/Cytoperm solution (BD Biosciences, Cat. #554722) for 1 hour at 4°C and washed once with BD Perm/Wash buffer (BD Biosciences, Cat. #554723). Intracellular antibody dilutions were prepared in BD Perm/Wash buffer and cells were incubated in them for 30 minutes at room temperature. Afterwards, cells were washed one time in BD Perm/Wash buffer. For annexin V staining, cells were incubated in annexin V binding buffer (BioLegend, Cat. #422201) containing fluorescently labeled annexin V. Samples were run on a BD LSRFortessa Cell Analyzer or a Sony ID7000 Spectral Cell Analyzer, and data was analyzed using FlowJo software (RRID: SCR_008520).

Statistical Analysis

Statistical analyses for all *in vitro* and *in vivo* experiments were performed using GraphPad Prism 9 (RRID: SCR_002798). Bulk RNA-seq data were analyzed in RStudio (RRID: SCR_000432).

Data Availability

The raw experimental data supporting the findings of this study are available from the corresponding author upon reasonable request. Bulk RNA-seq data have been

deposited in the NCBI Sequence Read Archive (SRA) under the project ID: PRJNA1282222 and BioSample accessions: SAMN49644584, SAMN49644585, SAMN49644586, SAMN49644587, SAMN49644588, SAMN49644589.

Results

PD-1 signal ablation in activated mouse T cells leads to increased AICD in vitro

We first assessed the role of PD-1 signaling on T cell activation through mitogen stimulation of mouse splenocytes from wild-type (WT) and PD-1$^{-/-}$ T cells *in vitro*. Following activation, WT T cells upregulated PD-1 in contrast to PD-1$^{-/-}$ T cells (Supplementary Fig. 1a). Stimulated PD-1$^{-/-}$ T cells displayed increased activation compared to their WT counterparts seen by upregulation of T cell activation markers CD25 and CD69 (Fig. 1a-b). Higher IFN-γ and TNF production was also present in the PD-1$^{-/-}$ T cells (Fig. 1c, Supplementary Fig. 1b-c). Interestingly, with increased activation, we observed significantly fewer live PD-1$^{-/-}$ T cells compared to WT controls (Fig. 1d, Supplementary Fig. 1d-e). This reduction in live PD-1$^{-/-}$ T cells correlated with increased binding of annexin V consistent with increased apoptosis (Fig. 1e).

AICD on activated T cells is affected by IFNGR signaling

IFN-γ has been associated with inducing AICD on T cells[19]. Accordingly, we observed that mitogen-activated IFNGR$^{-/-}$ mouse splenocytes displayed increased cellularity and live T cell numbers along with decreased apoptosis indicating reduced AICD (Fig. 1g-h, Supplementary Fig. 1f). Concurrently, this was associated with reduced expression of CD95 (FasR), a key receptor mediating apoptosis (Fig. 1h). Despite similar baseline percentages of CD4+ and CD8+ T cells with WT T cells, activated IFNGR$^{-/-}$ T cells had a significantly higher proportion of CD4+ T cells (Fig. 1i, Supplementary Fig. 1g). This aligns with previous reports showing that CD4+ T cells are more susceptible to IFN-γ-mediated AICD compared to CD8+ T cells[30,31]. To validate the pro-apoptotic role of IFN-

γ, IFN-γ was added to WT T cells during activation where it increased annexin V binding (Fig. 1j). Together, our results indicate that while PD-1 signal ablation enhances T cell activation, it concurrently increases T cell apoptosis and subsequent cell death mediated possibly in part by increased IFN-γ production and signaling, with the greatest effects on CD4+ T cells.

In vivo PD-1 ablation or blockade enhances early T cell activation but impairs long-term persistence

Building upon our *in vitro* findings that PD-1 loss enhances T cell activation but increases apoptosis, we evaluated this phenomenon *in vivo*. WT or PD-1$^{-/-}$ C57BL/6J splenocytes were adoptively transferred into sub-lethally irradiated NSG mice (Fig. 2a). The MHC mismatch between C57BL/6J donors (H-2^{b}) and NSG hosts (H-2^{g7}) drives robust T cell activation and expansion. At 7 days post-transfer, peripheral blood analysis revealed a higher frequency of circulating PD-1$^{-/-}$ donor T cells compared to WT controls along with elevated CD69 expression indicative of greater activation (Fig. 2b, Supplementary Fig. 2a). However, by day 21, the frequency of PD-1$^{-/-}$ T cells was significantly reduced in both blood and spleen (Fig. 2c, Supplementary Fig. 2b,). qPCR confirmed PD-1 deficiency in the donor PD-1$^{-/-}$ cells in the spleen (Supplementary Fig. 2c). Flow cytometry analysis showed that PD-1$^{-/-}$ T cells exhibited greater annexin V binding and increased CD95 expression – both by frequency and mean fluorescence intensity (MFI) – consistent with increased apoptosis and our *in vitro* data (Fig. 2d-f). To confirm these effects were not due to germline PD-1 knockout, we transferred WT T cells and treated recipient mice with an anti-mouse PD-1 blocking antibody (anti-mPD-

1) (Fig. 2g). Similarly, on day 7, anti-mPD-1-treated mice exhibited increased donor T cell numbers and elevated expression of CD25, CD69, and Ki67 indicating enhanced activation and proliferation (Fig. 2h-j, Supplementary Fig. 2d). Serum IFN-γ and TNF levels were also elevated (Fig. 2k, Supplementary Fig. 2e). By day 21, however, donor T cell frequencies in the spleen were significantly reduced in anti-mPD-1-treated mice relative to controls (Fig. 2l). We subsequently performed a side-by-side adoptive transfer of donor PD-1$^{-/-}$ C57BL/6J splenocytes or WT C57BL/6J splenocytes with anti-mPD-1 treatment and confirmed that genetic ablation and blockade of PD-1 similarly reduced long-term donor T cell engraftment (Supplementary Fig. 2f-j). Overall, these results align with our *in vitro* AICD data, indicating that while PD-1 signaling constrains early T cell activation it limits AICD and supports long-term persistence.

PD-1 signal modulation using a PD-1-CD28 chimeric switch receptor results in early proliferation but also impaired engraftment of canine CAR T cells

PD-1 blockade has been attempted to augment CAR T cell therapy with negative or equivocal clinical data being reported[25–27]. To determine whether the absence of PD-1 signaling translate cross-species, we employed a canine CAR T cell model. Canine T cells were isolated from whole blood, activated, and transduced with retrovirus encoding a CAR targeting canine CD20, either alone or in combination with a canine PD-1/CD28 chimeric switch receptor (CSR)[32,33]. The CAR consisted of an anti-cCD20 scFv fused to canine CD3ζ and 4-1BB intracellular signaling domains while the CSR consisted of the extracellular domain of canine PD-1 fused to a canine CD28 intracellular domain, designed to convert inhibitory PD-1 signaling into a costimulatory signal (Fig. 3a). T cell

transduction efficiencies post-expansion for the CAR WT and CAR+CSR constructs were comparable (Supplementary Fig. 3a-b). Both CAR T cell products were then co-cultured *in vitro* with target K562 cells expressing cCD20, cPD-L1, and GFP-firefly luciferase (K562/cCD20/cPD-L1/GFP-ffLuc). Live-cell imaging (via Incucyte) revealed CAR T cells expressing the CSR exhibited modestly enhanced cytotoxicity relative to CAR-only T cells (Supplementary Fig. 3c–d). ELISA on co-culture supernatants further showed increased production of canine IFN-γ by CSR-expressing CAR T cells (Fig. 3b). These results are supportive that lack of PD-1 signaling results in initially greater T cell activation. Next, we assessed canine CAR T cell engraftment *in vivo* in a tumor-bearing environment. To test this, NSG mice were injected intravenously (i.v.) with K562/cCD20/cPD-L1/GFP-ffLuc cells on day 0 and treated with either CAR WT or CAR+CSR T cells on day 10 (Fig. 3c). Early on, on day 17, mice treated with CAR+CSR T cells had higher numbers of CAR T cells in the spleen and bone marrow compared to the CAR WT group (Fig. 3d). However, by day 24, CAR+CSR T cells were significantly reduced in all tissues analyzed, including blood, despite sustained expression of the activation marker CD25 while in contrast, CAR WT T cells showed continued expansion over time (Fig. 3e, Supplementary Fig. 3e). This decline was specific to the CAR population, as the proportion of CAR-positive T cells was reduced in the bone marrow of mice treated with CAR+CSR T cells despite similar transduction efficiencies at baseline (Fig. 3f, Supplementary Fig. 3a). Moreover, annexin V binding was higher in the CAR+CSR group, suggesting increased apoptosis as the mechanism of reduced persistence (Fig. 3g). These findings may explain why, despite greater cytotoxic function *in vitro*, *in vivo* tumor control was comparable between treatment groups

(Supplementary Fig. 3f). Overall, these results demonstrate in another species that PD-1 signal modulation is linked to increased AICD and reduces CAR T cell persistence.

PD-1 inhibition increases activation but also AICD of both human T and CAR T cells

To evaluate the effects of PD-1 signal inhibition on human T cells, we first xenografted human peripheral blood mononuclear cells (PBMCs) into NSG mice and treated with pembrolizumab, an FDA-approved human anti-PD-1 blocking antibody with a mutated (S228P) IgG4 to prevent Fc receptor engagement (Supplementary Fig. 4a). As previously reported, human T cells become activated in this model via recognition of murine MHC molecules, leading to proliferation and eventual development of xenogeneic graft-versus-host disease (GVHD)[34]. By day 15 post-infusion, human T cells in the peripheral blood of NSG mice exhibited robust PD-1 expression, consistent with T cell activation (Supplementary Fig. 4b). Pembrolizumab treatment further increased the frequency of circulating human T cells and enhanced HLA-DR expression, indicating greater T cell activation compared to untreated controls (Supplementary Fig. 4c, d). This increased activation was further corroborated by an increase in the severity of acute GVHD observed in pembrolizumab-treated mice (Supplementary Fig. 4e). However, by day 25, human T cell frequency, particularly in the spleen, was reduced in treated mice mirroring the loss of persistence observed in murine and canine T cell models following PD-1 signal disruption (Supplementary Fig. 4f). This reduction appeared more prominent in the $CD4^+$ T cell population compared to $CD8^+$ T cells (Supplementary Fig. 4g)

To further evaluate the effects of PD-1 signal blockade in human T cells under conditions of strong antigen stimulation, we engineered CAR T cells to target three antigens: CD19, CD20, and CD22 (Supplementary Fig. 5a). We co-cultured these trivalent CAR T cells with Raji cells, which express all 3 antigens and observed significant upregulation of PD-1 on CAR T cells more so in CD4+ than CD8+ T cells (Supplementary Fig. 5b-d). To test the effects of PD-1 signaling on human CAR T cells, we then utilized a Raji line expressing human PD-L1 (Supplementary Fig. 6a). Co-culture of CAR T cells with PD-L1-positive Raji cells resulted in reduced CAR T cell cytotoxicity, measured by live-cell imaging (Incucyte), and decreased expression of CD25, Ki67, CD107a, IL-2, and IFN-γ (Supplementary Fig. 6b-d). Blockade of PD-1 using pembrolizumab restored CAR T cell activation *in vitro* observed by increased IL-2 and IFN-γ production, and upregulated CD25 and CD107a expression (Supplementary Fig. 7b–e). However, it also led to elevated expression of CD95 and annexin V binding, indicating increased apoptosis and AICD (Supplementary Fig. 7f–g). To investigate whether blocking PD-1/PD-L1 interactions impacts CAR T cell persistence *in vivo*, NSG mice were injected i.v. day 0 with PD-L1+ Raji cells, and on day 9 with CAR T cells, with the addition of an anti-hPD-1 antibody on days 9, 13, and 17 (Fig. 4a). On day 15, we observed comparable numbers of CAR T cells in the bone marrow of untreated and treated mice (Supplementary Fig. 8a-c). However, CAR T cells from anti-PD-1-treated mice exhibited greater activation, as evidenced by increased expression of CD69 and HLA-DR (Fig. 4b-c). Serum cytokine analysis on day 17 also revealed elevated IFN-γ, IL-2, and TNF in the anti-PD-1-treated group (Fig. 4d, Supplementary Fig. 8d). On day 19, CAR T cells from both spleen and bone marrow maintained an activated phenotype

with upregulation of CD25, CD69, granzyme B, HLA-DR, and Ki67 (Supplementary Fig. 9a-e, 10a-c). Despite sustained activation, in anti-hPD-1-treated mice there was a marked decrease in CAR T cell numbers in both the spleen and bone marrow (Fig. 4e, Supplementary Fig. 9f, 10d). This was further correlated with increased CD95 expression and annexin V binding in the recovered CAR T cells, indicating increased apoptosis and AICD (Fig. 4f-g, Supplementary Fig. 10e-f). This loss was more pronounced in the CD4+ subset compared to CD8+ T cells, paralleling our mouse data with activated IFNGR$^{-/-}$ T cells, suggesting IFN-γ–mediated susceptibility to apoptosis (Fig. 4h, Supplementary Fig. 9g–h, 10g–h). RNA sequencing of sorted human CD3+ T cells sorted from spleens of untreated and anti-PD-1-treated mice revealed transcriptional upregulation of pathways involved in T cell activation, DNA replication, protein translation, and apoptosis, along with downregulation of genes associated with T cell survival (Fig. 4i-j, Supplementary Fig. 11a-e). These results using both human T and CAR T cells are consistent with our findings in murine and canine T cell models, demonstrating that while preventing PD-1 signaling enhances T cell activation, it consequently promotes apoptosis and AICD and limits long-term persistence.

PD-1 ablation or signal inhibition in both activated mouse T and human CAR T cells resulted in compensatory upregulation of LAG3, TIGIT, and TIM3

Previous studies have reported that PD-1 ablation or signal inhibition in mouse T cells leads to compensatory upregulation of other inhibitory receptors, demonstrating an intrinsic regulatory mechanism aimed at restraining excessive T cell activation. Our data are consistent with these findings and extends across both mouse and human T cell

models. In adoptive transfer experiments using WT or PD-1 KO C57BL/6 splenocytes transferred into allogeneic, MHC-mismatched NSG mice, PD-1 KO T cells exhibited significantly elevated expression of the co-inhibitory receptors Lag-3, TIGIT, and Tim-3, 7 days post-transfer (Fig. 5a-c). Similarly, the administration of anti-mPD-1 monoclonal antibody to NSG mice receiving WT splenocytes resulted in increased expression of the same inhibitory receptors compared to untreated controls (Fig. 5d-f). Notably, this compensatory upregulation was not limited to mouse T cells. In human CAR T cells isolated from tumor-bearing mice treated with anti-hPD-1 antibody, we observed a similar pattern of compensatory inhibitory receptor upregulation, with increased levels of Lag-3, TIGIT, and Tim-3 (Fig. 5g-i). These results indicate that the inhibition of PD-1 signaling triggers a broader upregulation of immune checkpoint receptors across species and T cell models.

IFNGR1 deletion in CAR T cells display reduced AICD, increased persistence, and stronger anti-tumor efficacy

To evaluate the effects of IFN-γ on activated human T cells, we incubated resting CAR T cells in media containing recombinant human IFN-γ (rhIFN-γ). After 24 hours, CAR T cells upregulated CD95 expression (Fig. 6a). They were then activated with TransAct for 24 hours where IFN-γ-treated CAR T cells exhibited reduced viability and increased annexin V binding relative to untreated controls, confirming that IFN-γ promotes apoptosis in activated human T cells (Fig. 6b–c). To determine whether this apoptotic effect could be mitigated, we used CRISPR-Cas9 with a guide RNA targeting *IFNGR1* to generate IFNGR1 knockout (KO) CAR T cells (Fig. 6d). CAR transduction efficiencies

were similar between wild-type (WT) and IFNGR1 KO T cells (Supplementary Fig. 12a). When co-cultured with irradiated Raji cells, IFNGR1 KO CAR T cells exhibited reduced expression of CD95 compared to WT CAR T cells, consistent with our findings in murine IFNGR$^{-/-}$ T cells (Fig. 6e). To further evaluate their resistance to AICD, both WT and IFNGR1 KO CAR T cells underwent repeated TransAct stimulation every 3 days. After three rounds of stimulation, IFNGR1 KO CAR T cells demonstrated enhanced long-term expansion compared to WT cells validated across three independent donors (Fig. 6f-g). Furthermore, IFNGR1 KO CAR T cells also showed significantly reduced annexin V binding, indicating less apoptosis and AICD (Fig. 6h). To assess these findings *in vivo*, NSG mice were injected i.v. with Raji tumor cells on day 0 and treated with WT or IFNGR1 KO CAR T cells on day 9 (Fig. 6i). Bioluminescent imaging showed that IFNGR1 KO CAR T cells mediated superior tumor control compared to WT CAR T cells, reproduced in two independent experiments using CAR T cells derived from different donors (Fig. 6j–k, Supplementary Fig. 12b–c). Flow cytometric analysis of bone marrow from tumor-bearing mice on day 19 revealed higher engraftment of IFNGR1 KO CAR T cells relative to WT controls (Fig. 6l). This correlated with reduced CD95 expression and lower annexin V binding on IFNGR1 KO CAR T cells, indicating reduced apoptosis (Fig. 6m–n). Moreover, although the initial CD4+/CD8+ ratios were equivalent between groups, recovered IFNGR1 KO CAR T cells possessed a higher proportion of CD4+ T cells consistent with our data evaluating activated murine IFNGR$^{-/-}$ T cells (Fig. 6o). Overall, these findings spanning T cell models from three different species – mouse, canine, and human – provide strong evidence that IFN-γ signaling contributes to AICD in activated human T cells, particularly affecting the CD4+ subset. PD-1 signal inhibition,

whether through genetic ablation or antibody blockade, enhances T cell activation but may simultaneously increase AICD, possibly through elevated IFN-γ production. Targeting the IFN-γ signaling axis, through knockout of IFNGR via CRISPR-Cas9-mediated deletion of *IFNGR1*, may represent a promising therapeutic strategy to reduce apoptosis, enhance CAR T cell persistence, and improve anti-tumor efficacy.

Discussion

IFN-γ plays a dichotomous role in immune regulation by both promoting and inhibiting T cell responses as well as anti-tumor efficacy[35]. It can also have direct cytostatic and inhibitory effects on tumors as lack of tumor IFN-γ sensitivity is associated with reduced T and CAR T cell anti-tumor responses[36,37]. IFN-γ promotes cytotoxic effector function, and increased tissue infiltration, but also contributes to increased apoptosis and AICD resulting in T cell contraction[38]. Our results presented here demonstrate that PD-1 signaling limits AICD during strong T cell activation via TCR triggering pathways in part by inhibiting IFN-γ production and downstream CD95 induction. This was demonstrated through multiple means of PD-1 signal abrogation – by genetic ablation, signal modulation, or antibody blockade – and across murine, canine, and human T cell models in which either mitogen stimulation, allogeneic activation, or CAR triggering occurred. Loss of PD-1 signaling augmented TCR-mediated T cell activation and IFN-γ production, which in turn increased CD95 expression and apoptosis. Importantly, these effects occurred following strong and sustained T cell stimulation through mitogen exposure, allogeneic responses, or CAR triggering suggesting that PD-1 protects from AICD primarily strong stimulatory conditions are present. In contrast, immune checkpoint blockade alone appears to result in increased T cell activation and anti-tumor efficacy pointing to the need for high activation conditions to simultaneously be present. This may reconcile some of the negative or equivocal clinical data with PD-1 blockade and CAR T cell therapies in which it was predicted to result in increased activation and efficacy. Given the strength of CAR T signaling, these pro-apoptotic effects may be more problematic in settings

where sustained CAR activity is needed. AICD's impact on CAR efficacy may also depend on tumor-intrinsic factors affecting CAR activation, such as antigen density, as well as the specific CAR signaling domains used. It remains to be determined whether varying the dosage or timing of anti-PD-1/PD-L1 administration might modulate the extent of T cell AICD. Exploring alternative dosing strategies could help determine the thresholds at which PD-1 inhibition transitions from promoting T cell activation to inducing activation-associated loss, which may inform more effective clinical applications.

It is important to note that AICD is not limited to CD95-mediated apoptosis alone. IFN-γ is also known to upregulate TNF-related apoptosis-inducing ligand (TRAIL) expression on CD4+ T cells, which can increase sensitivity to TRAIL-mediated apoptosis via caspase activation and IRF-1 upregulation[39]. TRAIL interacts with death receptors DR4 and DR5, the latter of which has been implicated in promoting apoptosis specifically in CD4+ but not CD8+ T cells[40]. This receptor selectivity may help explain why, in our studies, apoptosis was more prominent, though not exclusive to, in the CD4+ T cell population. While the upregulation of CD95 we observed is compelling, future studies are needed to delineate the individual contributions of the CD95 and TRAIL pathways to AICD. Such studies may also build upon our findings by clarifying how these pathways differentially affect CD4+ and CD8+ T cell survival following strong activation stimuli.

Previous work with PD-1$^{-/-}$ and anti-mPD-1-treated mice has demonstrated impaired memory T cell formation in the absence of PD-1 signaling, suggesting that PD-1 promotes antigen-specific T cell survival[4,41]. Our findings extend this concept by

identifying AICD prevention as one mechanism by which PD-1 contributes to enhanced T cell persistence. However, PD-1 likely affects additional cellular pathways influencing long-term T cell maintenance. For example, in models of chronic LCMV infection, antigen-specific T cells lacking PD-1 signaling exhibit greater dysfunction and terminal exhaustion, compromising their long-term engraftment and function[42]. Thus, the PD-1/PDL-1 pathway may play roles in protecting T cells during initial activation but also with chronic stimulation in maintaining the population.

While targeting IFNGR on T cells could protect from AICD, IFN-γ is likely not the sole cytokine mediator involved. Other induced cytokines such as TNF can also promote AICD independently of CD95[43–45]. Similarly, it was observed that PD-1 inhibition not just elevated serum IFN-γ but also increased TNF which may contribute to AICD (Supplementary Fig. 2j, 8e). Consistent with this, other studies have shown that blocking TNF alongside PD-1 inhibition enhances T cell persistence[46]. It remains to be determined if concurrent targeting of TNFR2 on T cells would yield similar improvements in engraftment, as observed with IFNGR deletion.

The role of pro-inflammatory cytokines in promoting AICD brings us to an important clinical consideration. Since pro-inflammatory cytokines play a central role in mediating T cell AICD, the cytoreductive conditioning applied in most CAR therapies while promoting CAR engraftment and activation, may also augment subsequent CAR AICD. In addition, other patient-intrinsic characteristics such as individuals with chronic inflammatory conditions or with aging and obesity may result in inflammatory conditions that drive T cells to AICD[47]. Additionally, PD-1 blockade has been shown to induce compensatory upregulation of other inhibitory receptors, such as TIM3, LAG3, and

TIGIT (Fig. 5a-i)[48,49]. While this phenomenon supports the rationale for combined checkpoint inhibition to increase activation or reverse exhaustion, it also raises concerns that simultaneous inhibition of multiple checkpoints may exacerbate T cell AICD. Future studies investigating the potential effects of combined checkpoint blockade on T cell survival and exploring strategies to mitigate pro-apoptotic effects while preserving activation are likely to be translationally impactful.

We focused on IFN-γ's role in AICD because PD-1 inhibition clearly increases its production. Using $IFNGR^{-/-}$ mouse T cells we found that loss of IFN-γ signaling reduced apoptosis and enhanced T cell persistence post-activation. We further corroborated these findings by developing IFNGR1 KO human CAR T cells, which displayed reduced AICD without impairing IFN-γ's direct anti-tumor effects, maintaining T cell survival and function.

In conclusion, our findings reveal a critical role for PD-1 signaling in protecting T cells from AICD during strong and sustained activation. While PD-1 signal abrogation enhances early T cell activation, it subsequently predisposes T cells to apoptosis and impaired persistence through increased IFN-γ production and subsequent CD95 upregulation. Disruption of IFN-γ signaling by IFNGR deletion attenuates AICD allowing for improved T cell expansion, persistence, and anti-tumor effects. This strategy offers a promising avenue to enhance the therapeutic potential of CAR T cells, particularly in settings such as solid tumors, where durable CAR T cell responses remain a significant hurdle and where clinical successes have been limited.

Acknowledgements

This research was supported by funding from CIRM TRAN1-13996, NIH/NCI P30 CA093373, NIH/NCI P01 CA065493, NIH/NIAID R37 AI34495, and NIH/ORIP S10 RR026825. We thank Dr. Bruce Blazar (University of Minnesota Medical School) for supplying PD-1$^{-/-}$ C57BL/6 mice. We also thank Dr. Nicola Mason (University of Pennsylvania School of Veterinary Medicine) and Sonam Srivastava – for supplying target cells and lentiviral constructs for generating canine WT and CSR CAR T cells and providing their technical expertise. We thank Dr. Robert Rebhun (University of California Davis) for supplying canine donor blood for our canine CAR T studies. We are further grateful to Dr. Ying Xiong and Caring Cross for providing lentivirus used in the generation of human CAR T cells, along with their technical support and culturing protocols. Additionally, we thank Dr. Joseph Tuscano and Dr. Joshua Meckler for providing anti-human PD-1 (pembrolizumab). Finally, we thank Dr. Xiao-Jing Wang and the UC Davis Molecular Pharmacology Shared Resource Core for access to their Incucyte Live-Cell Analysis System; Jonathan Van Dyke of the UC Davis Flow Cytometry Shared Resource Core (funded by for technical assistance; and Dr. Kyle Fink and Dr. John Albeck for access to their Neon Electroporation Systems.

References

1. Greenwald, R. J., Freeman, G. J. & Sharpe, A. H. THE B7 FAMILY REVISITED. *Annu. Rev. Immunol.* **23**, 515–548 (2005).

2. Moseman, J. E., Rastogi, I., Jeon, D. & McNeel, D. G. PD-1 blockade employed at the time CD8+ T cells are activated enhances their antitumor efficacy. *J. Immunother. Cancer* **13**, e011145 (2025).

3. Chamoto, K., Yaguchi, T., Tajima, M. & Honjo, T. Insights from a 30-year journey: function, regulation and therapeutic modulation of PD1. *Nat. Rev. Immunol.* **23**, 682–695 (2023).

4. Pauken, K. E. *et al.* The PD-1 Pathway Regulates Development and Function of Memory CD8+ T Cells following Respiratory Viral Infection. *Cell Rep.* **31**, 107827 (2020).

5. Mittelbrunn, M. & Kroemer, G. Hallmarks of T cell aging. *Nat. Immunol.* **22**, 687–698 (2021).

6. Day, C. L. *et al.* PD-1 expression on HIV-specific T cells is associated with T-cell exhaustion and disease progression. *Nature* **443**, 350–354 (2006).

7. Jin, H.-T. *et al.* Cooperation of Tim-3 and PD-1 in CD8 T-cell exhaustion during chronic viral infection. *Proc. Natl. Acad. Sci.* **107**, 14733–14738 (2010).

8. Liu, B. *et al.* Temporal single-cell tracing reveals clonal revival and expansion of precursor exhausted T cells during anti-PD-1 therapy in lung cancer. *Nat. Cancer* **3**, 108–121 (2021).

9. Blackburn, S. D., Shin, H., Freeman, G. J. & Wherry, E. J. Selective expansion of a subset of exhausted CD8 T cells by PD-L1 blockade.

10. Barber, D. L. *et al.* Restoring function in exhausted CD8 T cells during chronic viral infection. *Nature* **439**, 682–687 (2006).

11. Nagata, S. Fas Ligand-Induced Apoptosis. *Annu. Rev. Genet.* **33**, 29–55 (1999).

12. Ashwell, J. D., Cunningham, R. E., Noguchi, P. D. & Hernandez, D. Cell growth cycle block of T cell hybridomas upon activation with antigen. *J. Exp. Med.* **165**, 173–194 (1987).

13. Peter, M. E. *et al.* The role of CD95 and CD95 ligand in cancer. *Cell Death Differ.* **22**, 549–559 (2015).

14. Krammer, P. H. CD95's deadly mission in the immune system. *Nature* **407**, 789–795 (2000).

15. Brunner, T. *et al.* Cell-autonomous Fas (CD95)/Fas-ligand interaction mediates activation-induced apoptosis in T-cell hybridomas. *Nature* **373**, 441–444 (1995).

16. Dhein, J. & Walczak, H. Autocrine T-cell suicide mediated by APO-l/(Fas/CD95). **373**, (1995).

17. Kischkel, F. C. *et al.* Cytotoxicity-dependent APO-1 (Fas/CD95)-associated proteins form a death-inducing signaling complex (DISC) with the receptor. *EMBO J.* **14**, 5579–5588 (1995).

18. Li, J. H. *et al.* Interferon- Augments CD95(APO-1/Fas) and Pro- Caspase-8 Expression and Sensitizes Human Vascular Endothelial Cells to CD95-Mediated Apoptosis. **161**, (2002).

19. Refaeli, Y., Van Parijs, L., Alexander, S. I. & Abbas, A. K. Interferon γ Is Required for Activation-induced Death of T Lymphocytes. *J. Exp. Med.* **196**, 999–1005 (2002).

20. Curran, M. A., Montalvo, W., Yagita, H. & Allison, J. P. PD-1 and CTLA-4 combination blockade expands infiltrating T cells and reduces regulatory T and myeloid cells within B16 melanoma tumors. *Proc. Natl. Acad. Sci.* **107**, 4275–4280 (2010).

21. Liakou, C. I. *et al.* CTLA-4 blockade increases IFN -producing CD4 ICOShi cells to shift the ratio of effector to regulatory T cells in cancer patients.

22. Peng, W. *et al.* PD-1 Blockade Enhances T-cell Migration to Tumors by Elevating IFN-γ Inducible Chemokines. *Cancer Res.* **72**, 5209–5218 (2012).

23. Zhu, J. *et al.* Resistance to cancer immunotherapy mediated by apoptosis of tumor-infiltrating lymphocytes. *Nat. Commun.* **8**, 1404 (2017).

24. Tomsitz, D. *et al.* Development of Lymphopenia during Therapy with Immune Checkpoint Inhibitors Is Associated with Poor Outcome in Metastatic Cutaneous Melanoma. *Cancers* **14**, 3282 (2022).

25. Wang, Z. *et al.* Phase I study of CAR-T cells with PD-1 and TCR disruption in mesothelin-positive solid tumors. *Cell. Mol. Immunol.* **18**, 2188–2198 (2021).

26. Chong, E. A. *et al.* Pembrolizumab for B-cell lymphomas relapsing after or refractory to CD19-directed CAR T-cell therapy. *Blood* **139**, 1026–1038 (2022).

27. Bagley, S. J. *et al.* Repeated peripheral infusions of anti-EGFRvIII CAR T cells in combination with pembrolizumab show no efficacy in glioblastoma: a phase 1 trial. *Nat. Cancer* **5**, 517–531 (2024).

28. Wei, J. *et al.* PD-1 silencing impairs the anti-tumor function of chimeric antigen receptor modified T cells by inhibiting proliferation activity. *J. Immunother. Cancer* **7**, 209 (2019).

29. Kalinin, R. S. *et al.* Engineered Removal of PD-1 From the Surface of CD19 CAR-T Cells Results in Increased Activation and Diminished Survival. *Front. Mol. Biosci.* **8**, 745286 (2021).

30. Hamad, A. R. A. & Schneck, J. P. Antigen-Induced T Cell Death Is Regulated by CD4 Expression. *Int. Rev. Immunol.* **20**, 535–546 (2001).

31. Berner, V. *et al.* IFN-γ mediates CD4+ T-cell loss and impairs secondary antitumor responses after successful initial immunotherapy. *Nat. Med.* **13**, 354–360 (2007).

32. Rotolo, A., Atherton, M. J., Kasper, B. T., Haran, K. P. & Mason, N. J. Genetic re-direction of canine primary T cells for clinical trial use in pet dogs with spontaneous cancer. *STAR Protoc.* **2**, 100905 (2021).

33. Yoshimoto, S. *et al.* Validation of a PD-1/CD28 chimeric switch receptor to augment CAR-T function in dogs with spontaneous B cell lymphoma. *iScience* **27**, 110863 (2024).

34. King, M. A. *et al.* Human peripheral blood leucocyte non-obese diabetic-severe combined immunodeficiency interleukin-2 receptor gamma chain gene mouse model of xenogeneic graft- *versus* -host-like disease and the role of host major histocompatibility complex. *Clin. Exp. Immunol.* **157**, 104–118 (2009).

35. Jorgovanovic, D., Song, M., Wang, L. & Zhang, Y. Roles of IFN-γ in tumor progression and regression: a review. *Biomark. Res.* **8**, 49 (2020).

36. Garcia-Diaz, A. *et al.* Interferon Receptor Signaling Pathways Regulating PD-L1 and PD-L2 Expression. *Cell Rep.* **19**, 1189–1201 (2017).

37. Larson, R. C. *et al.* CAR T cell killing requires the IFNγR pathway in solid but not liquid tumours. *Nature* **604**, 563–570 (2022).

38. Bhat, P., Leggatt, G., Waterhouse, N. & Frazer, I. H. Interferon-γ derived from cytotoxic lymphocytes directly enhances their motility and cytotoxicity. *Cell Death Dis.* **8**, e2836–e2836 (2017).

39. Park, S. *et al.* IFN-γ enhances TRAIL-induced apoptosis through IRF-1. *Eur. J. Biochem.* **271**, 4222–4228 (2004).

40. Herbeuval, J.-P. CD4+ T-cell death induced by infectious and noninfectious HIV-1: role of type 1 interferon-dependent, TRAIL/DR5-mediated apoptosis. *Blood* **106**, 3524–3531 (2005).

41. Ahn, E. *et al.* Role of PD-1 during effector CD8 T cell differentiation. *Proc. Natl. Acad. Sci.* **115**, 4749–4754 (2018).

42. Odorizzi, P. M., Pauken, K. E., Paley, M. A., Sharpe, A. & Wherry, E. J. Genetic absence of PD-1 promotes accumulation of terminally differentiated exhausted CD8+ T cells. *J. Exp. Med.* **212**, 1125–1137 (2015).

43. Zheng, L. *et al.* Induction of apoptosis in mature T cells by tumour necrosis factor. *Nature* **377**, 348–351 (1995).

44. Twu, Y., Gold, M. R. & Teh, H. TNFR1 delivers pro-survival signals that are required for limiting TNFR2-dependent activation-induced cell death (AICD) in $CD8^+$ T cells. *Eur. J. Immunol.* **41**, 335–344 (2011).

45. Otano, I. *et al.* Human CD8 T cells are susceptible to TNF-mediated activation-induced cell death. *Theranostics* **10**, 4481–4489 (2020).

46. Bertrand, F. *et al.* TNFα blockade overcomes resistance to anti-PD-1 in experimental melanoma. *Nat. Commun.* **8**, 2256 (2017).

47. Vick, L. V. *et al.* Aging augments obesity-induced thymic involution and peripheral T cell exhaustion altering the “obesity paradox”. *Front. Immunol.* **13**, 1012016 (2023).

48. Huang, R.-Y., Francois, A., McGray, A. R., Miliotto, A. & Odunsi, K. Compensatory upregulation of PD-1, LAG-3, and CTLA-4 limits the efficacy of single-agent checkpoint blockade in metastatic ovarian cancer. *OncoImmunology* **6**, e1249561 (2017).

49. Koyama, S. *et al.* Adaptive resistance to therapeutic PD-1 blockade is associated with upregulation of alternative immune checkpoints. *Nat. Commun.* **7**, 10501 (2016).

50. Cooke, K. *et al.* An experimental model of idiopathic pneumonia syndrome after bone marrow transplantation: I. The roles of minor H antigens and endotoxin. *Blood* **88**, 3230–3239 (1996).

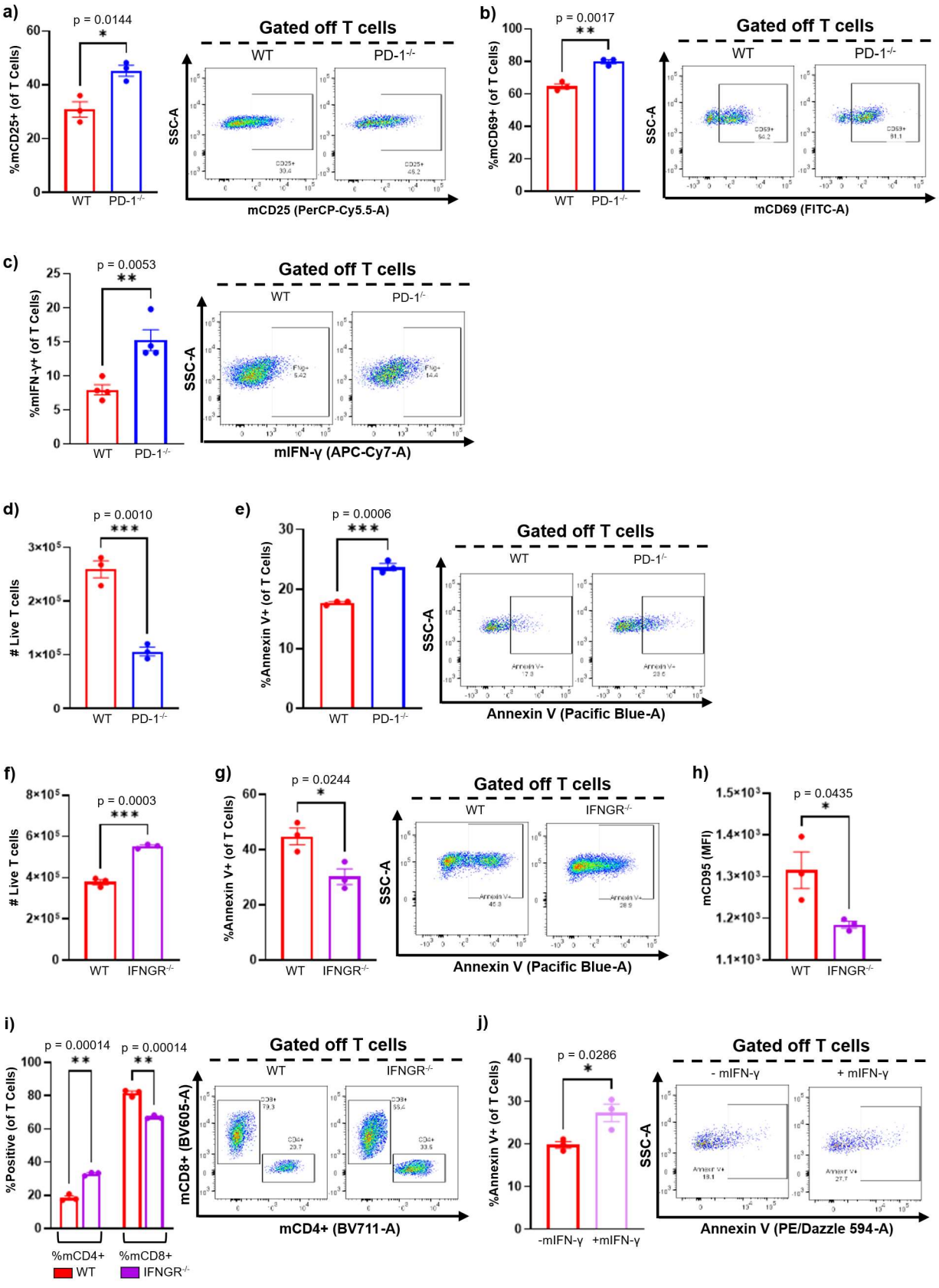
a)
p = 0.0144
*
%mCD25+ (of T Cells)
WT
PD-1-/-
Gated off T cells
WT
PD-1-/-
SSC-A
mCD25 (PerCP-Cy5.5-A)
b)
p = 0.0017
**
%mCD69+ (of T Cells)
WT
PD-1-/-
Gated off T cells
WT
PD-1-/-
SSC-A
mCD69 (FITC-A)
c)
p = 0.0053
**
%mIFN-γ+ (of T Cells)
WT
PD-1-/-
Gated off T cells
WT
PD-1-/-
SSC-A
mIFN-γ (APC-Cy7-A)
d)
p = 0.0010
***
Live T cells
WT
PD-1-/-
e)
p = 0.0006
***
%Annexin V+ (of T Cells)
WT
PD-1-/-
Gated off T cells
WT
PD-1-/-
SSC-A
Annexin V (Pacific Blue-A)
f)
p = 0.0003
***
Live T cells
WT
IFNGR-/-
g)
p = 0.0244
*
%Annexin V+ (of T Cells)
WT
IFNGR-/-
Gated off T cells
WT
IFNGR-/-
SSC-A
Annexin V (Pacific Blue-A)
h)
p = 0.0435
*
mCD95 (MFI)
WT
IFNGR-/-
i)
p = 0.00014
**
p = 0.00014
**
%Positive (of T Cells)
%mCD4+
%mCD8+
WT
IFNGR-/-
Gated off T cells
WT
IFNGR-/-
mCD8+ (BV605-A)
mCD4+ (BV711-A)
j)
p = 0.0286
*
%Annexin V+ (of T Cells)
-mIFN-γ
+mIFN-γ
Gated off T cells
- mIFN-γ
+ mIFN-γ
SSC-A
Annexin V (PE/Dazzle 594-A)

Figure 1: *In vitro,* PD-1 signal loss enhances mouse T cell activation but also increases subsequent cell death, potentially mediated by IFN-γ

Mouse splenocytes were activated in 0.625 µg/mL conA for 72 hours:

(a, b) Expression of CD25 (a) and CD69 (b) by flow cytometry in WT and IFNGR$^{-/-}$ C57BL/6 T cells.

(c) mIFN-γ expression in WT and PD-1$^{-/-}$ C57BL/6 T cells by flow cytometry.

(d) Number of live WT and PD-1$^{-/-}$ C57BL/6 T cells by trypan blue exclusion.

(e) Annexin V binding in WT and PD-1$^{-/-}$ T cells by flow cytometry.

(f) Number of live WT and IFNGR$^{-/-}$ C57BL/6 T cells by trypan blue exclusion.

(g) Annexin V binding in WT and IFNGR$^{-/-}$ T cells by flow cytometry.

(h) mCD95 expression in WT and IFNGR$^{-/-}$ C57BL/6 T cells.

(i) Percent of mCD4+ and mCD8+ WT and IFNGR$^{-/-}$ T cells by flow cytometry.

(j) Annexin V binding between T cells with and without mIFN-γ treatment.

Data is representative of two independent experiments performed in technical triplicates. Statistical comparisons were performed using a two-tailed unpaired Student's t test without Welch's correction. Data are presented as mean ± standard error of the mean (SEM), with individual data points shown where applicable.

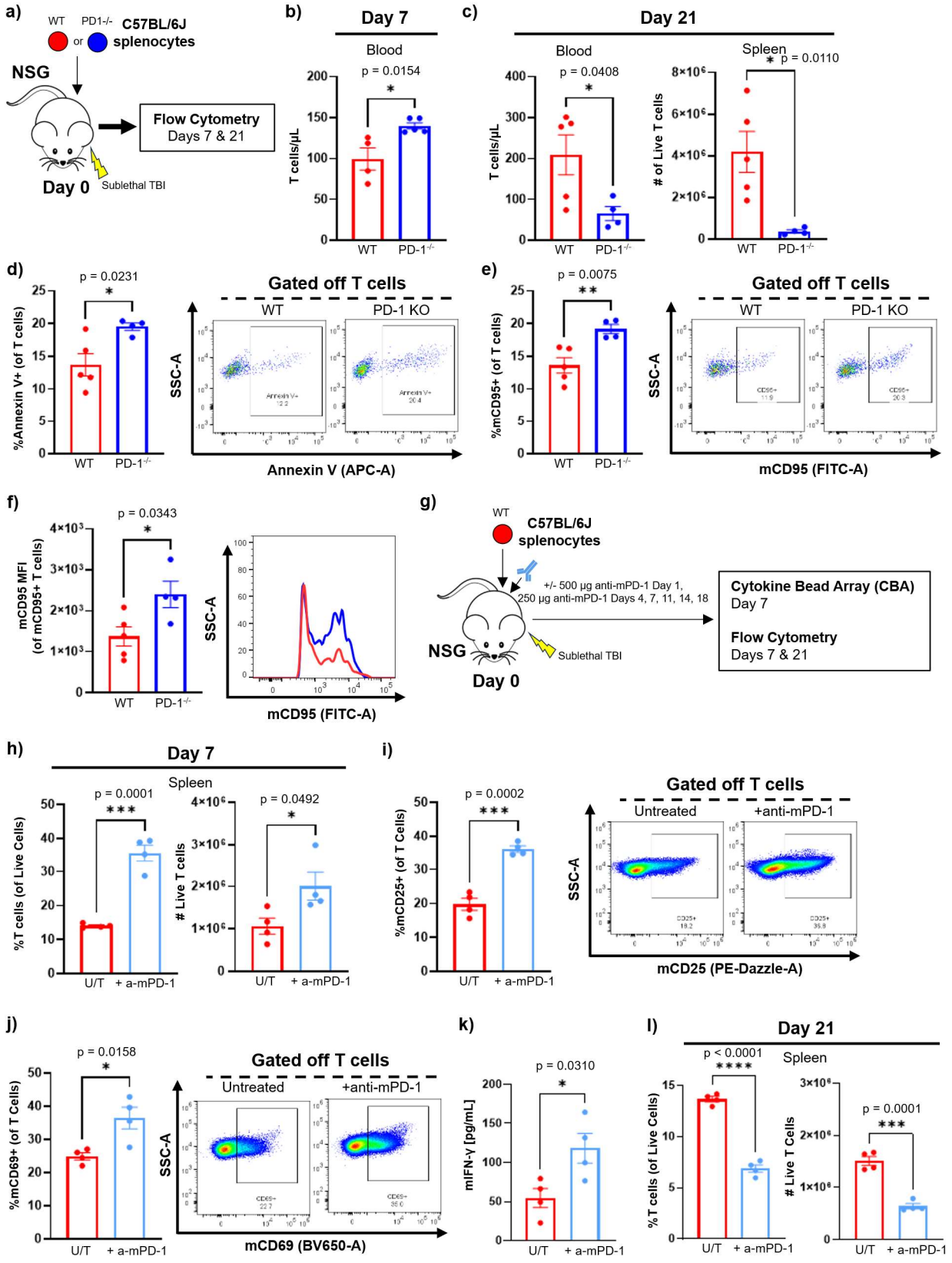
a)
WT
PD1-/-
or
C57BL/6J
splenocytes
NSG
Flow Cytometry
Days 7 & 21
Day 0
Sublethal TBI
b)
Day 7
Blood
p = 0.0154
T cells/µL
WT
PD-1-/-
c)
Day 21
Blood
p = 0.0408
T cells/µL
Spleen
p = 0.0110
# of Live T cells
d)
p = 0.0231
%Annexin V+ (of T cells)
Gated off T cells
WT
PD-1 KO
SSC-A
Annexin V (APC-A)
e)
p = 0.0075
%mCD95+ (of T cells)
Gated off T cells
mCD95 (FITC-A)
f)
p = 0.0343
mCD95 MFI
(of mCD95+ T cells)
mCD95 (FITC-A)
g)
C57BL/6J
splenocytes
+/- 500 µg anti-mPD-1 Day 1,
250 µg anti-mPD-1 Days 4, 7, 11, 14, 18
Cytokine Bead Array (CBA)
Day 7
Flow Cytometry
Days 7 & 21
h)
Day 7
Spleen
p = 0.0001
%T cells (of Live Cells)
p = 0.0492
# Live T cells
U/T
+ a-mPD-1
i)
p = 0.0002
%mCD25+ (of T Cells)
Gated off T cells
Untreated
+anti-mPD-1
mCD25 (PE-Dazzle-A)
j)
p = 0.0158
%mCD69+ (of T Cells)
Gated off T cells
mCD69 (BV650-A)
k)
p = 0.0310
mIFN-γ [pg/mL]
l)
Day 21
p < 0.0001
Spleen
%T cells (of Live Cells)
p = 0.0001
# Live T Cells

Figure 2: In an allogeneic adoptive transfer model, PD-1$^{-/-}$ and anti-PD-1-treated WT C57BL/6J T cells show increased activation and early expansion accompanied by elevated apoptosis compared to WT untreated controls

(a) Experimental schematic: C57BL/6J WT or PD1$^{-/-}$ splenocytes adoptively transferred into NSG mice.

(b) C57BL/6J WT and PD1$^{-/-}$ engrafted T cell numbers in the blood of NSG mice 7 days after infusion.

(c) C57BL/6J WT and PD1$^{-/-}$ engrafted T cell numbers in the blood and spleen of NSG mice 21 days after infusion.

(d) Annexin V binding in C57BL/6J WT and PD1$^{-/-}$ engrafted T cells in the spleen of NSG mice 21 days after infusion by flow cytometry.

(e) Percent mCD95 expression by flow cytometry in C57BL/6J WT and PD1$^{-/-}$ engrafted T cells in the spleen of NSG mice 21 days after infusion by flow cytometry.

(f) MFI of mCD95 expression by flow cytometry in mCD95-positive C57BL/6J WT and PD1$^{-/-}$ engrafted T cells in the spleen of NSG mice 21 days after infusion.

(g) Experimental schematic: C57BL/6J WT splenocytes are adoptively transferred into NSG mice and treated with or without anti-mPD-1.

(h) C57BL/6J engrafted T cell frequency and numbers in the spleen of NSG mice 7 days after treatment with and without anti-mPD-1 treatment.

(i, j) mCD25 (i) and mCD69 (j) expression by flow cytometry in C57BL/6J T cells engrafted in the spleens of NSG mice with and without anti-mPD-1 treatment 7 days after treatment.

(k) IFN-γ by CBA from the serum of NSG mice engrafted with C57BL/6J WT T cells with and without anti-mPD-1 treatment 7 days after treatment.
(l) C57BL/6J engrafted T cell numbers in the spleen of NSG mice 21 days after treatment with and without anti-mPD-1 treatment.

Data in b-f is representative of three independent experiments (n=4 or 5 per group), and in h-l is representative of two independent experiments (n=4 per group). Statistical comparisons were performed using a two-tailed unpaired Student's t test without Welch's correction. Data are presented as mean ± standard error of the mean (SEM), with individual data points shown where applicable.

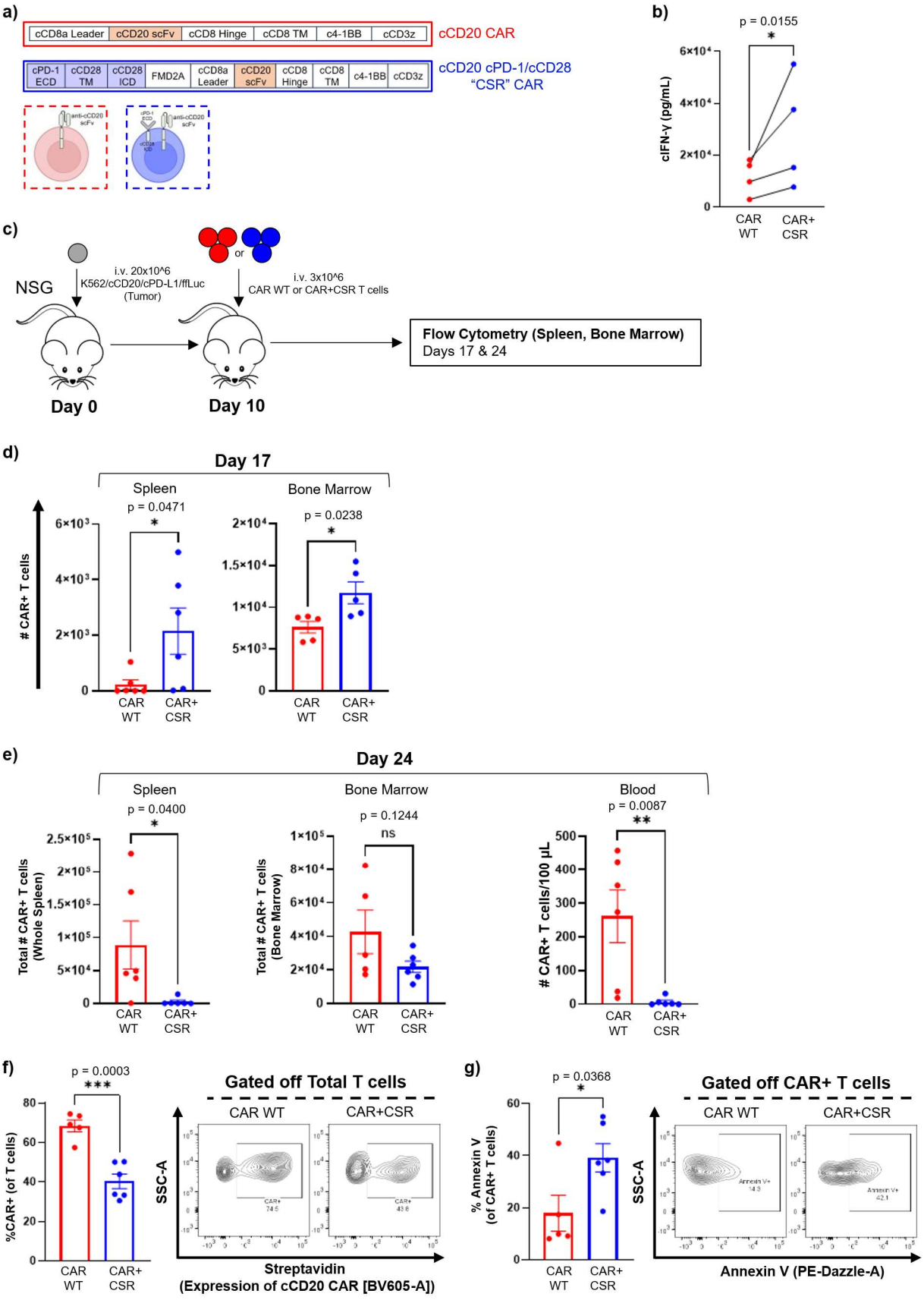
a)
cCD8a Leader
cCD20 scFv
cCD8 Hinge
cCD8 TM
c4-1BB
cCD3z
cCD20 CAR
cPD-1 ECD
cCD28 TM
cCD28 ICD
FMD2A
cCD8a Leader
cCD20 scFv
cCD8 Hinge
cCD8 TM
c4-1BB
cCD3z
cCD20 cPD-1/cCD28 "CSR" CAR
b)
p = 0.0155
*
cIFN-γ (pg/mL)
6×10⁴
4×10⁴
2×10⁴
0
CAR WT
CAR+ CSR
c)
NSG
i.v. 20x10^6 K562/cCD20/cPD-L1/ffLuc (Tumor)
or
i.v. 3x10^6 CAR WT or CAR+CSR T cells
Flow Cytometry (Spleen, Bone Marrow)
Days 17 & 24
Day 0
Day 10
d)
Day 17
Spleen
p = 0.0471
*
Bone Marrow
p = 0.0238
*
CAR+ T cells
6×10³
4×10³
2×10³
0
2×10⁴
1.5×10⁴
1×10⁴
5×10³
0
CAR WT
CAR+ CSR
e)
Day 24
Spleen
p = 0.0400
*
Bone Marrow
p = 0.1244
ns
Blood
p = 0.0087
**
Total # CAR+ T cells (Whole Spleen)
2.5×10⁵
2×10⁵
1.5×10⁵
1×10⁵
5×10⁴
0
Total # CAR+ T cells (Bone Marrow)
1×10⁵
8×10⁴
6×10⁴
4×10⁴
2×10⁴
0
CAR+ T cells/100 µL
500
400
300
200
100
0
CAR WT
CAR+ CSR
f)
p = 0.0003
***
%CAR+ (of T cells)
80
60
40
20
0
CAR WT
CAR+ CSR
Gated off Total T cells
CAR WT
CAR+CSR
SSC-A
Streptavidin
(Expression of cCD20 CAR [BV605-A])
g)
p = 0.0368
*
% Annexin V (of CAR+ T cells)
60
40
20
0
CAR WT
CAR+ CSR
Gated off CAR+ T cells
CAR WT
CAR+CSR
SSC-A
Annexin V (PE-Dazzle-A)

Figure 3: Canine CAR T cells engineered with a PD-1/CD28 chimeric switch receptor (CSR) exhibit enhanced IFN-γ production but also increased AICD

(a) Vector design of cCD20 CAR WT and cCD20 CAR+CSR constructs.

(b) cIFN-γ production between CAR WT and CAR+CSR after co-culture with K562/cCD20/cPD-L1 cells.

(c) Experimental schematic: K562/cCD20/cPD-L1/GFP-ffLuc tumor-bearing NSG mice treated with either CAR WT or CAR+CSR T cells.

(d) Day 17: Number of CAR WT and CAR+CSR T cells in spleens and bone marrow of tumor-bearing mice 7 days after infusion.

(e) Day 24: Number of CAR WT and CAR+CSR T cells in spleens, bone marrow, and blood of tumor-bearing mice 14 days after infusion.

(f) Day 24: Percentage of CAR+ T cells by flow cytometry gated off total T cells in bone marrow of tumor-bearing mice treated with CAR WT and CAR+CSR T cells 14 days after infusion.

(g) Day 24: Annexin V binding by flow cytometry on CAR WT and CAR+CSR T cells in NSG mice 14 days after infusion.

Data in b consists of CAR T cells made from 4 different donors (n=4), and in d-g is combined from two independent experiments (total n=5 or 6 per group). Statistical comparisons were performed either using a two-tailed unpaired (d-g) or paired (b) Student's t test without Welch's correction. Data are presented as mean ± standard error of the mean (SEM), with individual data points shown where applicable.

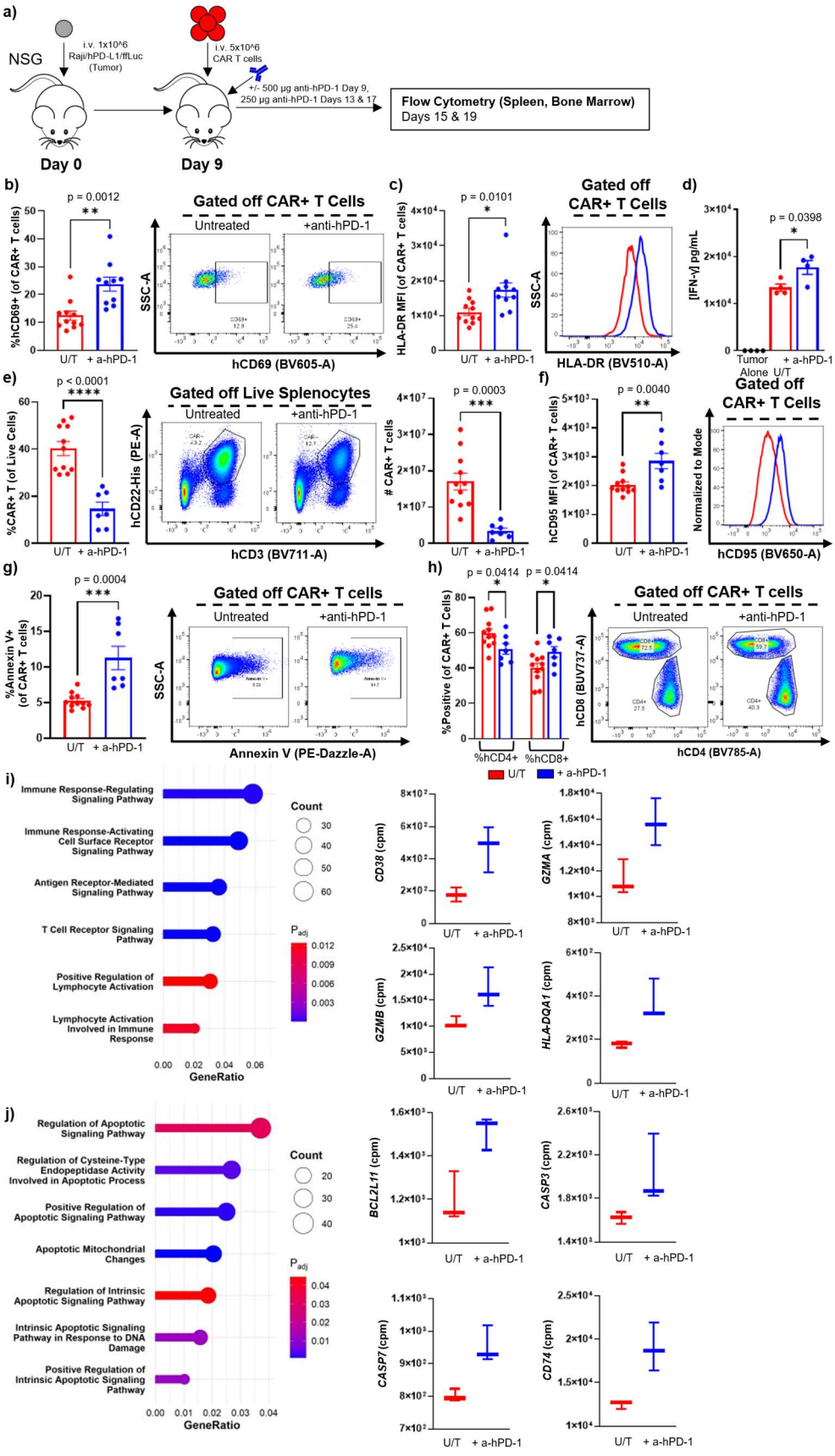
a)
NSG
i.v. 1x10^6
Raji/hPD-L1/ffLuc
(Tumor)
i.v. 5x10^6
CAR T cells
+/- 500 µg anti-hPD-1 Day 9,
250 µg anti-hPD-1 Days 13 & 17
Flow Cytometry (Spleen, Bone Marrow)
Days 15 & 19
Day 0
Day 9
b)
p = 0.0012
**
%hCD69+ (of CAR+ T cells)
U/T
+ a-hPD-1
Gated off CAR+ T Cells
Untreated
+anti-hPD-1
SSC-A
hCD69 (BV605-A)
c)
p = 0.0101
*
HLA-DR MFI (of CAR+ T cells)
Gated off CAR+ T Cells
SSC-A
HLA-DR (BV510-A)
d)
p = 0.0398
*
[IFN-γ] pg/mL
Tumor Alone
U/T
+ a-hPD-1
e)
p < 0.0001
****
%CAR+ T (of Live Cells)
Gated off Live Splenocytes
Untreated
+anti-hPD-1
hCD22-His (PE-A)
hCD3 (BV711-A)
p = 0.0003
***
CAR+ T cells
f)
p = 0.0040
**
hCD95 MFI (of CAR+ T cells)
Gated off CAR+ T Cells
Normalized to Mode
hCD95 (BV650-A)
g)
p = 0.0004
***
%Annexin V+ (of CAR+ T cells)
Gated off CAR+ T cells
Untreated
+anti-hPD-1
SSC-A
Annexin V (PE-Dazzle-A)
h)
p = 0.0414
p = 0.0414
*
*
%Positive (of CAR+ T Cells)
%hCD4+
%hCD8+
Gated off CAR+ T cells
Untreated
+anti-hPD-1
hCD8 (BUV737-A)
hCD4 (BV785-A)
U/T
+ a-hPD-1
i)
Immune Response-Regulating Signaling Pathway
Immune Response-Activating Cell Surface Receptor Signaling Pathway
Antigen Receptor-Mediated Signaling Pathway
T Cell Receptor Signaling Pathway
Positive Regulation of Lymphocyte Activation
Lymphocyte Activation Involved in Immune Response
Count
30
40
50
60
Padj
0.012
0.009
0.006
0.003
0.00 0.02 0.04 0.06
GeneRatio
CD38 (cpm)
GZMA (cpm)
GZMB (cpm)
HLA-DQA1 (cpm)
U/T
+ a-hPD-1
j)
Regulation of Apoptotic Signaling Pathway
Regulation of Cysteine-Type Endopeptidase Activity Involved in Apoptotic Process
Positive Regulation of Apoptotic Signaling Pathway
Apoptotic Mitochondrial Changes
Regulation of Intrinsic Apoptotic Signaling Pathway
Intrinsic Apoptotic Signaling Pathway in Response to DNA Damage
Positive Regulation of Intrinsic Apoptotic Signaling Pathway
Count
20
30
40
Padj
0.04
0.03
0.02
0.01
0.00 0.01 0.02 0.03 0.04
GeneRatio
BCL2L11 (cpm)
CASP3 (cpm)
CASP7 (cpm)
CD74 (cpm)
U/T
+ a-hPD-1

Figure 4: PD-1 blockade in activated human CAR T cells results in increased activation but also greater apoptosis and a lack of long-term persistence

(a) Experimental schematic: Raji/hPD-L1 tumor-bearing NSG mice were treated with human hCD19/hCD20/hCD22 tri-specific CAR T cells and treated with or without anti-hPD-1 blocking antibody (pembrolizumab).
(b, c) Day 15: expression of T cell activation markers hCD69 (b) and HLA-DR (c) by flow cytometry in CAR T cells in spleen of mice treated with and without anti-hPD-1 6 days post-CAR T infusion.
(d) Day 17: serum cytokine levels of hIFN-γ by CBA in mice treated with and without anti-hPD-1 8 days post-CAR T infusion.
(e) Day 19: frequency and number of CAR+ T cells by flow cytometry in spleens of mice treated with and without anti-hPD-1 10 days post-CAR T infusion.
(f, g) Day 19: expression of hCD95 (f) and annexin V binding (g) by flow cytometry in CAR T cells from spleens of mice treated with and without anti-hPD-1 10 days post-CAR T infusion.
(h) Day 19: proportion of hCD4+ and hCD8+ CAR T cells by flow cytometry in spleens of mice treated with and without anti-hPD-1 10 days post-CAR T infusion.
(i, j) Day 19: gene ontology analysis on activation (i) and apoptotic (j) pathways on sorted human CAR T cells from spleens of tumor-bearing mice treated with and without anti-hPD-1 10 days post-CAR T infusion; expression of select genes (cpm) from each pathway are shown.

Data in b-c and e-h is combined from 3 independent experiments (total n=11 for untreated group and n=10 or 7 for anti-hPD-1-treated group), and in d is from a single experiment (n=4 for all groups), and in i-j from a single experiment (n=3 for both groups). Statistical comparisons were performed using a two-tailed unpaired Student's t test without Welch's correction. Data are presented as mean ± standard error of the mean (SEM), with individual data points shown where applicable.

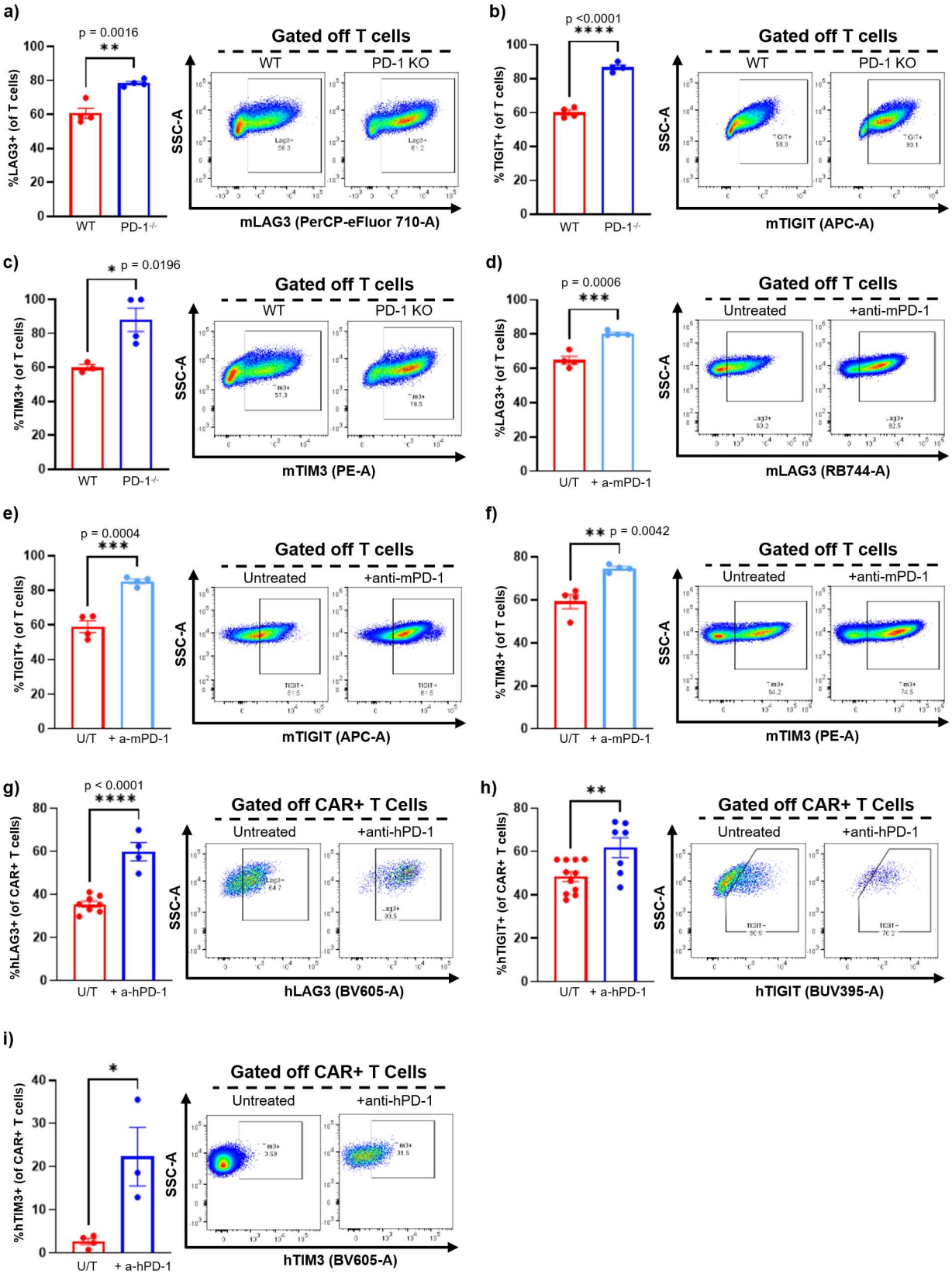
a)
p = 0.0016
**
%LAG3+ (of T cells)
WT
PD-1-/-
Gated off T cells
WT
PD-1 KO
SSC-A
mLAG3 (PerCP-eFluor 710-A)
b)
p <0.0001
****
%TIGIT+ (of T cells)
WT
PD-1-/-
Gated off T cells
WT
PD-1 KO
SSC-A
mTIGIT (APC-A)
c)
* p = 0.0196
%TIM3+ (of T cells)
WT
PD-1-/-
Gated off T cells
WT
PD-1 KO
SSC-A
mTIM3 (PE-A)
d)
p = 0.0006
***
%LAG3+ (of T cells)
U/T
+ a-mPD-1
Gated off T cells
Untreated
+anti-mPD-1
SSC-A
mLAG3 (RB744-A)
e)
p = 0.0004
***
%TIGIT+ (of T cells)
U/T
+ a-mPD-1
Gated off T cells
Untreated
+anti-mPD-1
SSC-A
mTIGIT (APC-A)
f)
** p = 0.0042
%TIM3+ (of T cells)
U/T
+ a-mPD-1
Gated off T cells
Untreated
+anti-mPD-1
SSC-A
mTIM3 (PE-A)
g)
p < 0.0001
****
%hLAG3+ (of CAR+ T cells)
U/T
+ a-hPD-1
Gated off CAR+ T Cells
Untreated
+anti-hPD-1
SSC-A
hLAG3 (BV605-A)
h)
**
%hTIGIT+ (of CAR+ T cells)
U/T
+ a-hPD-1
Gated off CAR+ T Cells
Untreated
+anti-hPD-1
SSC-A
hTIGIT (BUV395-A)
i)
*
%hTIM3+ (of CAR+ T cells)
U/T
+ a-hPD-1
Gated off CAR+ T Cells
Untreated
+anti-hPD-1
SSC-A
hTIM3 (BV605-A)

Figure 5: PD-1 ablation or signal blockade induces compensatory upregulation of other checkpoint molecules

(a-c) Day 7: mLAG3 (a), mTIGIT (b), mTIM3 (c) expression by flow cytometry in adoptively transferred C57BL/6J WT and PD1$^{-/-}$ engrafted T cells in the spleen of NSG mice.
(d-f) Day 7: mLAG3 (d), mTIGIT (e), mTIM3 (f) expression by flow cytometry in adoptively transferred C57BL/6J T cells engrafted in the spleens of NSG mice with and without anti-mPD-1 treatment.
(g-i) Day 19: hLAG3 (g), hTIGIT (h), and hTIM3 (i) expression by flow cytometry in human CAR T cells from spleens of tumor-bearing mice treated with and without anti-hPD-1 10 days post-infusion.

Data in a-f is representative of two independent experiments (n=4 in all groups). Data in g is combined from 2 independent experiments (g: n=8 for untreated group and n=4 for anti-hPD-1-treated group), from h is combined from 3 independent experiments (n=11 for untreated group and n=7 for anti-hPD-1 treated group), and from I from a single experiment (n=4 for untreated group and n=3 for anti-hPD-1 treated group). Statistical comparisons were performed using a two-tailed unpaired Student's t test without Welch's correction. Data are presented as mean ± standard error of the mean (SEM), with individual data points shown where applicable.

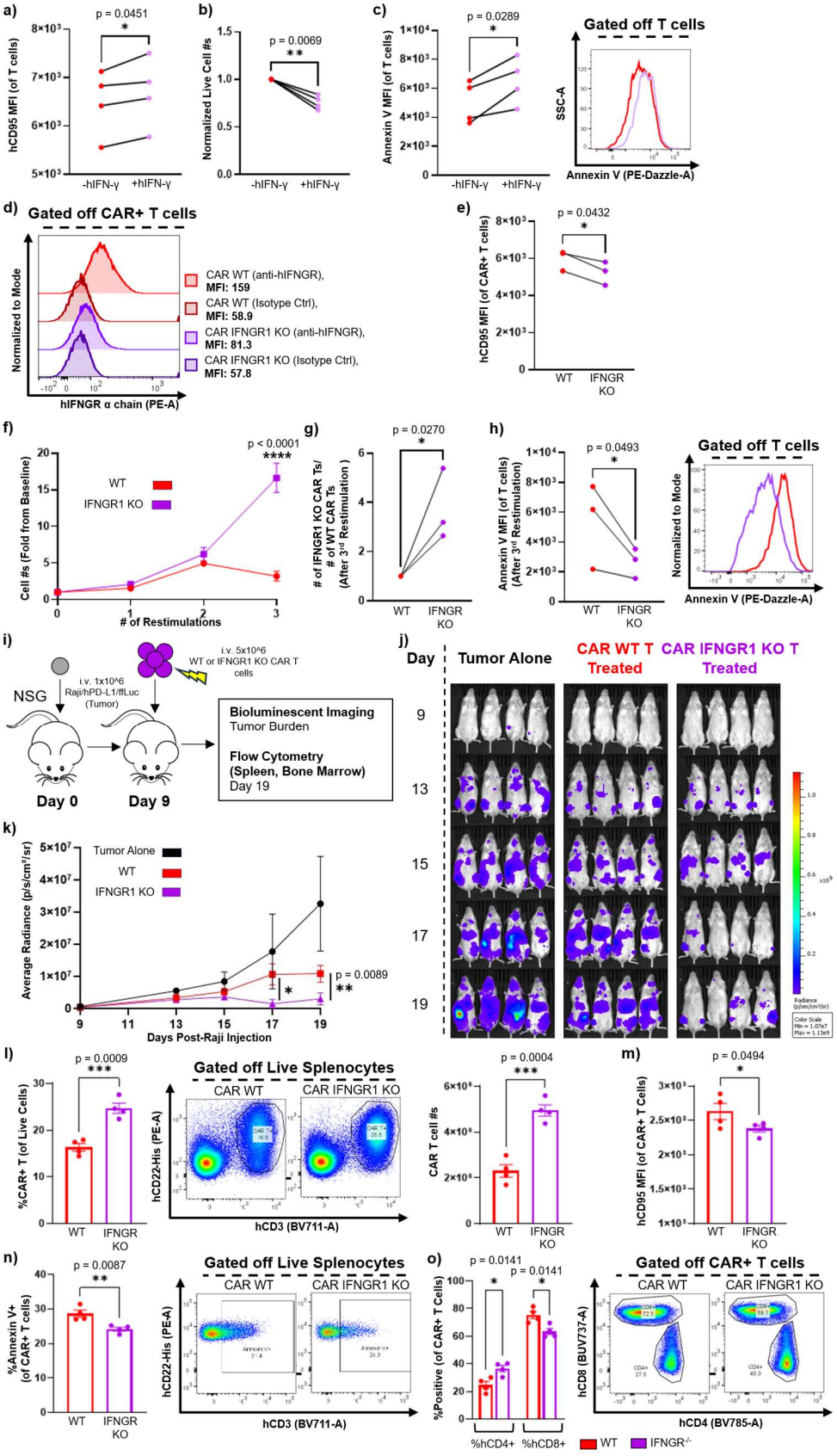
a)
p = 0.0451
*
hCD95 MFI (of T cells)
8×10³
7×10³
6×10³
5×10³
-hIFN-γ
+hIFN-γ
b)
p = 0.0069
**
Normalized Live Cell #s
1.5
1.0
0.5
0.0
-hIFN-γ
+hIFN-γ
c)
p = 0.0289
*
Annexin V MFI (of T cells)
1×10⁴
8×10³
6×10³
4×10³
2×10³
0
-hIFN-γ
+hIFN-γ
Gated off T cells
SSC-A
Annexin V (PE-Dazzle-A)
d)
Gated off CAR+ T cells
Normalized to Mode
CAR WT (anti-hIFNGR), MFI: 159
CAR WT (Isotype Ctrl), MFI: 58.9
CAR IFNGR1 KO (anti-hIFNGR), MFI: 81.3
CAR IFNGR1 KO (Isotype Ctrl), MFI: 57.8
hIFNGR α chain (PE-A)
e)
p = 0.0432
*
hCD95 MFI (of CAR+ T cells)
8×10³
6×10³
4×10³
2×10³
0
WT
IFNGR KO
f)
p < 0.0001
****
WT
IFNGR1 KO
Cell #s (Fold from Baseline)
20
15
10
5
0
0
1
2
3
# of Restimulations
g)
p = 0.0270
*
# of IFNGR1 KO CAR Ts/ # of WT CAR Ts (After 3rd Restimulation)
6
4
2
0
WT
IFNGR KO
h)
p = 0.0493
*
Annexin V MFI (of T cells) (After 3rd Restimulation)
1×10⁴
8×10³
6×10³
4×10³
2×10³
0
WT
IFNGR KO
Gated off T cells
Normalized to Mode
Annexin V (PE-Dazzle-A)
i)
NSG
i.v. 1x10^6 Raji/hPD-L1/ffLuc (Tumor)
i.v. 5x10^6 WT or IFNGR1 KO CAR T cells
Bioluminescent Imaging
Tumor Burden
Flow Cytometry
(Spleen, Bone Marrow)
Day 19
Day 0
Day 9
j)
Day
Tumor Alone
CAR WT T Treated
CAR IFNGR1 KO T Treated
9
13
15
17
19
k)
Tumor Alone
WT
IFNGR1 KO
Average Radiance (p/s/cm²/sr)
5×10⁷
4×10⁷
3×10⁷
2×10⁷
1×10⁷
0
p = 0.0089
**
*
9
11
13
15
17
19
Days Post-Raji Injection
l)
p = 0.0009
***
%CAR+ T (of Live Cells)
30
20
10
0
WT
IFNGR KO
Gated off Live Splenocytes
CAR WT
CAR IFNGR1 KO
hCD22-His (PE-A)
hCD3 (BV711-A)
p = 0.0004
***
CAR T cell #s
6×10⁶
4×10⁶
2×10⁶
0
WT
IFNGR KO
m)
p = 0.0494
*
hCD95 MFI (of CAR+ T Cells)
3×10³
2.5×10³
2×10³
1.5×10³
1×10³
WT
IFNGR KO
n)
p = 0.0087
**
%Annexin V+ (of CAR+ T cells)
40
30
20
10
0
WT
IFNGR KO
Gated off Live Splenocytes
CAR WT
CAR IFNGR1 KO
hCD22-His (PE-A)
hCD3 (BV711-A)
o)
p = 0.0141
p = 0.0141
*
*
%Positive (of CAR+ T Cells)
100
80
60
40
20
0
%hCD4+
%hCD8+
Gated off CAR+ T cells
CAR WT
CAR IFNGR1 KO
hCD8 (BUV737-A)
hCD4 (BV785-A)
WT
IFNGR-/-

Figure 6: IFNGR knockout human CAR T cells show reduced AICD and prolonged persistence correlated with increased anti-tumor efficacy

(a) hCD95 expression by flow cytometry in WT CAR T cells with and without 24 hours of rhIFN-γ treatment.

(b) Cell counts of TransAct-activated (24 hours) WT CAR T cells treated with and without initial rhIFN-γ treatment (normalized to # of CAR T cells without rhIFN-γ treatment).

(c) Annexin V binding by flow cytometry of TransAct-activated (24 hours) WT CAR T cells treated with and without initial rhIFN-γ treatment.

(d) Validation of IFNGR1 KO CAR T cells by flow cytometry.

(e) hCD95 expression in WT and IFNGR1 KO CAR T cells by flow cytometry 3 days after co-culture with irradiated Raji WT cells.

(f) Cell counts of WT and IFNGR1 KO CAR T cells after 3 rounds of restimulation with TransAct.

(g) Fold difference in IFNGR1 KO-to-WT CAR T cells after 3 rounds of restimulation with TransAct.

(h) Annexin V binding by flow cytometry in WT and IFNGR1 KO CAR T cells after 3 rounds of restimulation with TransAct.

(i) Experimental schematic: Raji/hPD-L1 tumor-bearing NSG mice were treated with human hCD19/hCD20/hCD22 tri-specific WT or IFNGR1 KO CAR T cells.

(j, k) Tumor burden by bioluminescent imaging after WT or IFNGR1 KO CAR T cell treatment.

(l) Day 19: frequency of CAR+ T cells by flow cytometry in bone marrow of mice treated with WT and IFNGR1 KO CAR T cells 10 days post-CAR T infusion.
(m, n) Day 19: expression of hCD95 (m) and annexin V binding (n) in WT and IFNGR1 KO CAR T cells from bone marrow of treated mice by flow cytometry 10 days post-CAR T infusion.
(o) Day 19: proportion of hCD4+ and hCD8+ WT and IFNGR1 KO CAR T cells from bone marrow of treated mice by flow cytometry 10 days post-CAR T infusion.

Data consists in a-c CAR WT T cells generated from 4 individual donors (n=4) and in e, g, and h, CAR WT and IFNGR1 KO T cells from 3 different donors (n=3), and in f is representative two independent experiments co-cultured in technical triplicates, and in j-o is representative of two independent experiments (n=4 per group). Statistical comparisons were performed either using a two-tailed (l, n, o) or one-tailed (m) unpaired Student's t test without Welch's correction, a two-tailed paired (a-c) or ratio paired (e, g-h) Student's t test, or a two-way ANOVA with Tukey's correction (f, k) for multiple comparisons. Data are presented as mean ± standard error of the mean (SEM), with individual data points shown where applicable.

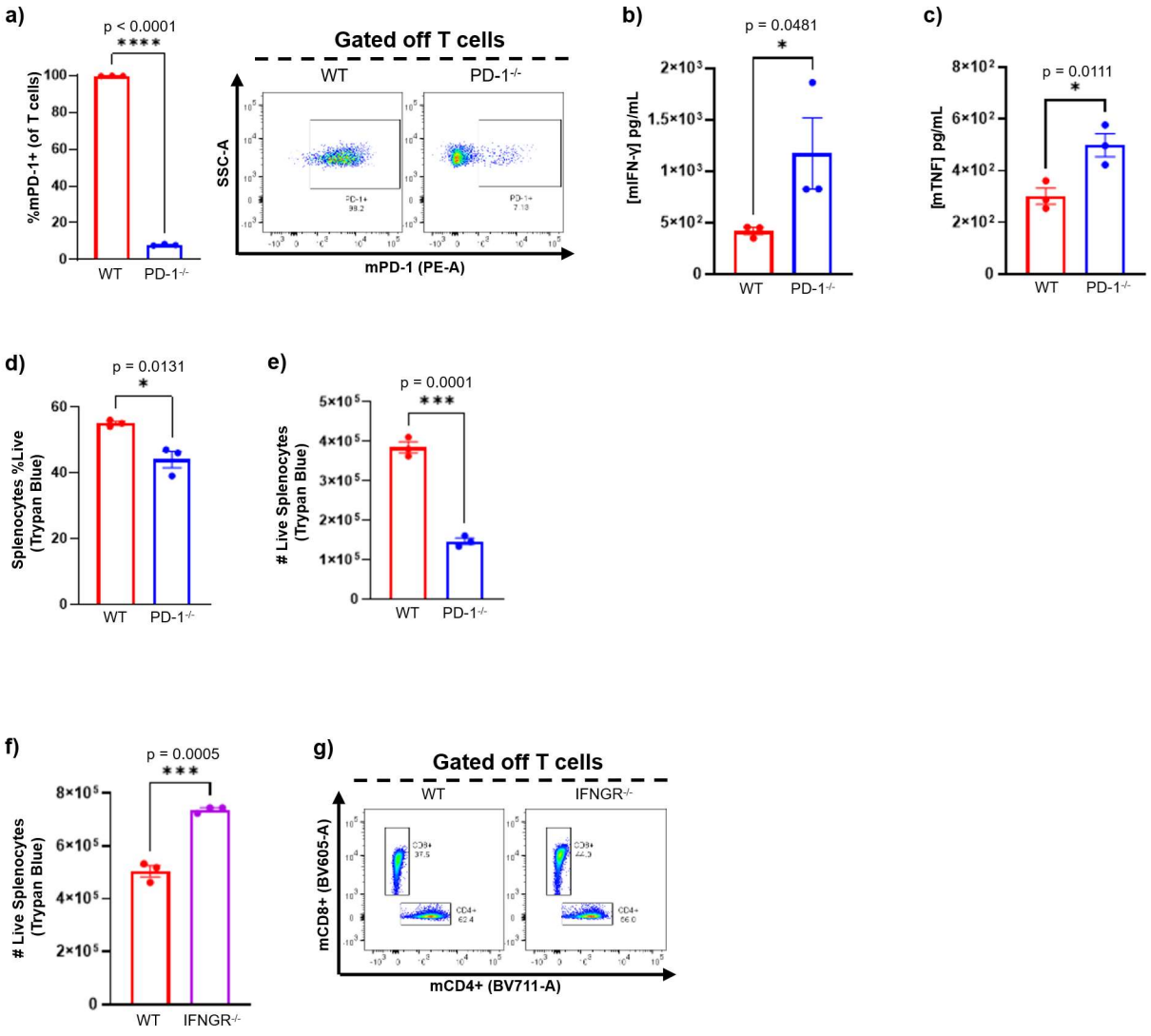
a)
p < 0.0001
****
%mPD-1+ (of T cells)
WT
PD-1-/-
Gated off T cells
WT
PD-1-/-
SSC-A
mPD-1 (PE-A)
b)
p = 0.0481
*
[mIFN-γ] pg/mL
c)
p = 0.0111
*
[mTNF] pg/mL
d)
p = 0.0131
*
Splenocytes %Live (Trypan Blue)
e)
p = 0.0001
***
Live Splenocytes (Trypan Blue)
f)
p = 0.0005
***
Live Splenocytes (Trypan Blue)
IFNGR-/-
g)
Gated off T cells
WT
IFNGR-/-
mCD8+ (BV605-A)
mCD4+ (BV711-A)

Supplementary Figure 1: Additional phenotype data of activated PD-1$^{-/-}$ and IFNGR$^{-/-}$ mouse T cells *in vitro*

(a) Expression of PD-1 in conA-activated WT and PD-1$^{-/-}$ C57BL/6 T cells by flow cytometry.

(b, c) IFN-γ & TNF levels of WT and PD-1$^{-/-}$ C57BL/6 splenocytes after conA activation measured by ELISA.

(d, e) Live splenocyte counts (d) and viability (e) of conA-activated WT and PD-1$^{-/-}$ C57BL/6 splenocytes by trypan blue exclusion.

(f) Live splenocyte counts of conA-activated WT and IFNGR$^{-/-}$ C57BL/6 splenocytes by trypan blue exclusion.

(g) Baseline mCD4+ and mCD8+ percentages of WT and IFNGR$^{-/-}$ T cells by flow cytometry.

Data is representative of two independent experiments performed in technical triplicates. Statistical comparisons were performed using either a two-tailed (a, c, d, e, f) or one-tailed unpaired Student's t test (b) without Welch's correction. Data are presented as mean ± standard error of the mean (SEM), with individual data points shown where applicable.

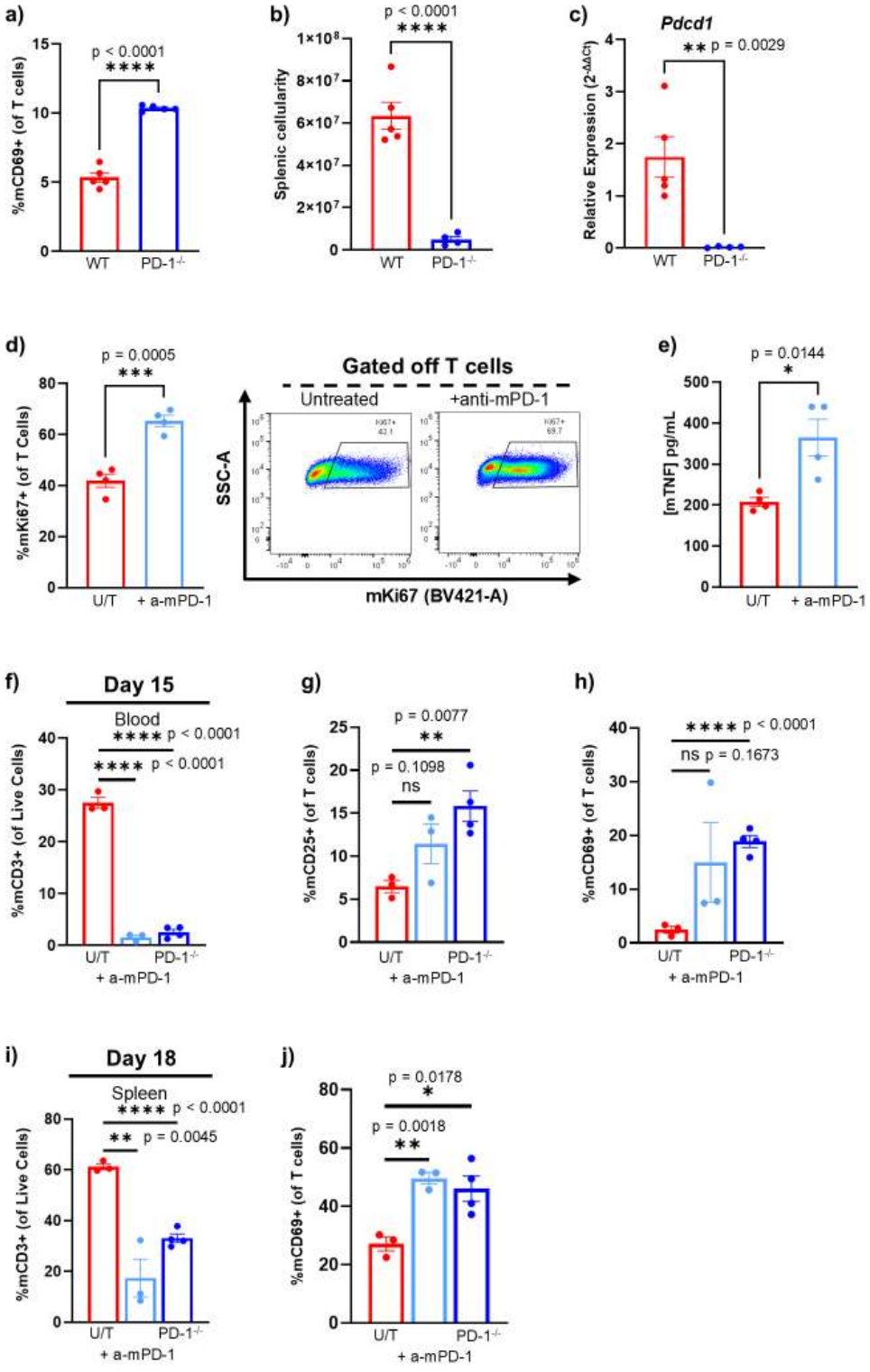
a)
%mCD69+ (of T cells)
p < 0.0001
****
WT
PD-1-/-
b)
Splenic cellularity
p < 0.0001
****
c)
Pdcd1
Relative Expression (2-ΔΔCt)
** p = 0.0029
d)
%mKi67+ (of T Cells)
p = 0.0005
***
U/T
+ a-mPD-1
Gated off T cells
Untreated
+anti-mPD-1
SSC-A
mKi67 (BV421-A)
e)
[mTNF] pg/mL
p = 0.0144
*
f)
Day 15
Blood
%mCD3+ (of Live Cells)
**** p < 0.0001
g)
%mCD25+ (of T cells)
p = 0.0077
**
p = 0.1098
ns
h)
%mCD69+ (of T cells)
**** p < 0.0001
ns p = 0.1673
i)
Day 18
Spleen
** p = 0.0045
j)
p = 0.0178
*
p = 0.0018

Supplementary Figure 2: Additional phenotype of donor WT, PD-1$^{-/-}$, and anti-mouse PD-1-treated WT C57BL/6 T cells from allogenic adoptive transfer experiments

(a) mCD69 expression by flow cytometry in donor C57BL/6J WT and PD-1$^{-/-}$ T cells in the blood of recipient NSG mice 7 days after engraftment.
(b) Splenic cellularity of recipient NSG mice receiving adoptive transfer of C57BL/6J WT and PD-1$^{-/-}$ T cells 21 days after engraftment.
(c) mPD-1 expression by qPCR of recipient NSG spleens receiving adoptive transfer of C57BL/6J WT and PD-1$^{-/-}$ T cells 21 days after engraftment.
(d) mKi67 expression in C57BL/6J T cells engrafted in the spleens of NSG mice with and without anti-mPD-1 treatment 7 days after treatment.
C57BL/6J engrafted T cell numbers in the spleen of NSG mice 7 days after treatment with and without anti-mPD-1 treatment.
(e) TNF from the serum of NSG mice engrafted with C57BL/6J WT T cells with and without anti-mPD-1 treatment 7 days after treatment.
(f) Percent CD3+ donor C57BL/6J WT, PD-1$^{-/-}$, or WT with anti-mPD-1 treatment T cells (gated off live) in blood of recipient NSG mice 21 days after engraftment.
(g, h) mCD25 (g) and mCD69 (h) expression in donor C57BL/6J WT, PD-1$^{-/-}$, or WT with anti-mPD-1 treatment T cells in blood of recipient NSG mice 21 days after engraftment.
(i) Percent CD3+ donor C57BL/6J WT, PD-1$^{-/-}$, or WT with anti-mPD-1 treatment T cells (gated off live) in spleen of recipient NSG mice 21 days after engraftment.

(j) mCD69 expression in donor C57BL/6J WT, PD-1$^{-/-}$, or WT with anti-mPD-1 treatment T cells in blood of recipient NSG mice 21 days after engraftment.

Data in a-c is representative of two independent experiments (n=4 or 5 per group), in d-e is representative of two independent experiments (n=4 per group), and in f-j is from a single experiment (n=3 or 4 per group). Statistical comparisons were performed using a two-tailed unpaired Student's t test without Welch's correction. Data are presented as mean ± standard error of the mean (SEM), with individual data points shown where applicable.

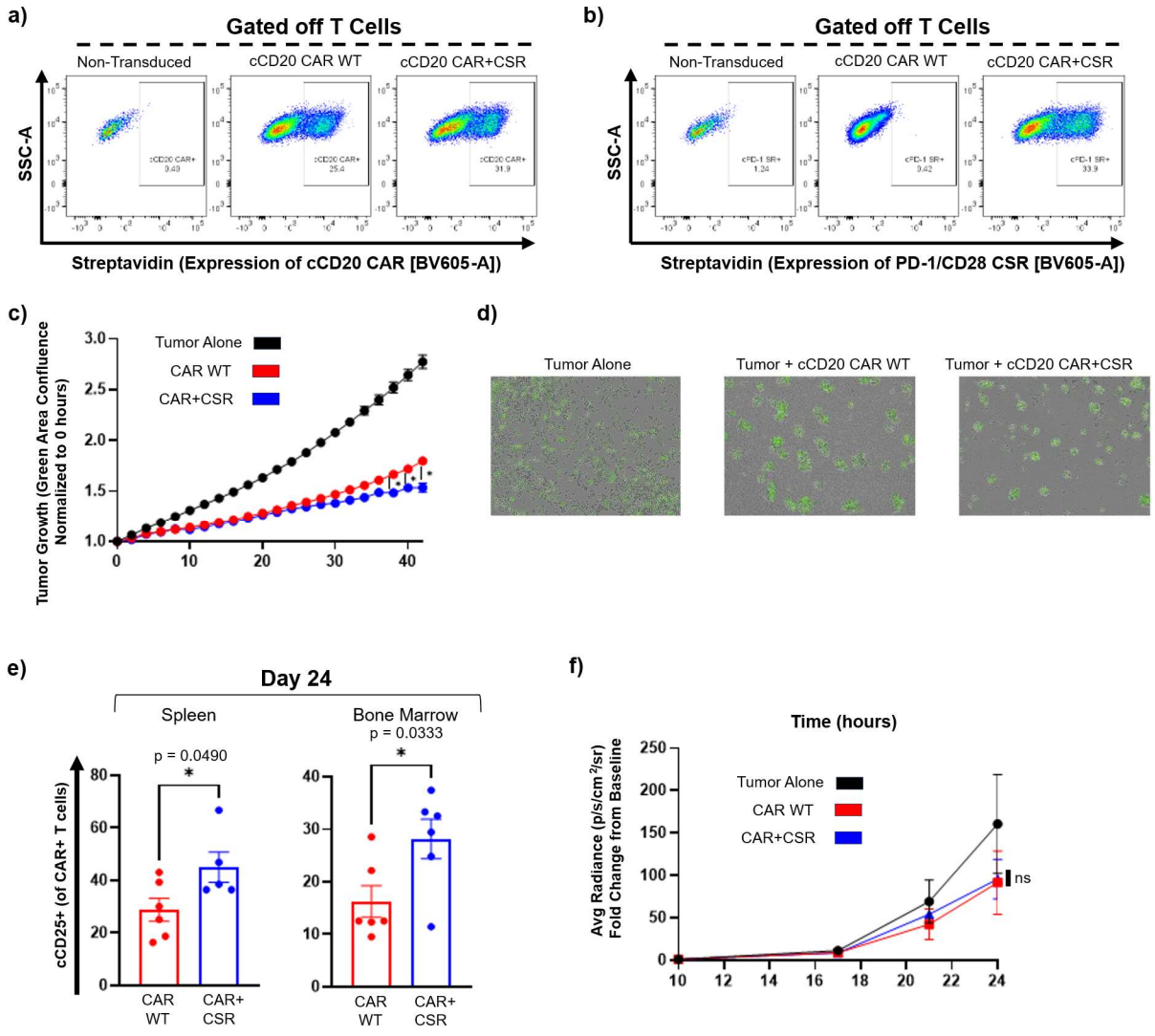
a)
Gated off T Cells
Non-Transduced
cCD20 CAR WT
cCD20 CAR+CSR
SSC-A
Streptavidin (Expression of cCD20 CAR [BV605-A])
b)
Gated off T Cells
Non-Transduced
cCD20 CAR WT
cCD20 CAR+CSR
SSC-A
Streptavidin (Expression of PD-1/CD28 CSR [BV605-A])
c)
Tumor Growth (Green Area Confluence Normalized to 0 hours)
Tumor Alone
CAR WT
CAR+CSR
d)
Tumor Alone
Tumor + cCD20 CAR WT
Tumor + cCD20 CAR+CSR
e)
Day 24
Spleen
Bone Marrow
p = 0.0490
p = 0.0333
cCD25+ (of CAR+ T cells)
CAR WT
CAR+ CSR
f)
Time (hours)
Avg Radiance (p/s/cm²/sr) Fold Change from Baseline
Tumor Alone
CAR WT
CAR+CSR
ns

Supplementary Figure 3: Additional phenotype data of cCD20 CAR WT and cCD20 CAR+CSR T cells

(a) *In vivo* pre-infusion CAR transduction efficiency between CAR WT and CAR+CSR T cells.

(b) *In vivo* pre-infusion CSR transduction efficiency between CAR WT and CAR+CSR T cells.

(c-d) *In vitro* cytotoxicity of CAR WT and CAR+CSR T cells against K562/cCD20/cPD-L1/GFP-ffLuc cells via live cell imaging using an Incucyte® including representational images of tumor killing (d).

(e) Day 24: cCD25 expression on CAR WT and CAR+CSR T cells in bone marrow of tumor-bearing mice 14 days after infusion.

(f) Tumor (K562/cCD20/cPD-L1/GFP-ffLuc) burden of NSG mice treated with CAR WT and CAR+CSR T cells over time.

Data in e-f is combined from two independent experiments (n=5 or 6 per group). Statistical comparisons were performed using a two-tailed unpaired Student's t test without Welch's correction (e) or 2-way analysis of variance (ANOVA) with Tukey's multiple comparisons test (c, f). Data are presented as mean ± standard error of the mean (SEM), with individual data points shown where applicable.

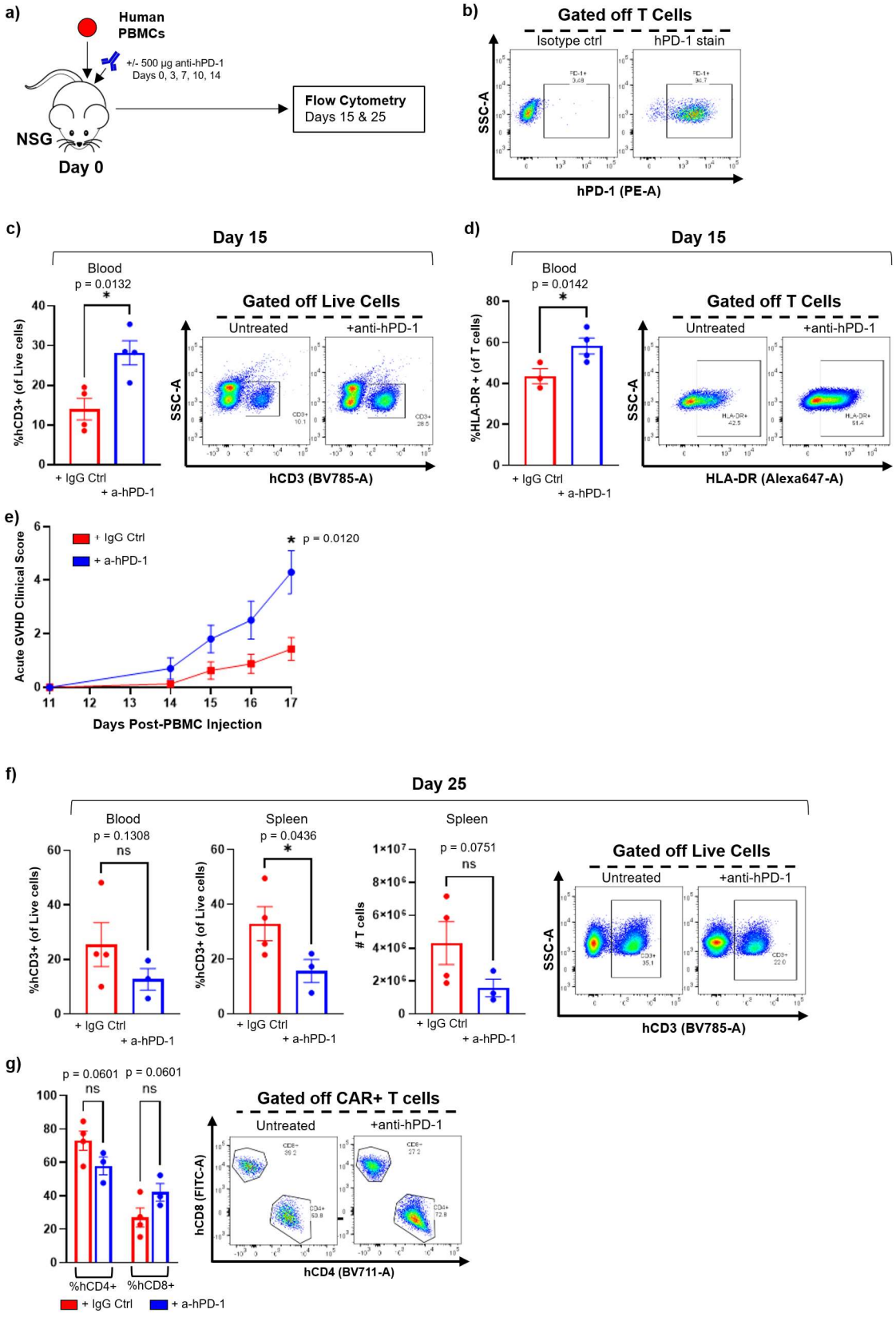
a)
Human PBMCs
+/- 500 µg anti-hPD-1
Days 0, 3, 7, 10, 14
NSG
Day 0
Flow Cytometry
Days 15 & 25
b)
Gated off T Cells
Isotype ctrl
hPD-1 stain
SSC-A
hPD-1 (PE-A)
c)
Day 15
Blood
p = 0.0132
%hCD3+ (of Live cells)
+ IgG Ctrl
+ a-hPD-1
Gated off Live Cells
Untreated
+anti-hPD-1
SSC-A
hCD3 (BV785-A)
d)
Day 15
Blood
p = 0.0142
%HLA-DR + (of T cells)
+ IgG Ctrl
+ a-hPD-1
Gated off T Cells
Untreated
+anti-hPD-1
SSC-A
HLA-DR (Alexa647-A)
e)
+ IgG Ctrl
+ a-hPD-1
p = 0.0120
Acute GVHD Clinical Score
Days Post-PBMC Injection
f)
Day 25
Blood
p = 0.1308
ns
%hCD3+ (of Live cells)
Spleen
p = 0.0436
%hCD3+ (of Live cells)
Spleen
p = 0.0751
ns
T cells
+ IgG Ctrl
+ a-hPD-1
Gated off Live Cells
Untreated
+anti-hPD-1
SSC-A
hCD3 (BV785-A)
g)
p = 0.0601
ns
p = 0.0601
ns
%hCD4+
%hCD8+
+ IgG Ctrl
+ a-hPD-1
Gated off CAR+ T cells
Untreated
+anti-hPD-1
hCD8 (FITC-A)
hCD4 (BV711-A)

Supplementary Figure 4: PD-1 blockade in xenogeneic activated human T cells results in increased activation but also reduced persistence

(a) Experimental schematic: NSG mice engrafted with human PBMCs.
(b) Day 15: representative flow expression of hPD-1 in human T cells engrafted in the blood of NSG mice without anti-hPD-1 15 days after infusion.
(c) Day 15: human T cell frequency by flow cytometry in the blood of NSG mice with and without anti-hPD-1 15 days after infusion.
(d) Day 15: expression of HLA-DR in human T cells engrafted in the blood of NSG mice with and without anti-hPD-1 15 days after infusion.
(e) Acute GVHD clinical scoring of NSG mice engrafted with human PBMCs with and without anti-hPD-1.
(f) Day 25: human T cell frequency by flow cytometry in the blood and spleens of NSG mice with and without anti-hPD-1 25 days after infusion.
(g) Day 25: proportion of hCD4+ and hCD8+ T cells in spleens of mice treated with and without anti-hPD-1 25 days after infusion.

Data in c-d and f-g is representative of 2 independent experiments (n=3 or 4 per group) and in e is combined from 3 experiments (n=10 total). Statistical comparisons were performed either using a two-tailed (c, d) or one-tailed (f, g) unpaired Student's t test without Welch's correction or two-way ANOVA (e). Data are presented as mean ± standard error of the mean (SEM), with individual data points shown where applicable.

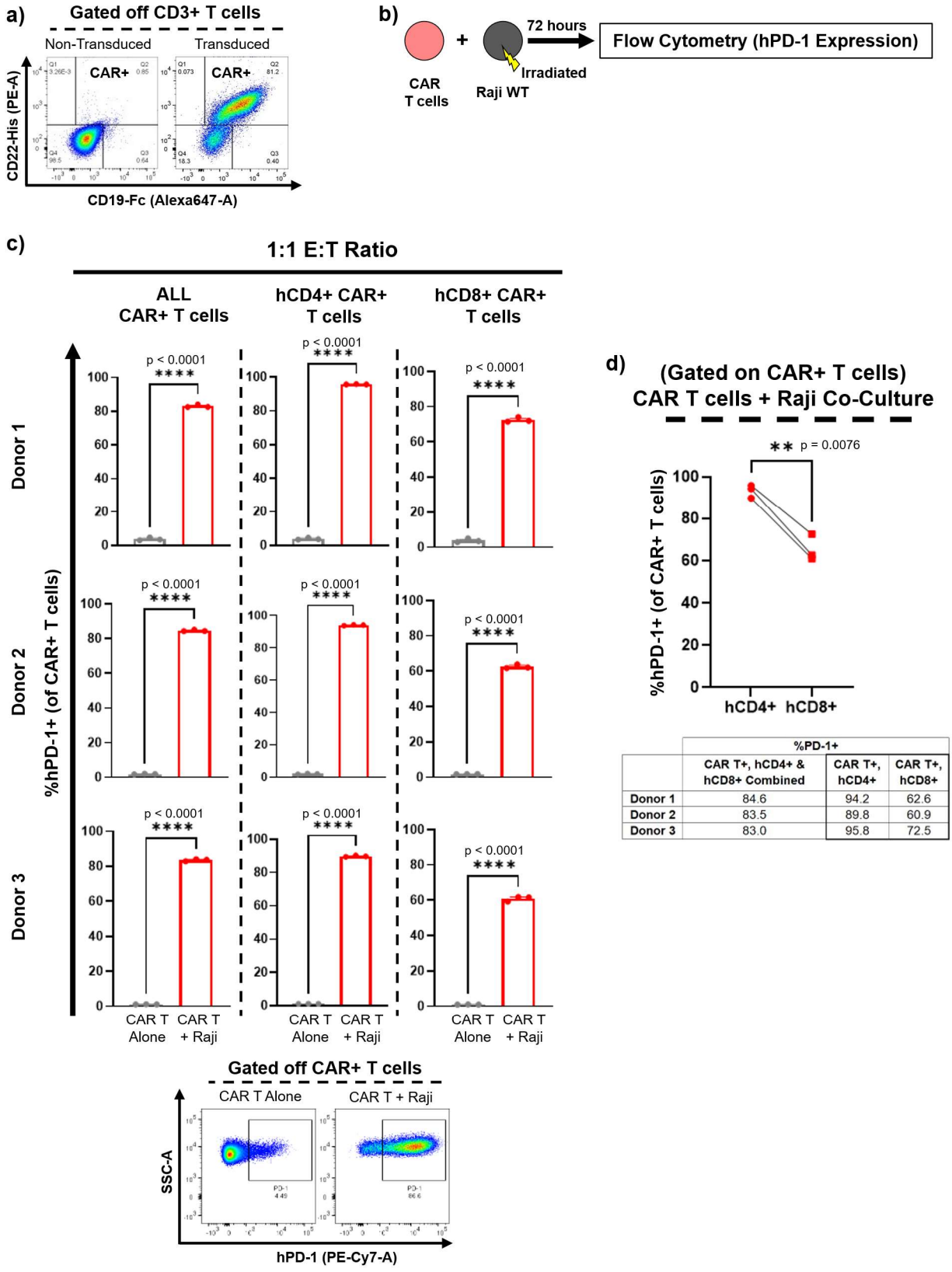

	%PD-1+		
	CAR T+, hCD4+ & hCD8+ Combined	CAR T+, hCD4+	CAR T+, hCD8+
Donor 1	84.6	94.2	62.6
Donor 2	83.5	89.8	60.9
Donor 3	83.0	95.8	72.5

Supplementary Figure 5: Human CAR T cells upregulate PD-1 expression upon antigen stimulation; CD4+ CAR+ T cells more so than CD8+ CAR+ T cells

(a) Flow cytometry validation of hCD19/hCD20/hCD22-trispecific CAR T cell transduction efficiency using hCD19-Fc and hCD22-His recombinant proteins with subsequent respective secondary antibody staining.
(b) Schematic (*in vitro*): CAR T cells from 3 donors were incubated at a 1:1 E:T ratio with irradiated Raji cells for 3 days and evaluated for hPD-1 expression by flow cytometry
(c) Flow cytometry staining of CAR T cels for hPD-1 expression after co-culturing with Raji cells for 72 hours. Experiments were performed in technical triplicates for each donor.
(d) Comparison of hPD-1 expression (by flow cytometry) between hCD4+CAR+ and hCD8+CAR+ T cells.

Data is from CAR T cells generated from 3 different donors (n=3) and co-cultured in technical triplicates. Statistical comparisons were performed either using a two-tailed unpaired Student's t test without Welch's correction (c) or a two-tailed paired t test (d). Data are presented as mean ± standard error of the mean (SEM), with individual data points shown where applicable.

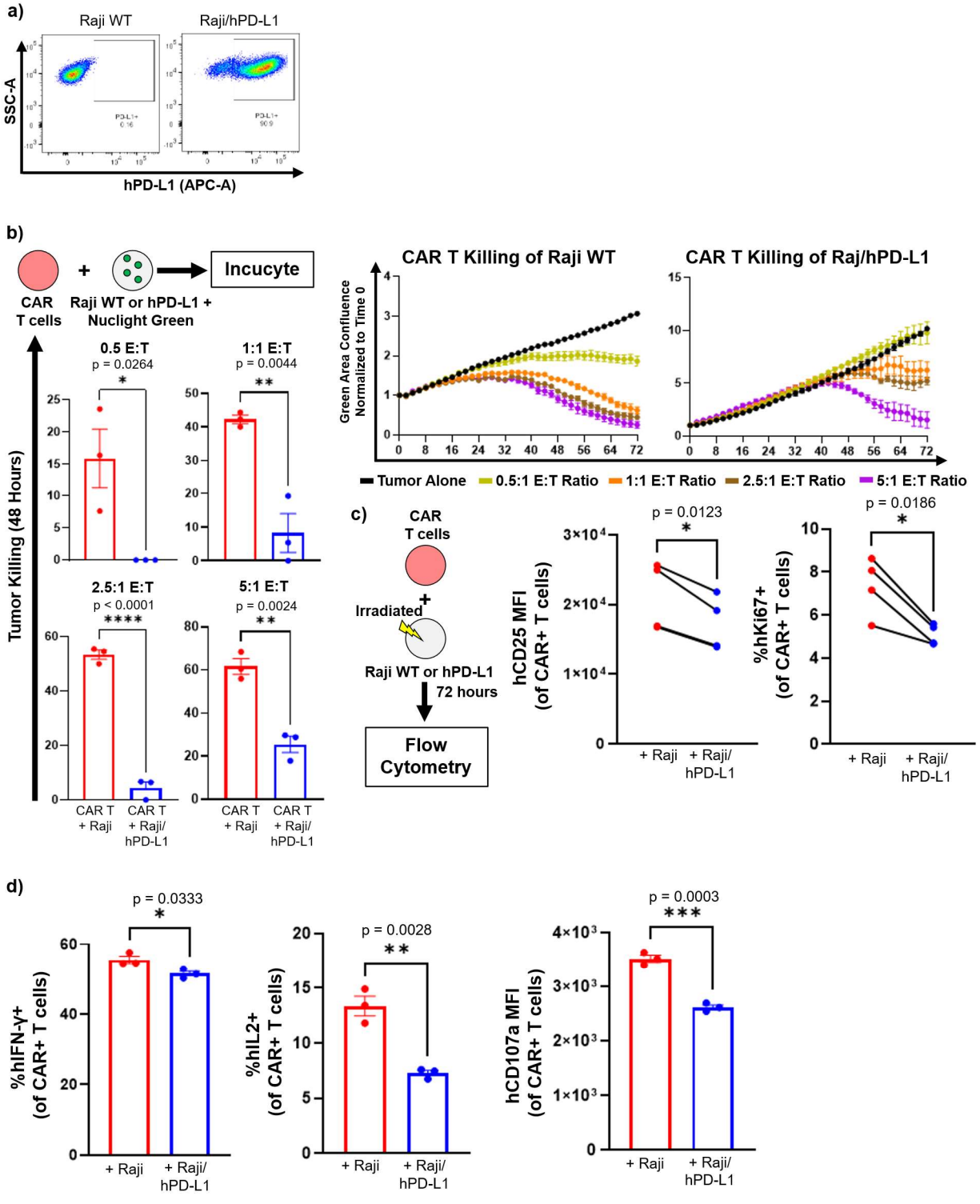
a)
Raji WT
Raji/hPD-L1
SSC-A
hPD-L1 (APC-A)
b)
CAR T cells
Raji WT or hPD-L1 + Nuclight Green
Incucyte
Tumor Killing (48 Hours)
0.5 E:T
p = 0.0264
1:1 E:T
p = 0.0044
2.5:1 E:T
p < 0.0001
5:1 E:T
p = 0.0024
CAR T + Raji
CAR T + Raji/ hPD-L1
CAR T Killing of Raji WT
CAR T Killing of Raj/hPD-L1
Green Area Confluence Normalized to Time 0
Tumor Alone
0.5:1 E:T Ratio
1:1 E:T Ratio
2.5:1 E:T Ratio
5:1 E:T Ratio
c)
CAR T cells
Irradiated
Raji WT or hPD-L1
72 hours
Flow Cytometry
hCD25 MFI (of CAR+ T cells)
p = 0.0123
%hKi67+ (of CAR+ T cells)
p = 0.0186
+ Raji
+ Raji/ hPD-L1
d)
%hIFN-γ+ (of CAR+ T cells)
p = 0.0333
%hIL2+ (of CAR+ T cells)
p = 0.0028
hCD107a MFI (of CAR+ T cells)
p = 0.0003

Supplementary Figure 6: PD-L1 expression on tumor cells downregulates CAR T cell effector function

(a) Flow cytometry staining of Raji WT and PD-L1-engineered cells for PD-L1 expression.
(b) Raji WT or Raji/hPD-L1 cells engineered with Nuclight Green were incubated in an Incucyte® Live-Cell Analysis System with fluorescence measured over time. Tumor killing was computed by the following formula: (normalized green area [tumor+CAR T cells])/(normalized green area [tumor alone]) * 100.
(c) CAR T cells from 4 donors were co-cultured with either Raji WT or PD-L1 expressing cells for 72 hours. Expression of the activation marker CD25 and the proliferation marker Ki67 by flow cytometry.
(d) IFN-γ, IL2, and CD107a expression of CAR T cells by flow cytometry after co-culturing.

Data in b and d is representative of two independent experiments using the same donor CAR T cells co-cultured in technical triplicates. Data in c consists of CAR T cells made from 4 different donors (n=4). Statistical comparisons were performed either using a two-tailed unpaired (b, d) or paired (c) Student's t test without Welch's correction. Data are presented as mean ± standard error of the mean (SEM), with individual data points shown where applicable.

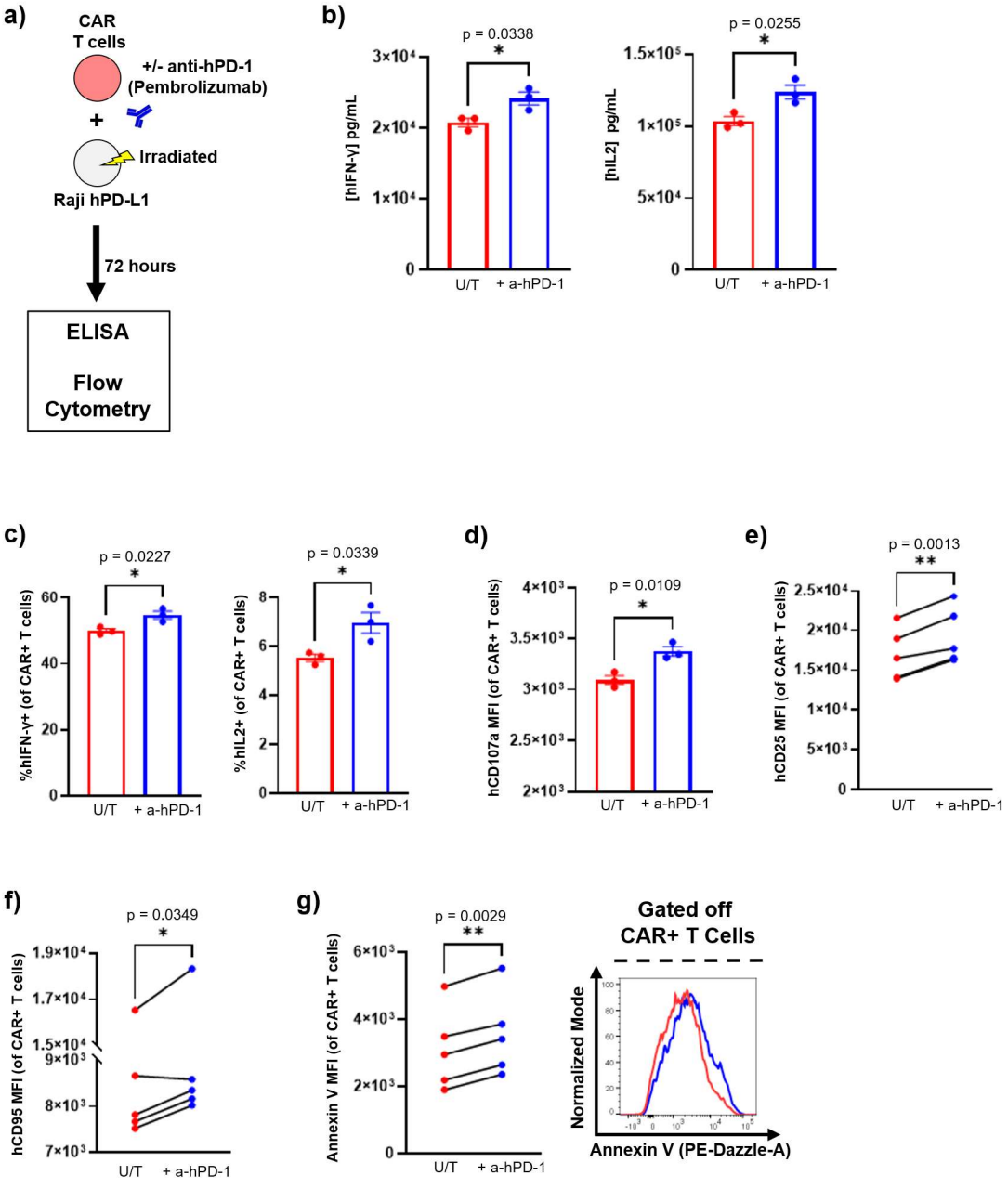
a)
CAR
T cells
+/- anti-hPD-1
(Pembrolizumab)
+
Irradiated
Raji hPD-L1
72 hours
ELISA
Flow
Cytometry
b)
p = 0.0338
*
[hIFN-γ] pg/mL
3×10⁴
2×10⁴
1×10⁴
0
U/T
+ a-hPD-1
p = 0.0255
*
[hIL2] pg/mL
1.5×10⁵
1×10⁵
5×10⁴
0
U/T
+ a-hPD-1
c)
p = 0.0227
*
%hIFN-γ+ (of CAR+ T cells)
60
40
20
0
U/T
+ a-hPD-1
p = 0.0339
*
%hIL2+ (of CAR+ T cells)
8
6
4
2
0
U/T
+ a-hPD-1
d)
p = 0.0109
*
hCD107a MFI (of CAR+ T cells)
4×10³
3.5×10³
3×10³
2.5×10³
2×10³
U/T
+ a-hPD-1
e)
p = 0.0013
**
hCD25 MFI (of CAR+ T cells)
2.5×10⁴
2×10⁴
1.5×10⁴
1×10⁴
5×10³
0
U/T
+ a-hPD-1
f)
p = 0.0349
*
hCD95 MFI (of CAR+ T cells)
1.9×10⁴
1.7×10⁴
1.5×10⁴
9×10³
8×10³
7×10³
U/T
+ a-hPD-1
g)
p = 0.0029
**
Annexin V MFI (of CAR+ T cells)
6×10³
4×10³
2×10³
0
U/T
+ a-hPD-1
Gated off
CAR+ T Cells
Normalized Mode
Annexin V (PE-Dazzle-A)

Supplementary Figure 7: *In vitro,* blocking PD-1/PD-L1 signaling in CAR T cells increases activation but also apoptosis

(a) Experimental Schematic: CAR T cells were co-cultured with Raji hPD-L1 expressing cells for 72 hours with and without anti-hPD-1 and ELISA and flow cytometry were performed.
(b, c) hIFN-γ and hIL2 production detected by ELISA in supernatants of co-cultured cells (b) and by flow cytometry (c).
(d, e) hCD107a and hCD25 expression by flow cytometry in CAR T cells after co-culture
(f, g) hCD95 expression and annexin V binding by flow cytometry in CAR T cells after co-culture.

Data in b-d is representative of two independent experiments using the same donor CAR T cells co-cultured in technical triplicates. Data in e-g consists of CAR T cells made from 5 different donors (n=5). Statistical comparisons were performed either using a two-tailed unpaired Student's t test without Welch's correction (b-d) or a two-tailed paired t test (e-g). Data are presented as mean ± standard error of the mean (SEM), with individual data points shown where applicable.

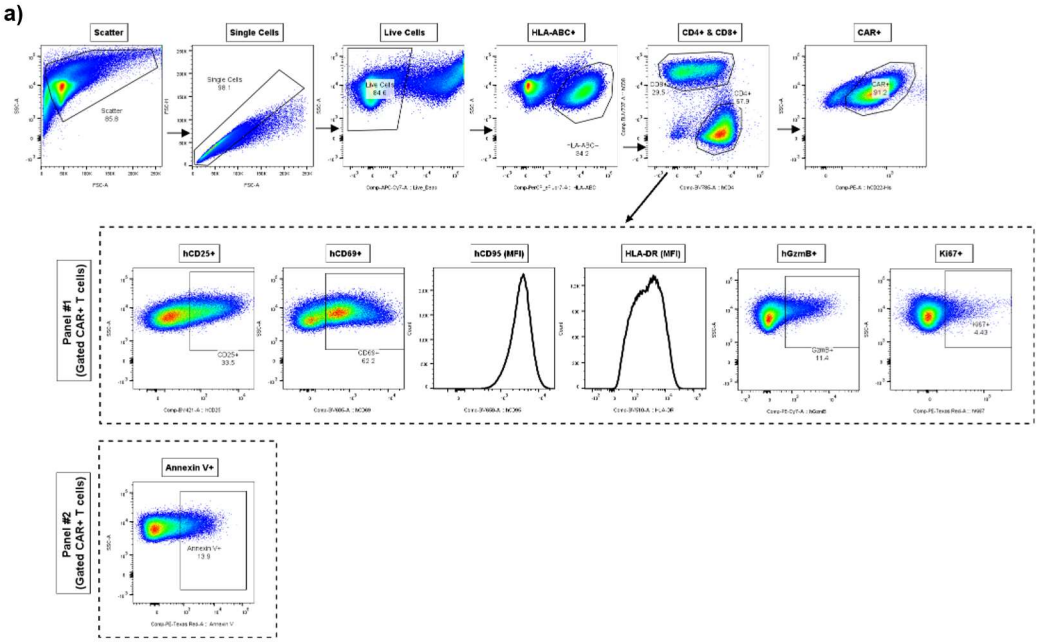
a)
Scatter
Single Cells
Live Cells
HLA-ABC+
CD4+ & CD8+
CAR+
Panel #1 (Gated CAR+ T cells)
hCD25+
hCD69+
hCD95 (MFI)
HLA-DR (MFI)
hGzmB+
Ki67+
Panel #2 (Gated CAR+ T cells)
Annexin V+

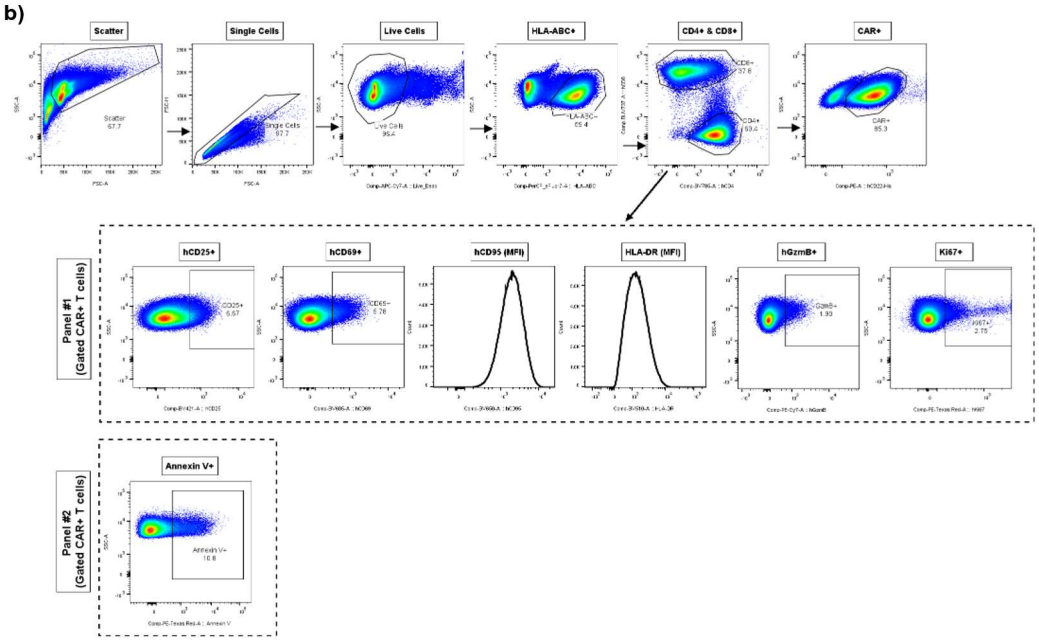
b)
Scatter
Single Cells
Live Cells
HLA-ABC+
CD4+ & CD8+
CAR+
Panel #1 (Gated CAR+ T cells)
hCD25+
hCD69+
hCD95 (MFI)
HLA-DR (MFI)
hGzmB+
Ki67+
Panel #2 (Gated CAR+ T cells)
Annexin V+

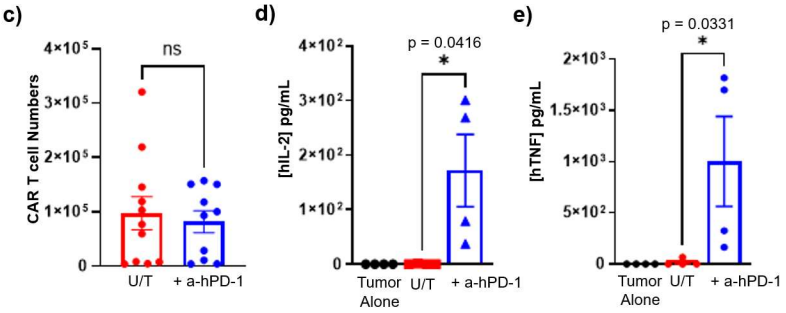
c)
CAR T cell Numbers
ns
U/T
+ a-hPD-1
d)
[hIL-2] pg/mL
p = 0.0416
*
Tumor Alone
U/T
+ a-hPD-1
e)
[hTNF] pg/mL
p = 0.0331
*
Tumor Alone
U/T
+ a-hPD-1

Supplementary Figure 8: Gating strategy for human CAR T cell phenotype; some additional phenotype of CAR T cells from tumor-bearing mice treated with and without anti-hPD-1

(a) Gating strategy for phenotyping CAR T cells from bone marrow of tumor-bearing mice.
(b) Gating strategy for phenotyping CAR T cells from spleen of tumor-bearing mice.
(c) Day 15: CAR T cell numbers in bone marrow of tumor-bearing mice treated with and without anti-hPD-1 6 days post-CAR T infusion.
(d, e) Day 17 (8 days post-CAR T infusion) serum cytokine levels of hIL2 (d) and hTNF (e) by CBA from tumor-bearing mice treated with and without anti-hPD-1.

Data in c is combined from 3 independent experiments (n=11 in untreated group and n=10 in anti-hPD-1-treated group) and in d-e is from a single experiment (n=4 in all groups). Statistical comparisons were performed either using a two-tailed (c, d) or one-tailed (e) unpaired Student's t test without Welch's correction. Data are presented as mean ± standard error of the mean (SEM), with individual data points shown where applicable.

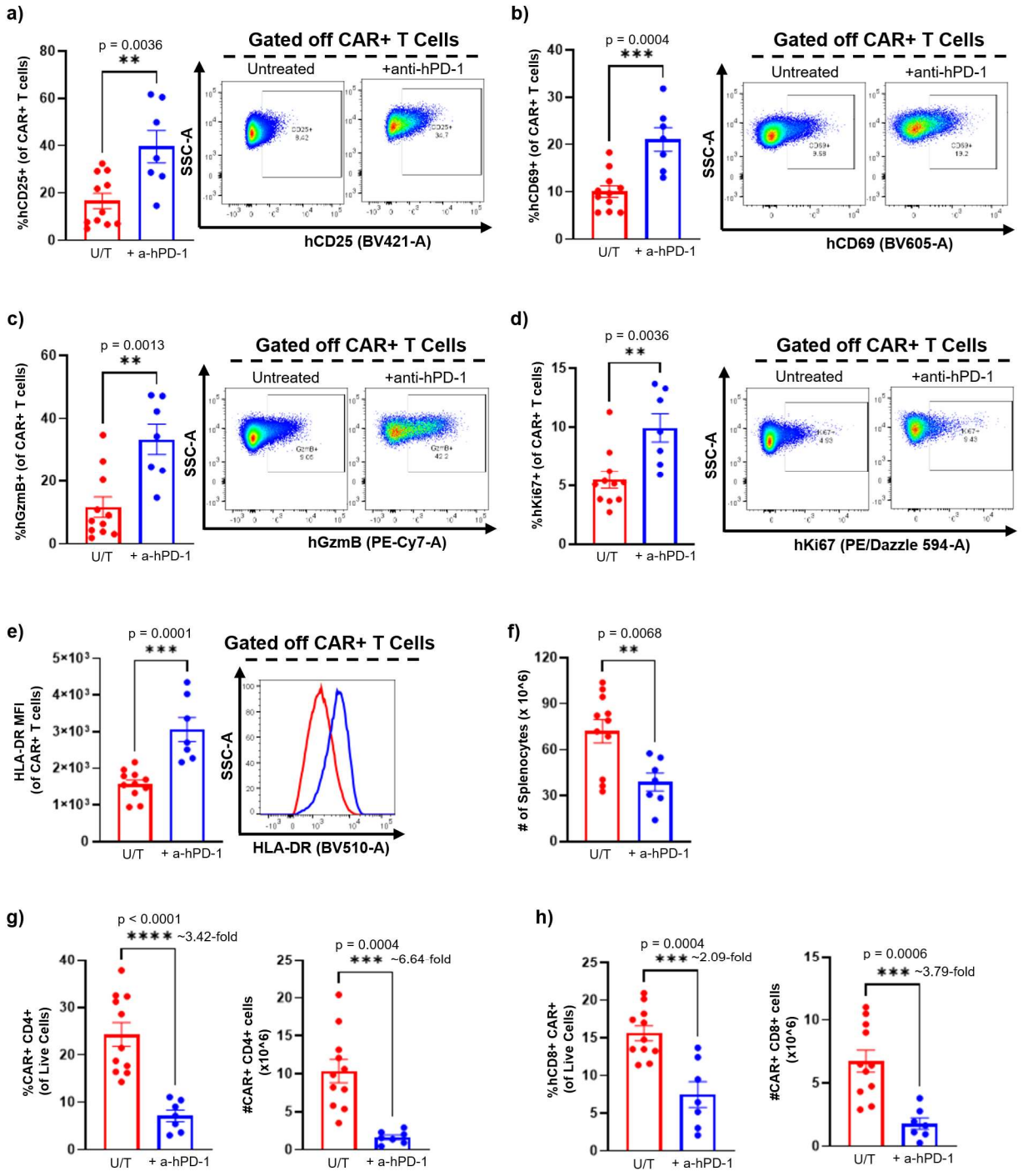
a)
p = 0.0036
**
%hCD25+ (of CAR+ T cells)
U/T
+ a-hPD-1
Gated off CAR+ T Cells
Untreated
+anti-hPD-1
SSC-A
hCD25 (BV421-A)
b)
p = 0.0004
***
%hCD69+ (of CAR+ T cells)
hCD69 (BV605-A)
c)
p = 0.0013
%hGzmB+ (of CAR+ T cells)
hGzmB (PE-Cy7-A)
d)
p = 0.0036
%hKi67+ (of CAR+ T cells)
hKi67 (PE/Dazzle 594-A)
e)
p = 0.0001
***
HLA-DR MFI (of CAR+ T cells)
HLA-DR (BV510-A)
f)
p = 0.0068
# of Splenocytes (x 10^6)
g)
p < 0.0001
**** ~3.42-fold
%CAR+ CD4+ (of Live Cells)
p = 0.0004
*** ~6.64-fold
#CAR+ CD4+ cells (x10^6)
h)
p = 0.0004
*** ~2.09-fold
%hCD8+ CAR+ (of Live Cells)
p = 0.0006
*** ~3.79-fold
#CAR+ CD8+ cells (x10^6)

Supplementary Figure 9: Additional phenotype of CAR T cells isolated from spleens of tumor-bearing mice treated with and without anti-hPD-1

(a-e) Day 19: expression of T cell activation markers hCD25 (a), hCD69 (b), hGzmB (c), hKi67 (d), HLA-DR (e) by flow cytometry in CAR T cells in spleen of mice treated with and without anti-hPD-1 10 days post-CAR T infusion.
(f) Day 19: splenic cellularity of mice treated with and without anti-hPD-1 10 days post-CAR T infusion.
(g, h) Day 19: frequency and number of hCD4+ (g) and hCD8+ (h) CAR T cells by flow cytometry in spleens of mice treated with and without anti-hPD-1 10 days post-CAR T infusion.

Data in is combined from 3 independent experiments (n=11 for untreated group and n=7 for anti-hPD-1-treated group. Statistical comparisons were performed using a two-tailed unpaired Student's t test without Welch's correction. Data are presented as mean ± standard error of the mean (SEM), with individual data points shown where applicable.

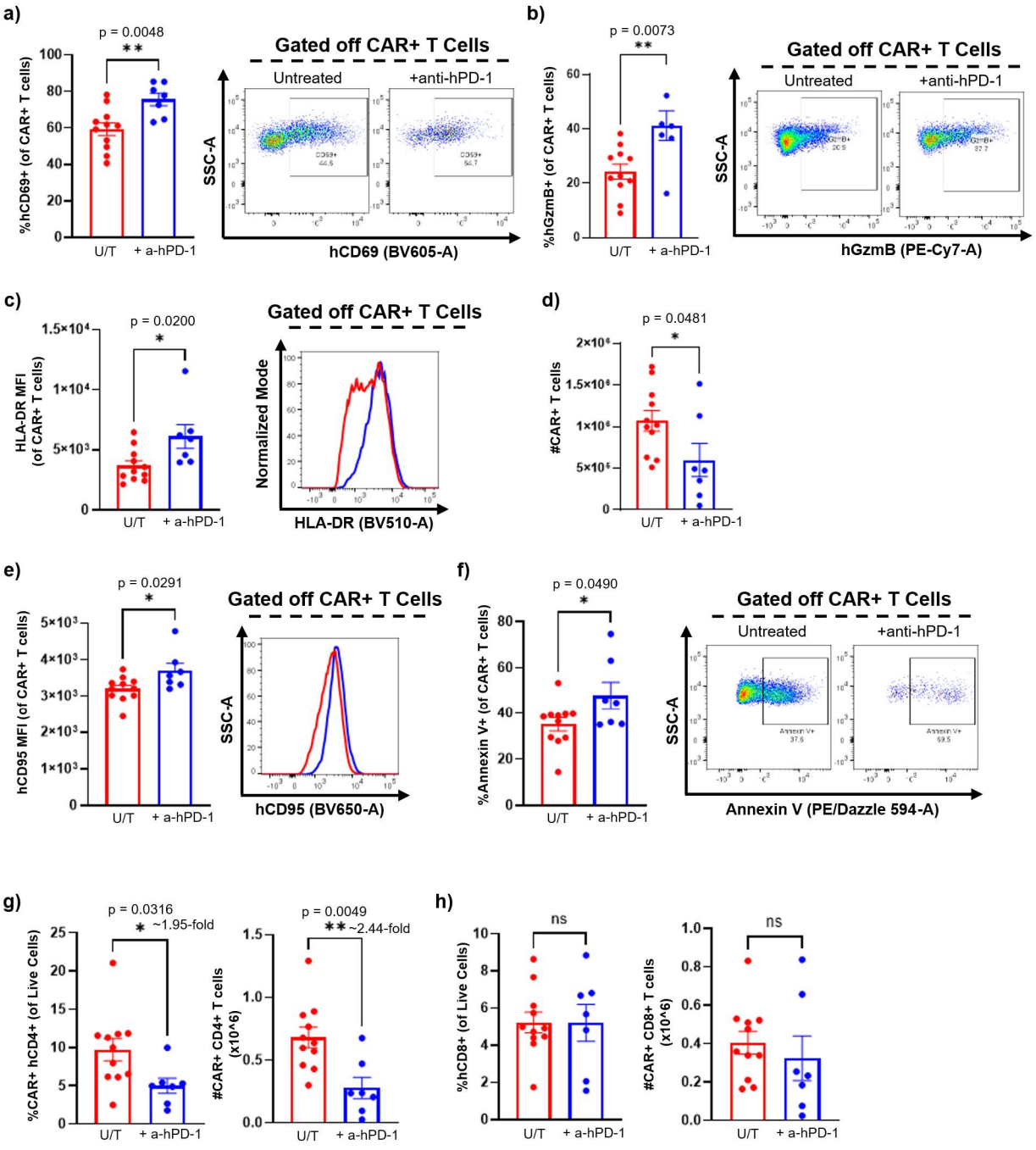
a)
p = 0.0048
**
%hCD69+ (of CAR+ T cells)
U/T
+ a-hPD-1
Gated off CAR+ T Cells
Untreated
+anti-hPD-1
SSC-A
hCD69 (BV605-A)
b)
p = 0.0073
**
%hGzmB+ (of CAR+ T cells)
U/T
+ a-hPD-1
Gated off CAR+ T Cells
Untreated
+anti-hPD-1
SSC-A
hGzmB (PE-Cy7-A)
c)
p = 0.0200
*
HLA-DR MFI (of CAR+ T cells)
U/T
+ a-hPD-1
Gated off CAR+ T Cells
Normalized Mode
HLA-DR (BV510-A)
d)
p = 0.0481
*
#CAR+ T cells
U/T
+ a-hPD-1
e)
p = 0.0291
*
hCD95 MFI (of CAR+ T cells)
U/T
+ a-hPD-1
Gated off CAR+ T Cells
SSC-A
hCD95 (BV650-A)
f)
p = 0.0490
*
%Annexin V+ (of CAR+ T cells)
U/T
+ a-hPD-1
Gated off CAR+ T Cells
Untreated
+anti-hPD-1
SSC-A
Annexin V (PE/Dazzle 594-A)
g)
p = 0.0316
* ~1.95-fold
%CAR+ hCD4+ (of Live Cells)
U/T
+ a-hPD-1
p = 0.0049
** ~2.44-fold
#CAR+ CD4+ T cells (x10^6)
U/T
+ a-hPD-1
h)
ns
%hCD8+ (of Live Cells)
U/T
+ a-hPD-1
ns
#CAR+ CD8+ T cells (x10^6)
U/T
+ a-hPD-1

Supplementary Figure 10: Phenotype of CAR T cells isolated from the bone marrow of tumor-bearing mice treated with anti-hPD-1 show increased activation induced cell death mirroring phenotype from spleen

(a-c) Day 19: expression of T cell activation markers hCD69 (a), hGzmB (b), and HLA-DR (c) by flow cytometry in CAR T cells in bone marrow of mice treated with and without anti-hPD-1 10 days post-CAR T infusion.
(d) Day 19: CAR T cell numbers in bone marrow of mice treated with and without anti-hPD-1 10 days post-CAR T infusion.
(e, f) Day 19: expression of hCD95 (e) and annexin V binding (f) by flow cytometry in CAR T cells from bone marrow of mice treated with and without anti-hPD-110 days post-CAR T infusion.
(g, h) Day 19: frequency and number of hCD4+ (g) and hCD8+ (h) CAR T cells by flow cytometry in bone marrow of mice treated with and without anti-hPD-1 10 days post-CAR T infusion.

Data in is combined from 3 independent experiments (n=11 for untreated group and n=7 for anti-hPD-1-treated group). Statistical comparisons were performed using a two-tailed unpaired Student's t test without Welch's correction. Data are presented as mean ± standard error of the mean (SEM), with individual data points shown where applicable.

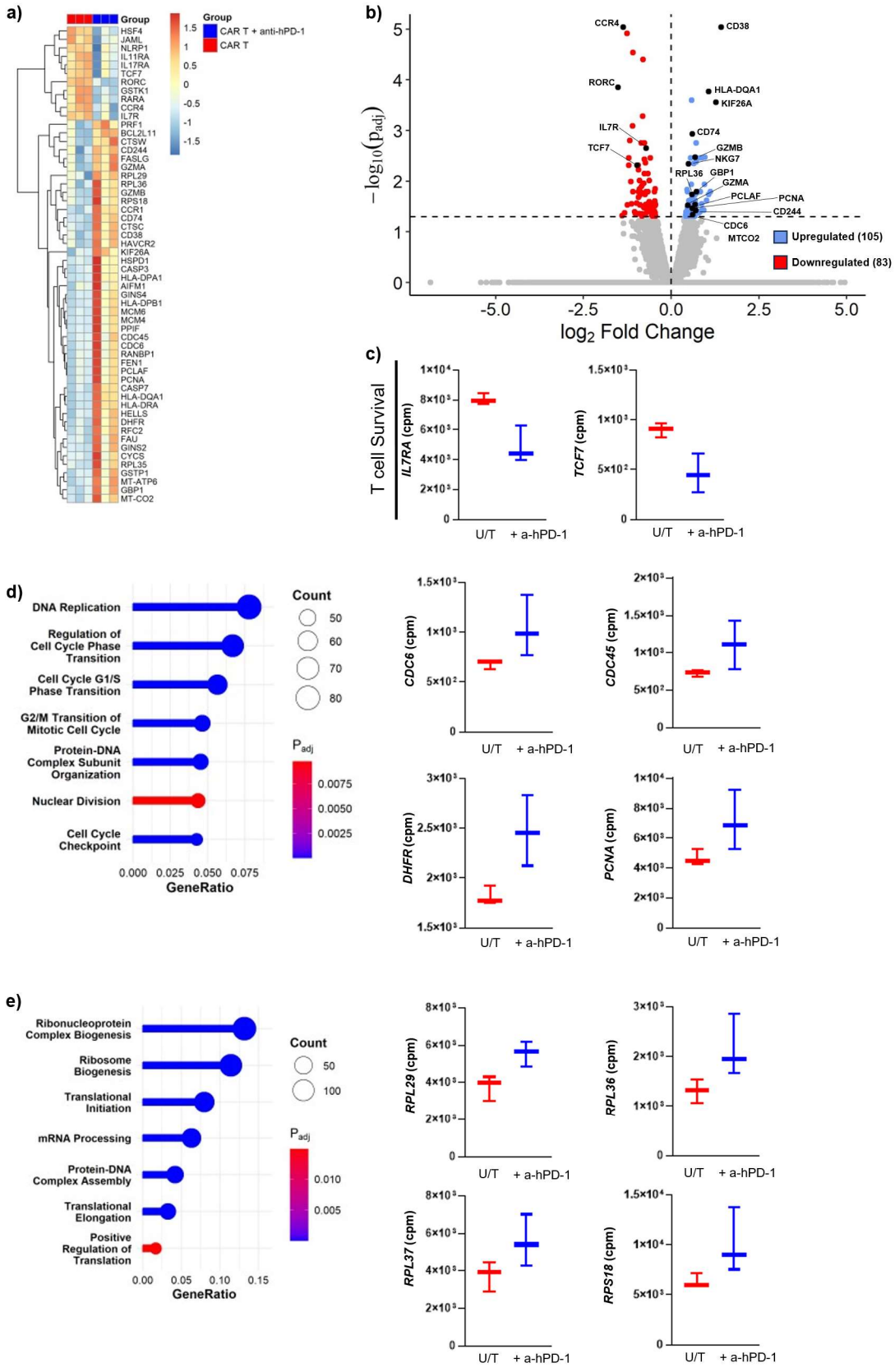
a)
Group
CAR T + anti-hPD-1
CAR T
HSF4
JAML
NLRP1
IL11RA
IL17RA
TCF7
RORC
GSTK1
RARA
CCR4
IL7R
PRF1
BCL2L11
CTSW
CD244
FASLG
GZMA
RPL29
RPL36
GZMB
RPS18
CCR1
CD74
CTSC
CD38
HAVCR2
KIF26A
HSPD1
CASP3
HLA-DPA1
AIFM1
GINS4
HLA-DPB1
MCM6
MCM4
PPIF
CDC45
CDC6
RANBP1
FEN1
PCLAF
PCNA
CASP7
HLA-DQA1
HLA-DRA
HELLS
DHFR
RFC2
FAU
GINS2
CYCS
RPL35
GSTP1
MT-ATP6
GBP1
MT-CO2
b)
$-\log_{10}(p_{adj})$
$\log_2$ Fold Change
CCR4
CD38
RORC
HLA-DQA1
KIF26A
IL7R
CD74
TCF7
GZMB
NKG7
RPL36
GBP1
GZMA
PCLAF
PCNA
CD244
CDC6
MTCO2
Upregulated (105)
Downregulated (83)
c)
T cell Survival
IL7RA (cpm)
TCF7 (cpm)
U/T
+ a-hPD-1
d)
DNA Replication
Regulation of Cell Cycle Phase Transition
Cell Cycle G1/S Phase Transition
G2/M Transition of Mitotic Cell Cycle
Protein-DNA Complex Subunit Organization
Nuclear Division
Cell Cycle Checkpoint
GeneRatio
Count
P_{adj}
CDC6 (cpm)
CDC45 (cpm)
DHFR (cpm)
PCNA (cpm)
e)
Ribonucleoprotein Complex Biogenesis
Ribosome Biogenesis
Translational Initiation
mRNA Processing
Protein-DNA Complex Assembly
Translational Elongation
Positive Regulation of Translation
RPL29 (cpm)
RPL36 (cpm)
RPL37 (cpm)
RPS18 (cpm)

Supplementary Figure 11: Additional bulk RNA-seq data of of CAR T cells isolated from the bone marrow of tumor-bearing mice with and without anti-hPD-1 treatment

(a) Heat map showing differential expression of genes of CAR T cells in spleens of mice treated with and without anti-hPD-1.
(b) Volcano plot showing differential expression of genes upregulated and downregulated CAR T cells in spleens of mice treated with anti-hPD-1 compared to those from mice without treatment
(c) Normalized cpm reads for IL7RA and TCF7, genes important for T cell survival, between CAR T cells from spleens with and without anti-hPD-1.
(d) Gene ontology analysis of DNA replication pathways and normalized cpm reads several activation genes between CAR T cells from spleens of mice treated with and without anti-hPD-1.
(e) Gene ontology analysis of protein translation pathways and normalized cpm reads several apoptosis genes between CAR T cells from spleens of mice treated with and without anti-hPD-1.

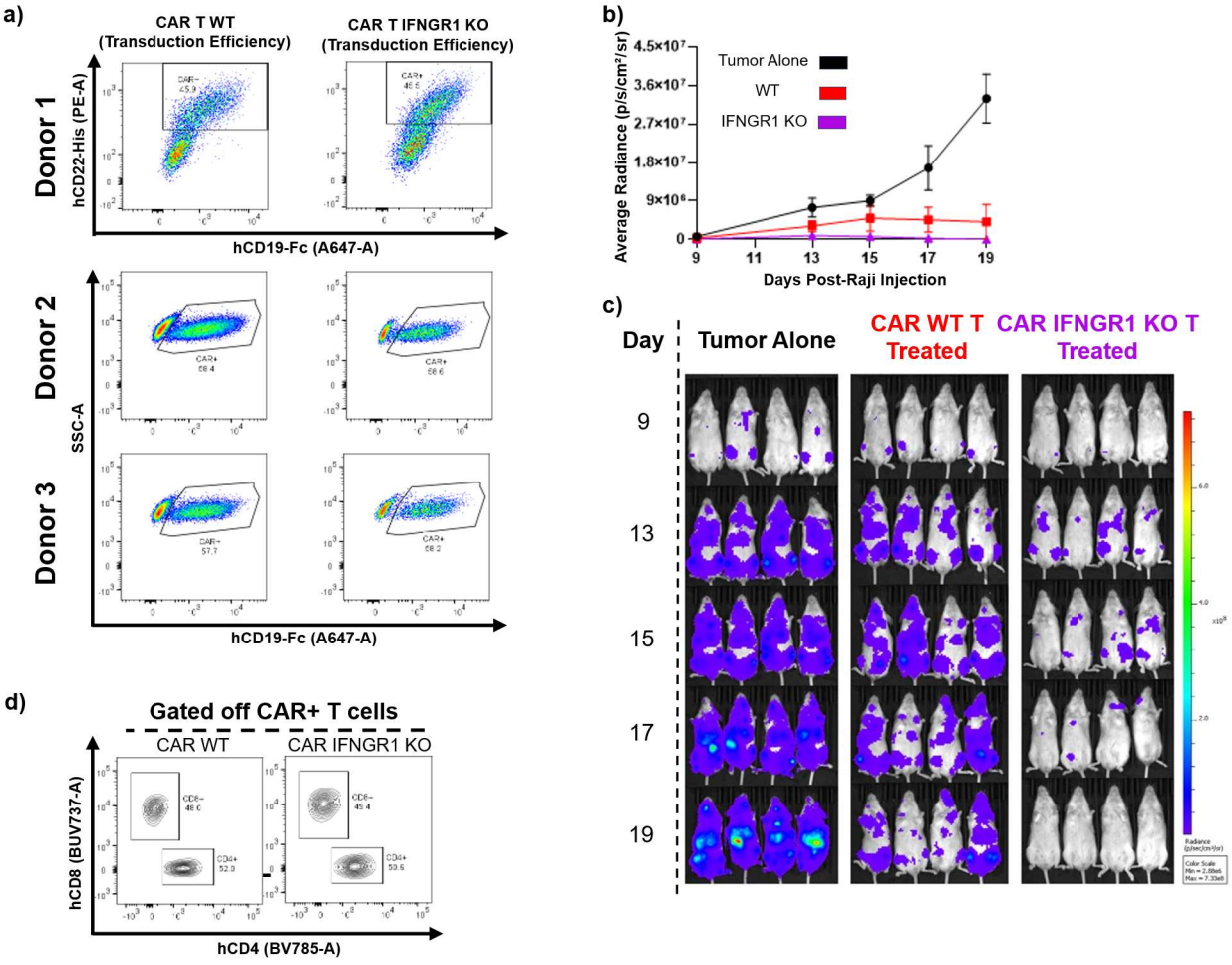
a)
CAR T WT
(Transduction Efficiency)
CAR T IFNGR1 KO
(Transduction Efficiency)
Donor 1
hCD22-His (PE-A)
hCD19-Fc (A647-A)
Donor 2
Donor 3
SSC-A
hCD19-Fc (A647-A)
b)
Tumor Alone
WT
IFNGR1 KO
Average Radiance (p/s/cm²/sr)
Days Post-Raji Injection
c)
Day
Tumor Alone
CAR WT T
Treated
CAR IFNGR1 KO T
Treated
9
13
15
17
19
d)
Gated off CAR+ T cells
CAR WT
CAR IFNGR1 KO
hCD8 (BUV737-A)
hCD4 (BV785-A)

Supplementary Figure 12: Additional phenotype and data from CAR IFNGR1 KO T cell experiments

(a) CAR transduction efficiencies from 3 donors with and without knocking out *IFNGR1*.
(b, c) Tumor burden by bioluminescent imaging after WT or IFNGR1 KO CAR T cell treatment (repeat).
(d) Baseline proportion of CD4+ and CD8+ WT and IFNGR1 KO CAR T cells by flow cytometry.

Data from b-c is representative of two independent experiments (repeat of anti-tumor efficacy study in Fig. 5j-k). Data are presented as mean ± standard error of the mean (SEM), with individual data points shown where applicable.

CHAPTER 3: Evidence of Allogeneic-Directed Anti-Tumor Effects by CAR T cells in Preclinical Modeling

Michael K. Sheng[1], Kelly Loi[1], Logan V. Vick[1], Craig P. Collins[1], Ryan N. Nielsen[1], Wahed A. Firoz[1], Ying Xiong[2], Zhongyu Zhu[2], Yanping Xie[2], Robert J. Canter[3], Arta M. Monjazeb[4], Anthony E. Zamora[5], William J. Murphy[1*]

1. Department of Dermatology, University of California Davis School of Medicine, Davis, Sacramento, CA, USA

2. Caring Cross, Gaithersburg, MD, USA

3. Department of Surgery, University of California Davis School of Medicine, Davis, Sacramento, CA, USA

4. Department of Radiation Oncology, University of California Davis School of Medicine, Davis, Sacramento, CA, USA

5. Department of Medicine, Medical College of Wisconsin, Milwaukee, WI, USA

***Corresponding Author:**

Dr. William J. Murphy, Distinguished Professor, Department of Dermatology, School of Medicine, University of California, Davis, Sacramento, CA 95817, USA,

Phone: (916) 703-9397, E-mail: wmjmurphy@health.ucdavis.edu

Abstract

Chimeric antigen receptor (CAR) T cells are highly potent and FDA-approved for treating several hematological malignancies. Despite these clinical successes, however, CAR T cell efficacy remains variable amongst patients due to tumor-intrinsic resistance, antigen modulation, and systemic toxicities; furthermore, they also remain therapeutically limited in solid tumors. Developing novel and improved CAR T cell products relies heavily on testing on preclinical models that can accurately recapitulate tumor biology and predict clinical outcomes. For this purpose, typically immortalized tumor cell lines, such as the Burkitt's lymphoma Raji cell line, are used. In this study, we observed that CD19-specific CAR (CAR19) T cells demonstrated cytotoxicity not only against Raji wild-type (WT) cells expressing CD19, but also unexpectedly against CD19-negative Raji cells. This reactivity was seen both *in vitro* and *in vivo* and was associated with increased expression of T cell activation markers such as CD25, CD69, HLA-DR, PD-1, the proliferation marker Ki-67, and elevated cytokine production – all features consistent with endogenous T cell receptor (TCR) engagement. To exclude the possibility of CAR tonic signaling as the cause of this reactivity, we also generated non-transduced (NT) T cells and found that they exhibited similar activation and cytokine responses against Raji cells. Interestingly, NT T cells did not respond to other B cell leukemia/lymphoma or solid tumor cell lines *in vitro.* These findings highlight that certain tumor cell lines, such as Raji, can unintendedly trigger T cell activation, possibly through alloreactivity mediated by the TCR. This reveals a key limitation in preclinical modeling for CAR T cell therapies, where false-positive efficacy data may arise from T cell responses unrelated to CAR specificity to antigen.

Introduction

In chimeric antigen receptor (CAR) T cell therapy, T cells are taken, typically autologously, from a patient and genetically modified to express an artificial receptor – termed a 'CAR' – that enables antigen-specific recognition and subsequent activation and cytotoxicity against tumor cells. This approach has profoundly revolutionized cancer immunotherapy, achieving unprecedented clinical success, particularly in hematological malignancies, and providing a highly curative alternative to conventional cancer treatments.

Large-scale international clinical trials, including ELIANA/ENSIGN, ELARA, and ZUMA-1, have routinely reported objective response rates eclipsing 80%, complete response rates exceeding 60%, and 12-month survival rates surpassing 50% in patients with relapsed or refractory (R/R) B-cell acute lymphoblastic leukemia (B-ALL) and diffuse large B-cell lymphoma (DLBCL).[1–4] In contrast, the SCHOLAR-1 study, which evaluated conventional salvage chemotherapy regimens in R/R DLBCL, reported overall and complete response rates of only 26% and 7% respectively, and a median overall survival of 6.3 months.[5]

Despite clinical success, CAR T cell therapy still faces significant limitations. Not all patients respond positively due to key challenges including systemic toxicities, antigen escape, poor T cell persistence, and an immunosuppressive and hypoxic tumor microenvironment characteristic of many cancers; moreover, CAR T cells have demonstrated limited efficacy in solid tumors.[6,7] These challenges have necessitated the development of novel next-generation CAR T cell therapies with enhanced persistence and anti-tumor activity in hostile tumor environments, such as armored CAR

T cells and T cells redirected for universal cytokine-mediated killing (TRUCKs).[8] However, before translation to the clinic, these therapies must be validated in rigorous preclinical model testing.

Preclinical evaluation of CAR T cells typically relies heavily on using CAR antigen-expressing tumor cell lines as targets for *in vitro* and *in vivo* studies. In studies of CAR T cells directed against lymphoma, the Burkitt's lymphoma cell line Raji is commonly used due to its distinction of being the first hematopoietic cell line and high expression of several CAR-targeted antigens such as CD19, CD20, and CD22.[9–12] In our studies using CD19-specific CAR (CAR19) T cells, however, we unexpectedly observed T cell reactivity against Raji cells that had genetic ablation of CD19 (Raji CD19 KO). CAR19 T cells exhibited cytotoxicity against Raji CD19 KO cells both *in vitro* and *in vivo*, along with increased expression of T cell activation and proliferation markers and elevated cytokine production. Furthermore, non-transduced (NT) T cells also exhibited a similar reactivity demonstrating that this effect was not solely due to CAR tonic signaling. Additionally, this phenomenon was not observed with other leukemia/lymphoma or solid tumor cell lines tested, suggesting instead that there are Raji-intrinsic factors capable of eliciting a strong T cell response. These findings suggest that Raji cells may present uniquely immunogenic peptides onto major histocompatibility (MHC) molecules or exhibit other tumor-intrinsic properties that promote T cell activation across multiple donors, raising concerns about its reliability in use as a preclinical model for evaluating CAR T cell efficacy.

Methods

Tumor Cell Lines and Culture

The wild-type (WT) and CD19 knockout (KO) human Burkitt's lymphoma, Raji, cell lines were engineered to constitutively express firefly luciferase (ffLuc) and were gifted by Caring Cross. The Raji CD19 KO cell line was validated by staining with anti-human CD19 (BioLegend, Cat. #: 302206) and analyzing with flow cytometry. Raji WT and CD19 cells expressing Incucyte Nuclight Green were generated by transducing parental lines with lentivirus encoding for Incucyte Nuclight Green at an MOI of 3 in the presence of 5 µg/mL polybrene. The transduced cells were selected for Nuclight Green expression in media containing 1 µg/mL puromycin (Gibco, Cat. #: A1113803). The human lymphoid leukemia cell line, NALM6, was also provided by Caring Cross. The K562 cell line was purchased from ATCC (ATCC, Cat. #: CCL-243). The SKMEL-28 cell line was provided by Dr. Jose Guevara (Moffitt Cancer Center). A-673 cells were purchased from ATCC (ATCC, Cat. #: CRL-1598). Granta, Ramos, and REH cell lines were received from Dr. Joseph Tuscano (UC Davis School of Medicine). Raji, Granta, NALM6, Ramos, and REH cell lines were cultured in media made of: 90% RPMI 1640 without glutamine (Gibco, Cat. #: 21870084), 10% Nu-Serum (Corning, Cat. #: 355100), 2 mM L-glutamine (Gibco, Cat. #: 25030081), 1x MEM non-essential amino acids (Gibco, Cat. #: 11140050), 1 mM sodium pyruvate (Gibco, Cat. #: 11360070), 1% penicillin/streptomycin (Gibco, Cat. #: 15140122), 1 mM HEPES (Gibco, Cat. #: 15630080) and passaged twice a week to maintain high cell viability (>90%). SKMEL-28 and A-673 cells were cultured in media made of 90% DMEM (Gibco, Cat. #: 11995081), 10% Nu-Serum (Corning, Cat. #: 355100), 2 mM L-glutamine (Gibco, Cat. #:

25030081), 1% penicillin/streptomycin (Gibco, Cat. #: 15140122), 1 mM HEPES (Gibco, Cat. #: 15630080) and passaged once a week to maintain high cell viability (>90%).

Mice

Female NOD.Cg-*Prkdc*^{scid} *Il2rg*^{tm1Wjl}/SzJ (NSG) mice (Jackson Laboratory, Cat. #005557) were purchased from the Jackson Laboratory. Mice were housed in groups of four per cage under specific pathogen-free (SPF) conditions at the University of California, Davis (UC Davis) Institute for Regenerative Cures, an AAALAC-accredited animal facility. Animals were maintained on a 12-hour light/dark cycle with ad libitum access to food (NIH-31 chow) and water. All animal procedures were approved by the UC Davis Institutional Animal Care and Use Committee (IACUC) and carried out in accordance with institutional guidelines, ethical regulations, and humane endpoints.

Human PBMC/T cell Isolation

Leukocyte reduction chambers containing blood from healthy human donors were procured from (Vitalant) and diluted 1:1 with D-PBS containing 2% FBS. The diluted blood was placed into 50 mL SepMate PBMC isolation tubes pre-filled with 15 mL of lymphocyte separation media and centrifuged at 1200 x g for 10 minutes at room temperature with the brake on. The top layer containing the enriched PBMCs was poured into a new 50 mL conical tube and washed once with D-PBS containing 2% FBS. Afterwards, to remove residual red blood cells the purified human PBMCs were treated with 1x RBC lysis buffer for 5 minutes and washed once with D-PBS and 2% FBS. T cells were subsequently isolated from the enriched PBMCs using a MagniSort

human T cell enrichment kit (Invitrogen, Catalog #: 8804-6810-74) and cryopreserved in 90% FBS and 10% DMSO at -80°C for 24 to 72 hours. Isolated T cells were stored in liquid nitrogen for long-term storage until used for CAR T cell generation.

Human CAR and Non-Transduced (NT) T cell Generation, Expansion and Validation

Isolated T cells were thawed from liquid nitrogen on day 0 and resuspended in pre-warmed TexMACS GMP medium (Miltenyi Biotec, Cat. #: 170-076-307) and counted. To activate, T cells were resuspended to a concentration of 1x10^6 cells/mL in TexMACS containing 200 IU/mL rhIL2 and a 1:20 dilution of MACS GMP T cell TransAct (Miltenyi Biotec, Cat. #: 200-076-204). On day 1 post-activation, for CAR T cell transduction T cells were transduced with lentivirus encoding a CAR targeting hCD19 (provided by Caring Cross) at an MOI of 10. Cells that did not receive lentivirus were demarcated as non-transduced (NT). On day 3, T cells were collected, centrifuged at 1200 RPM for 5 minutes, and media was decanted. The T cells were then resuspended in pre-warmed TexMACS medium, counted, and subsequently resuspended to a concentration of 0.25x10^6 cells/mL in TexMACS containing 200 IU/mL rhIL2. On days 6, 8, and 10, the T cells were counted and resuspended to a concentration of 0.5x10^6 cells/mL in TexMACS containing 200 IU/mL rhIL2. CAR T cells were validated by primary staining with recombinant human CD19 Fc chimera protein (R&D Systems, Cat. #: 9269-CD-050) followed by secondary staining with Alexa Fluor 647 (AF647) goat anti-human Fc (Jackson ImmunoResearch, Cat. #: 109-606-098) and analyzed by flow cytometry. CAR T cells were used for experiments between days 10 and 12.

Human CAR and NT T cell In Vitro Studies

In a 96-well round bottom plate, CAR or NT T cells were co-cultured with irradiated (10,000 cGy) target cells for 72 hours at a 1:1 E:T ratio (1.0x10^5 cells of both) in TexMACS GMP medium. For cytokine analysis, supernatants were collected and IFN-γ and IL-2 levels were measured by cytokine bead array (CBA) (BD, Cat. #: 558270; BD, Cat. #: 558269). For flow cytometry, cells were then incubated with Zombie NIR viability dye, Fc blocked with a 1:20 dilution of human TruStain FcX (BioLegend, Cat. #: 422302), surface stained (anti-human CD19-Fc + AF647 anti-human Fc, BV711 anti-human CD3 [BD Biosciences, Cat. #: 563725], BV785 anti-human CD4 [BioLegend, Cat. #: 317442], BUV737 anti-human CD8 [BD Biosciences, Cat. #: 749367], BV421 anti-human CD25 [BioLegend, Cat. #: 302630], BV605 anti-human CD69 [BioLegend, Cat. #: 310938], BV510 anti-HLA-DR [BioLegend, Cat. #: 307646], PE anti-human PD-1 [BioLegend, Cat. #: 329906]), intracellular stained when applicable (PE/Cyanine7 anti-human Granzyme B [BioLegend, Cat. #: 372214], PE/Dazzle 594 anti-human Ki67 [BioLegend, Cat. #: 350534], BV605 anti-human CD107a [BioLegend, Cat. #: 328634]) and analyzed by flow cytometry. Incucyte cytotoxicity studies were done by plating CAR or NT T cells with either target Raji WT/Nuclight Green or Raji CD19 KO/Nuclight Green cells at different E:T ratios in a 96-well flat bottom plate. The plate was placed in an Incucyte Live-Cell Analysis System (Sartorius) for 72 hours and analyzed using Incucyte analysis software (Sartorius).

Human CAR and NT T cell Treatment of Tumor-Bearing Mice

NSG mice were injected i.v. with 1x10^6 Raji/ffLuc or Raji CD19 KO/ffLuc cells on day 0 and 5x10^6 CAR or NT T cells on day 7. On indicated timepoints, blood, spleens, and

bone marrow were harvested. Blood was collected in Microtainer Collection Tubes (BD Biosciences, Cat. #: 365967) and spun at 8000 x g for 10 minutes to acquire serum; serum was frozen at -80°C until used. Spleens and bone marrow were mechanically processed into single-cell suspensions in D-PBS + 2% FBS, filtered through a Falcon 70 µm cell strainer, treated with 5 mL of 1x RBC lysis buffer, washed once in D-PBS + 2% FBS, and counted using a Z1 Coulter Particle Counter. Cells from spleens and bone marrow were incubated with Zombie NIR viability dye, Fc blocked with a 1:20 dilution of human TruStain FcX and a 1:20 dilution of TruStain FcX anti-mouse CD16/32 (BioLegend, Cat. #: 101320), surface stained (anti-human CD19-Fc + AF647 anti-human Fc, BV711 anti-human CD3 [BD Biosciences, Cat. #: 563725], BV785 anti-human CD4 [BioLegend, Cat. #: 317442], BUV737 anti-human CD8 [BD Biosciences, Cat. #: 749367], BV421 anti-human CD25 [BioLegend, Cat. #: 302630], BV605 anti-human CD69 [BioLegend, Cat. #: 310938], BV510 anti-HLA-DR [BioLegend, Cat. #: 307646], PE anti-human PD-1 [BioLegend, Cat. #: 329906]), intracellular stained when applicable (PE/Cyanine7 anti-human Granzyme B [BioLegend, Cat. #: 372214], PE/Dazzle 594 anti-human Ki67 [BioLegend, Cat. #: 350534]) and analyzed by flow cytometry. Serum human IFN-γ levels were measured in serum samples using cytometric bead array. Tumor burden in mice was assessed at indicated timepoints by i.p. injection of 4.5 mg D-luciferin (Revvity, Cat. #: 122799) on indicated timepoints followed by bioluminescent imaging using the IVIS Lumina III system.

Trypan Blue Exclusion

Throughout the experiments, total splenocyte and bone marrow numbers were determined using a Z1 Coulter Particle Counter (Beckman Coulter). For cell counting during *in vitro* experiments, trypan blue exclusion was performed using a 1:1 dilution of cells-to-trypan blue (Gibco, Cat. #: 15250061) and recording total and live cell numbers using a BioRad TC20 automated cell counter (BioRad, Cat. #: 1450102).

Flow Cytometry

For CD107a staining, cells were incubated for 5 hours prior with a 1:1000 dilution of GolgiPlug (BD, Cat. #: 555029) and a 1:1500 dilution of GolgiStop (BD, Cat. #: 554724) prior to surface staining. Viability dye was prepared in D-PBS; all cells were incubated at room temperature during viability dye staining. Surface antibody dilutions were prepared and washing was performed in staining buffer consisting of D-PBS (Gibco, Cat. #14190-136) and 2% fetal bovine serum (FBS) (Gibco, Cat. #A5256701). Cells were incubated with surface antibodies on ice for 30 minutes per staining step and washed once in staining buffer between each step. For intracellular staining, cells were fixed and permeabilized using Cytofix/Cytoperm solution (BD Biosciences, Cat. #554722) for 1 hour at 4°C and washed once with BD Perm/Wash buffer (BD Biosciences, Cat. #554723). Intracellular antibody dilutions were prepared in BD Perm/Wash buffer and cells were incubated in them for 30 minutes at room temperature. Afterwards, cells were washed one time in BD Perm/Wash buffer. Samples were run on a BD LSRFortessa Cell Analyzer, and data was analyzed using FlowJo software.

Statistical Analysis

Statistical analyses for all *in vitro* and *in vivo* experiments were performed using GraphPad Prism 9.

Data Availability

The raw experimental data supporting the findings of this study are available from the corresponding author upon reasonable request.

Results

CAR19 T cells Demonstrate Reactivity to Both Raji WT and CD19 KO Cells In Vitro

We generated CAR19 T cells using a standard manufacturing protocol involving activation with anti-CD3/anti-CD28 agonist antibodies (TransAct), transduction with CAR-encoding lentivirus, and *ex vivo* expansion in media containing recombinant human IL-2 (rhIL-2) (Supplementary Fig. 1a). CAR19 T cell transduction efficiencies routinely exceeded 70% (Supplementary Fig. 1b). Following successful CAR19 T cell generation, cells were co-cultured *in vitro* with Raji WT and CD19 knockout (KO) (Fig. 1a). Raji CD19 KO cells were confirmed to be devoid of CD19 cell surface expression by flow cytometry (Fig. 1b). After co-culture with Raji WT cells, CAR19 T cells demonstrated robust upregulation of T cell activation markers such as CD25, CD69, GzmB, HLA-DR, and PD-1, and increased expression of the proliferation marker Ki67; notably, however, these same markers were upregulated, though to a lesser extent, following co-culture with Raji CD19 KO cells despite the absence of the CAR-specific antigen (Fig. 1c-e). This response was observed in CAR19 T cells made from five independent donors. This pattern of expression was consistent with TCR stimulation using TransAct, suggesting that CAR19 T cell reactivity to Raji CD19 KO cells may be mediated by TCR-dependent alloreactivity (Supplementary Fig. 1c). Furthermore, analysis of supernatants revealed increased levels of both IFN-γ and IL-2 in CAR19 T cell co-cultures with both Raji WT and CD19 KO cells. CAR19 T cells also exhibited both CD107a degranulation, a marker of cellular cytotoxicity, and demonstrated dose-dependent anti-tumor effects against both Raji and Raji CD19 KO cells (Fig. 1g, Supplementary Fig. e-f).

CAR19 T cells Exhibit Anti-Tumor Effects Against Raji CD19 KO Cells In Vivo

To evaluate whether CAR19 T cell reactivity also extended *in vivo*, we tested xenograft models using NSG mice. Mice were injected day 0 with Raji WT or CD19 KO cells, and on day 7 with CAR19 T cells (Fig. 2a). As expected, over 90% of Raji WT tumor-bearing mice survived to day 50. However, more than half of the mice bearing Raji CD19 KO tumors also survived to day 50 indicating that CAR19 T cells are capable of exerting anti-tumor effects leading to prolonged survival even in the absence of CD19 expression on Raji cells, consistent with the intermediate activation phenotype we observed *in vitro* (Fig. 2b). These anti-tumor effects varied based on the donor the CAR19 T cells were derived from, with CAR19 T cells from one donor in particular causing all Raji CD19 KO tumor-bearing mice to survive (Supplementary Fig. 2a). Using bioluminescent imaging (Raji WT and CD19 KO tumor cells were engineered with firefly luciferase), we further confirmed CAR19 T cell-mediated clearance in both Raji WT and CD19 KO tumor-bearing mice (Fig. 2c-d, Supplementary Fig. 2b).

Serum cytokine levels of human IFN-γ were upregulated at days 14 and 21 in both Raji WT and Raji CD19 KO tumor-bearing mice treated with CAR19 T cells (Fig. 2e, Supplementary Fig. 2c). Flow cytometry was also performed on cells harvested from the bone marrow and spleen (Supplementary Fig. 3a-b). On day 14, there were higher T cell frequencies in the bone marrow of treated Raji WT tumor-bearing mice relative to those bearing Raji CD19 KO tumors with a higher proportion of these T cells expressing the CAR (Fig. 2f, Supplementary Fig. 2d). By day 21, this trend reversed, possibly due to the complete clearance of Raji WT tumors, causing a contraction of the CAR T

population while the persistence of Raji CD19 KO tumor may have sustained T cell activation and expansion (Supplementary Fig. 2e).

In addition, T cells isolated from both Raji WT and CD19 KO tumor-bearing mice showed upregulation of CD25, GzmB, HLA-DR, PD-1, and Ki67, although these markers were more strongly expressed in T cells from the Raji CD19 KO group possibly because of ongoing TCR-mediated stimulation due to incomplete tumor clearance (Fig. 2g–h; Supplementary Fig. f). By day 28, T cell frequencies were higher in both the bone marrow and spleens of mice bearing Raji CD19 KO tumors relative to ones bearing Raji WT tumors, and these cells continued to exhibit an increased activation phenotype (Fig. 2i, Supplementary Fig. 2g, h).

Together, our *in vitro* and *in vivo* results demonstrate that CAR19 T cells are capable of becoming activated and mediating anti-tumor effects not only against antigen-expressing Raji WT cells, but also against antigen-negative Raji CD19 KO cells, and this reactivity may be driven by endogenous TCR signaling.

Non-Transduced T cells Also Demonstrate Reactivity to Raji Cells In Vitro and In Vivo

To confirm CAR19 T cell antigen-independent reactivity towards Raji cells was not due to CAR tonic signaling or an artifact of CD19 ablation in Raji cells, we also generated NT T cells that lacked CAR expression. NT T cells were then incubated *in vitro* with either Raji WT or CD19 KO cells (Fig. 3a). Following co-culture, NT T cells demonstrated augmented expression of CD25, CD69, GzmB, HLA-DR, PD-1, and Ki-67 (Fig. 3b-d). Furthermore, supernatants collected from these co-cultures contained

elevated levels of IFN-γ and IL-2 (Fig. 3e). NT T cells also mediated cytotoxicity against both Raji WT and CD19 KO targets (Fig. 3f).

To see if these effects extended *in vivo*, NSG mice were injected day 0 with Raji WT or CD19 KO cells, and on day 7 with NT T cells (Fig. 4a). Bioluminescent imaging of tumor burden revealed partial tumor clearance by NT T cells in both Raji WT and CD19 KO tumor-bearing mice (Fig. 4c). Anti-tumor activity was more pronounced in Raji CD19 KO tumor-bearing mice; notably, NT T cells from one donor prolonged survival of Raji CD19 KO tumor-bearing mice up until day 70, the survival endpoint (Fig. 4d, Supplementary Fig. 4a). Additionally, serum cytokine analysis confirmed the presence of IFN-γ in both treated groups (Fig. 4e). Furthermore, flow cytometry showed sustained T cell engraftment in both the bone marrow and spleen of tumor-bearing mice along with elevated expression of CD25, CD69, HLA-DR, PD-1, and Ki67 (Fig. 4f-h, Supplementary Fig. 4b-d).

Collectively, these *in vitro* and *in vivo* findings demonstrate that NT T cells, without CAR expression, can mediate anti-tumor activity against both Raji WT and CD19 KO cells. These results mirror our findings with CAR19 T cells and indicate that the observed reactivity is not attributable to CAR tonic signaling or CD19 gene deletion in Raji cells, but instead likely reflects an intrinsic reactivity of donor T cells toward Raji cells.

Other B cell Leukemia/Lymphoma or Solid Tumor Cell Lines Do Not Elicit T cell Activation Responses

To determine whether this observed T cell reactivity in other tumor cell lines, we co-cultured CAR19 or NT T cells with four additional non-Raji B cell leukemia/lymphoma cell lines: Granta, NALM6, Ramos, and REH. All 4 of these cell lines expressed homogenous surface levels of CD19 (Supplementary Fig. 5a). As expected, after co-culture, CAR T cells upregulated expression of CD25, CD69, GzmB, HLA-DR, and PD-1 (Supplementary Fig. 5b). In contrast, NT T cells did not augment expression of any of these activation markers nor Ki-67, indicating a lack of reactivity toward these cell lines (Fig. 5a-b). Similarly, we co-cultured NT T cells with two solid tumor cell lines: the melanoma line SKMEL28 and the Ewing sarcoma-like line A673 and neither cell line elicited T cell activation indicated by the absence of upregulated activation or proliferation markers (Supplementary Fig. 5c).

Discussion

Overall, our results demonstrate that Raji broadly stimulate T cells across multiple donors. This was observed both *in vitro* and *in vivo* by the upregulation of activation and proliferation markers, elevated cytokine production, and cytotoxicity towards both Raji WT and CD19 KO cells. However, this reactivity appears to be specific to Raji cells as neither other B cell leukemia/lymphoma lines (Granta, NALM6, Ramos, and REH) nor solid tumor lines (SKMEL28 and A673) were capable of inducing a similar activation response, suggesting that Raji cells possess unique tumor-intrinsic characteristics that allow them to elicit T cell activation independent of CAR expression.

A potential explanation for this donor-independent T cell activation against Raji cells comes from a prior study using humanized immune system mice (HIS), where immunodeficient mice were reconstituted with human CD34+ hematopoietic stem cells from ten donors. Researchers observed spontaneous regression of subcutaneously implanted Raji tumor cells in HIS mice reconstituted from all ten donor populations.[13] Depletion of human T cells prevented Raji tumor clearance and furthermore, tumor-infiltrating T cells isolated from the Raji-bearing HIS mice possessed an activated phenotype and displayed memory formation along with clonal expansion, all characteristics indicative of antigen-specific TCR engagement.

Mechanistically, their study also showed that antibody blockade of MHC class II partially attenuated IFN-γ production *in vitro*, suggesting that CD4+ T cell activation may be driven in part by peptide presentation onto MHC class II molecules. A possible explanation is that Raji cells are transformed with Epstein-Barr virus (EBV) and harbor approximately 50-60 complete copies of the EBV genome per cell.[14,15] This omnipresent

viral integration may result in the expression and presentation of highly immunogenic viral peptides onto MHC molecules, which may trigger alloreactive and/or cross-reactive T cell responses. To test this hypothesis, future experiments could evaluate whether other EBV-transformed B cell lines such as Akata, CBM1, Namalwa, or P3HR-1, induce similar T cell activation, cytotoxicity and cytokine release in our *in vitro* and *in vivo* studies. This comparative evaluation of inducing T cell responses using EBV-positive and EBV-negative cell lines would clarify whether EBV transformation can drive T cell immunogenicity, findings which would have major implications for the use of EBV transformation in generating immortalized lymphoblastoid cell lines, a widely employed technique.[16,17]

Alternatively, another hypothesis is that Raji cells may produce superantigens – microbial-derived proteins that induce widespread, non-specific T cell activation. Superantigens bypass conventional antigen processing by binding the region outside the MHC class II peptide-binding groove and directly cross-linking the MHC molecule to the Vβ region of the TCR region causing activation in up to 20% of all T cells regardless of antigen specificity.[18] Raji cells are highly effective at presenting superantigen, such as TSST-1 and SEA.[19,20] While superantigens are typically associated with microbial pathogens, the idea of superantigen-like molecules being secreted and presented by tumor cell lines such as Raji cells remains an intriguing hypothesis, albeit untested. To elucidate the mechanisms underlying Raji-induced T cell activation, future studies should focus on examining the roles of MHC class I and II on Raji cells in mediating T cell responses, whether through antibody blockade or CRISPR-mediated gene ablation. Additionally, the potential contribution of superantigen-like proteins or EBV-derived

antigens should be explored by assessing their presentation on MHC molecules via peptide-MHC profiling or mass spectrometry. Understanding the basis of this antigen-independent T cell activation is critical for improving the fidelity of preclinical models of CAR T cell efficacy to avoid generating false-positive efficacy data.

Acknowledgements

This research was supported by funding from CIRM TRAN1-13996, NCI P30 CA093373, and S10 RR026825. We are grateful to Dr. Ying Xiong and Caring Cross for providing lentivirus used in the generation of human CAR T cells, along with technical support and culturing protocols. Finally, we thank Dr. Xiao-Jing Wang and the UC Davis Molecular Pharmacology Shared Resource Core for access to the Incucyte Live-Cell Analysis System; and Jonathan Van Dyke of the UC Davis Flow Cytometry Shared Resource Core for technical assistance.

References

1. Neelapu, S. S. *et al.* Axicabtagene Ciloleucel CAR T-Cell Therapy in Refractory Large B-Cell Lymphoma. *N. Engl. J. Med.* 377, 2531–2544 (2017).

2. Maude, S. L. *et al.* Tisagenlecleucel in Children and Young Adults with B-Cell Lymphoblastic Leukemia. *N. Engl. J. Med.* 378, 439–448 (2018).

3. Fowler, N. H. *et al.* Tisagenlecleucel in adult relapsed or refractory follicular lymphoma: the phase 2 ELARA trial. *Nat. Med.* 28, 325–332 (2022).

4. Neelapu, S. S. *et al.* 5-Year Follow-Up Supports Curative Potential of Axicabtagene Ciloleucel in Refractory Large B-Cell Lymphoma (ZUMA-1). *Blood* blood.2022018893 (2023) doi:10.1182/blood.2022018893.

5. Crump, M. *et al.* Outcomes in refractory diffuse large B-cell lymphoma: results from the international SCHOLAR-1 study. *Blood* 130, 1800–1808 (2017).

6. Majzner, R. G. & Mackall, C. L. Clinical lessons learned from the first leg of the CAR T cell journey. *Nat. Med.* 25, 1341–1355 (2019).

7. Sterner, R. C. & Sterner, R. M. CAR-T cell therapy: current limitations and potential strategies. *Blood Cancer J.* 11, 69 (2021).

8. Tang, L., Pan, S., Wei, X., Xu, X. & Wei, Q. Arming CAR-T cells with cytokines and more: Innovations in the fourth-generation CAR-T development. *Mol. Ther.* 31, 3146–3162 (2023).

9. Drexler, H. G. & Minowada, J. History and Classification of Human Leukemia-Lymphoma Cell Lines. *Leuk. Lymphoma* 31, 305–316 (1998).

10. Wen, H. *et al.* Preclinical safety evaluation of chimeric antigen receptor-modified T cells against CD19 in NSG mice. *Ann. Transl. Med.* 7, 735–735 (2019).

11. Webster, B. *et al.* Self-driving armored CAR-T cells overcome a suppressive milieu and eradicate CD19+ Raji lymphoma in preclinical models. *Mol. Ther.* 29, 2691–2706 (2021).

12. Cordoba, S. *et al.* CAR T cells with dual targeting of CD19 and CD22 in pediatric and young adult patients with relapsed or refractory B cell acute lymphoblastic leukemia: a phase 1 trial. *Nat. Med.* 27, 1797–1805 (2021).

13. Patel, A. K. *et al.* Spontaneous tumor regression mediated by human T cells in a humanized immune system mouse model. *Commun. Biol.* 6, 444 (2023).

14. Takakuwa, T. *et al.* Integration of Epstein-Barr Virus into Chromosome 6q15 of Burkitt Lymphoma Cell Line (Raji) Induces Loss of BACH2 Expression. *Am. J. Pathol.* 164, 967–974 (2004).

15. Zuo, L. *et al.* The copy number of Epstein-Barr virus latent genome correlates with the oncogenicity by the activation level of LMP1 and NF-κB. *Oncotarget* 6, 41033–41044 (2015).

16. Wroblewski, J. M., Copple, A., Batson, L. P., Landers, C. D. & Yannelli, J. R. Cell surface phenotyping and cytokine production of Epstein–Barr Virus (EBV)-transformed lymphoblastoid cell lines (LCLs). *J. Immunol. Methods* 264, 19–28 (2002).

17. Omi, N. *et al.* Efficient and reliable establishment of lymphoblastoid cell lines by Epstein-Barr virus transformation from a limited amount of peripheral blood. *Sci. Rep.* 7, 43833 (2017).

18. Papageorgiou, A. C. & Acharya, K. R. Superantigens as immunomodulators: recent structural insights. *Structure* 5, 991–996 (1997).

19. Scholl, P. *et al.* Toxic shock syndrome toxin 1 binds to major histocompatibility complex class II molecules. *Proc Natl Acad Sci USA* (1989).

20. Fischer, H., Dohlsten, M., Lindvall, M., Sjögren, H. O. & Carlsson, R. Binding of staphylococcal enterotoxin A to HLA-DR on B cell lines. *J. Immunol. Baltim. Md 1950* 142, 3151–3157 (1989).

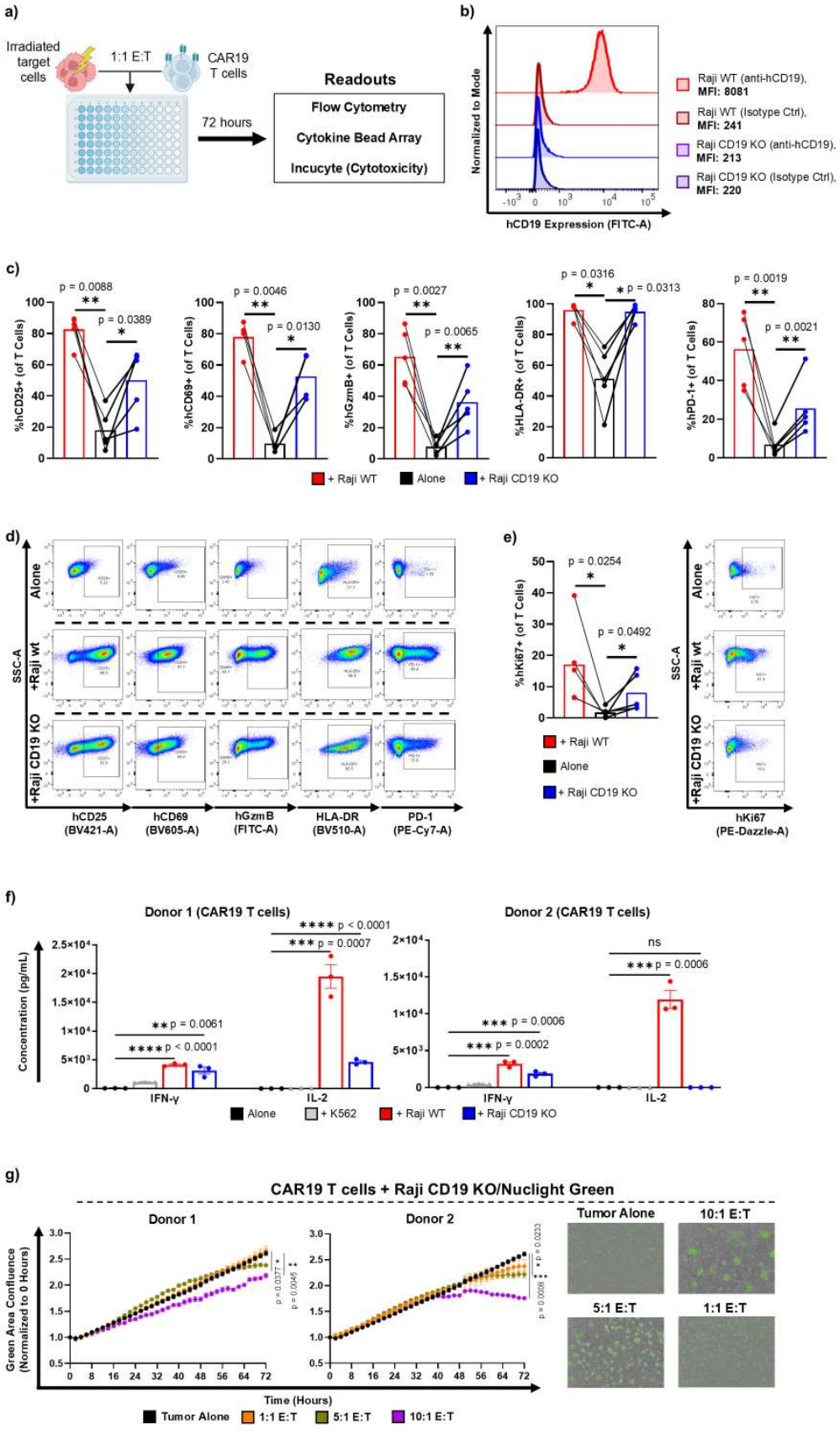
a)
Irradiated target cells
1:1 E:T
CAR19 T cells
72 hours
Readouts
Flow Cytometry
Cytokine Bead Array
Incucyte (Cytotoxicity)
b)
Normalized to Mode
hCD19 Expression (FITC-A)
Raji WT (anti-hCD19), MFI: 8081
Raji WT (Isotype Ctrl), MFI: 241
Raji CD19 KO (anti-hCD19), MFI: 213
Raji CD19 KO (Isotype Ctrl), MFI: 220
c)
%hCD25+ (of T Cells)
%hCD69+ (of T Cells)
%hGzmB+ (of T Cells)
%HLA-DR+ (of T Cells)
%hPD-1+ (of T Cells)
p = 0.0088
p = 0.0389
p = 0.0046
p = 0.0130
p = 0.0027
p = 0.0065
p = 0.0316
p = 0.0313
p = 0.0019
p = 0.0021
+ Raji WT
Alone
+ Raji CD19 KO
d)
Alone
+Raji wt
+Raji CD19 KO
SSC-A
hCD25 (BV421-A)
hCD69 (BV605-A)
hGzmB (FITC-A)
HLA-DR (BV510-A)
PD-1 (PE-Cy7-A)
e)
%hKi67+ (of T Cells)
p = 0.0254
p = 0.0492
hKi67 (PE-Dazzle-A)
f)
Donor 1 (CAR19 T cells)
Donor 2 (CAR19 T cells)
Concentration (pg/mL)
IFN-γ
IL-2
p = 0.0061
p < 0.0001
p = 0.0007
p = 0.0006
p = 0.0002
ns
Alone
+ K562
+ Raji WT
+ Raji CD19 KO
g)
CAR19 T cells + Raji CD19 KO/Nuclight Green
Donor 1
Donor 2
Green Area Confluence (Normalized to 0 Hours)
Time (Hours)
Tumor Alone
1:1 E:T
5:1 E:T
10:1 E:T

Figure 1: Human CAR19 T cells mediate anti-tumor activity against antigen-loss Raji CD19 KO cells *in vitro*, exhibiting a phenotype consistent with TCR-driven alloreactivity

(a) Staining of Raji and Raji CD19 KO cells for hCD19 expression by flow cytometry.
(b) Experimental schematic: Raji WT or CD19 KO cells were co-incubated with CAR19 T cells.
(c, d) Expression of T cell activation markers hCD25, hCD69, hGzmB, HLA-DR, and hPD-1 on CAR19 T cells by flow cytometry (c) and representational flow (d) after co-culture.
(e) Expression of T cell proliferation marker hKi67 on CAR19 T cells after co-culture.
(f) Cytokine levels of hIFN-γ and hIL2 after co-culture.
(g) Raji CD19 KO cells engineered with Nuclight Green were incubated with CAR19 T cells in an Incucyte Live-Cell Analysis System with fluorescence measured over time.

Data in c and e involves CAR19 T cells generated from 5 different donors (n=5 [except for hCD69 expression which is from 4 donors]), and in f-g contains involves CAR19 T cells generated from 2 different donors run in technical triplicates. Statistical comparisons were performed using a two-tailed paired ratio (c, e) or Student's t test without Welch's correction (f), or a two-way ANOVA (g). Data are presented as mean ± standard error of the mean (SEM), with individual data points shown where applicable.

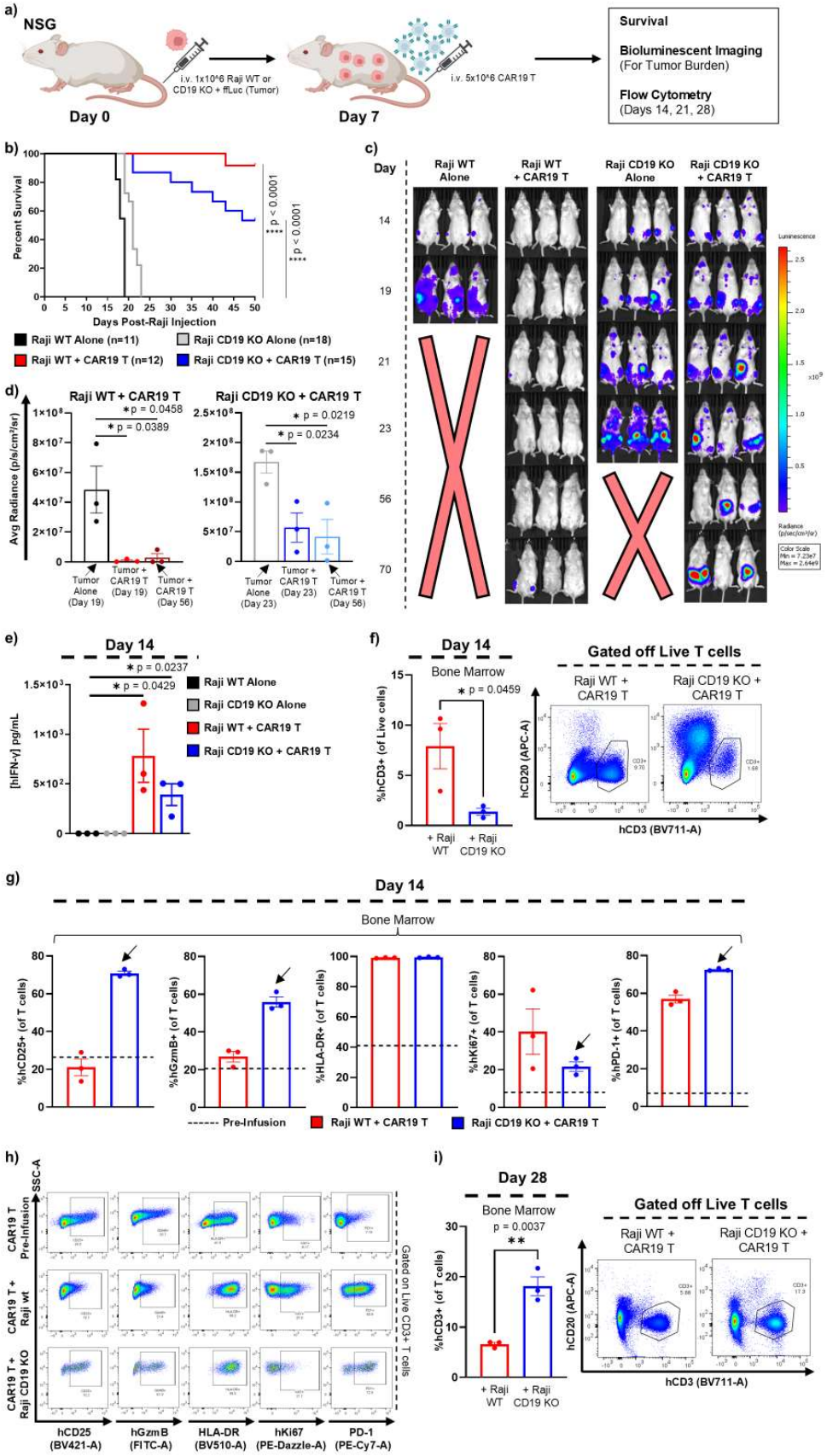
a)
NSG
i.v. 1x10^6 Raji WT or CD19 KO + ffLuc (Tumor)
Day 0
Day 7
i.v. 5x10^6 CAR19 T
Survival
Bioluminescent Imaging (For Tumor Burden)
Flow Cytometry (Days 14, 21, 28)
b)
Percent Survival
Days Post-Raji Injection
p < 0.0001
p < 0.0001
Raji WT Alone (n=11)
Raji CD19 KO Alone (n=18)
Raji WT + CAR19 T (n=12)
Raji CD19 KO + CAR19 T (n=15)
c)
Day
Raji WT Alone
Raji WT + CAR19 T
Raji CD19 KO Alone
Raji CD19 KO + CAR19 T
14
19
21
23
56
70
Luminescence
Radiance (p/sec/cm²/sr)
d)
Raji WT + CAR19 T
Raji CD19 KO + CAR19 T
Avg Radiance (p/s/cm²/sr)
* p = 0.0458
* p = 0.0389
* p = 0.0219
* p = 0.0234
Tumor Alone (Day 19)
Tumor + CAR19 T (Day 19)
Tumor + CAR19 T (Day 56)
Tumor Alone (Day 23)
Tumor + CAR19 T (Day 23)
Tumor + CAR19 T (Day 56)
e)
Day 14
* p = 0.0237
* p = 0.0429
[hIFN-γ] pg/mL
Raji WT Alone
Raji CD19 KO Alone
Raji WT + CAR19 T
Raji CD19 KO + CAR19 T
f)
Day 14
Bone Marrow
* p = 0.0459
%hCD3+ (of Live cells)
+ Raji WT
+ Raji CD19 KO
Gated off Live T cells
Raji WT + CAR19 T
Raji CD19 KO + CAR19 T
hCD20 (APC-A)
hCD3 (BV711-A)
g)
Day 14
Bone Marrow
%hCD25+ (of T cells)
%hGzmB+ (of T cells)
%HLA-DR+ (of T cells)
%hKi67+ (of T cells)
%hPD-1+ (of T cells)
------ Pre-Infusion
Raji WT + CAR19 T
Raji CD19 KO + CAR19 T
h)
SSC-A
CAR19 T Pre-Infusion
CAR19 T + Raji wt
CAR19 T + Raji CD19 KO
Gated on Live CD3+ T cells
hCD25 (BV421-A)
hGzmB (FITC-A)
HLA-DR (BV510-A)
hKi67 (PE-Dazzle-A)
PD-1 (PE-Cy7-A)
i)
Day 28
Bone Marrow
p = 0.0037
**
%hCD3+ (of T cells)
+ Raji WT
+ Raji CD19 KO
Gated off Live T cells
Raji WT + CAR19 T
Raji CD19 KO + CAR19 T
hCD20 (APC-A)
hCD3 (BV711-A)

Figure 2: Additionally, human CAR19 T cells mediate anti-tumor activity against antigen-loss Raji CD19 KO cells *in vivo* prolonging survival

(a) Experimental schematic: Raji WT or CD19 KO tumor-bearing NSG mice were treated with human hCD19-targeted CAR T cells derived from Donor 2.
(b) Survival curves of Raji WT or CD19 KO tumor-bearing NSG mice treated with human hCD19-targeted CAR T cells.
(c, d) Tumor burden by bioluminescent imaging of Raji WT or CD19 KO tumor-bearing NSG mice treated with human hCD19-targeted CAR T cells.
(e) Day 14: serum cytokine levels of hIFN-γ in Raji WT or CD19 KO tumor-bearing NSG mice treated with human hCD19-targeted CAR T cells.
(f) Day 14: frequency of T cells by flow cytometry in bone marrow of Raji WT or CD19 KO tumor-bearing NSG mice treated with human hCD19-targeted CAR T cells.
(g, h) Day 14: expression of T cell activation markers hCD25, hGzmB, HLA-DR, hPD-1, and the proliferation marker Ki67 by flow cytometry (g) and representational flow (h) on T cells in bone marrow of Raji WT or CD19 KO tumor-bearing NSG mice treated with human hCD19-targeted CAR T cells
(i) Day 28: frequency of T cells by flow cytometry in bone marrow of Raji WT or CD19 KO tumor-bearing NSG mice treated with human hCD19-targeted CAR T cells.

Data in b is combined survival from CAR19 T cells generated from 4 different donors and in c to i is representative of 2 independent experiments (n=3 per each group). Statistical comparisons were performed using a log-rank (Mantel-Cox) test (b) or a two-

tailed unpaired Student's t test without Welch's correction (d-f, i). Data are presented as mean ± standard error of the mean (SEM), with individual data points shown where applicable.

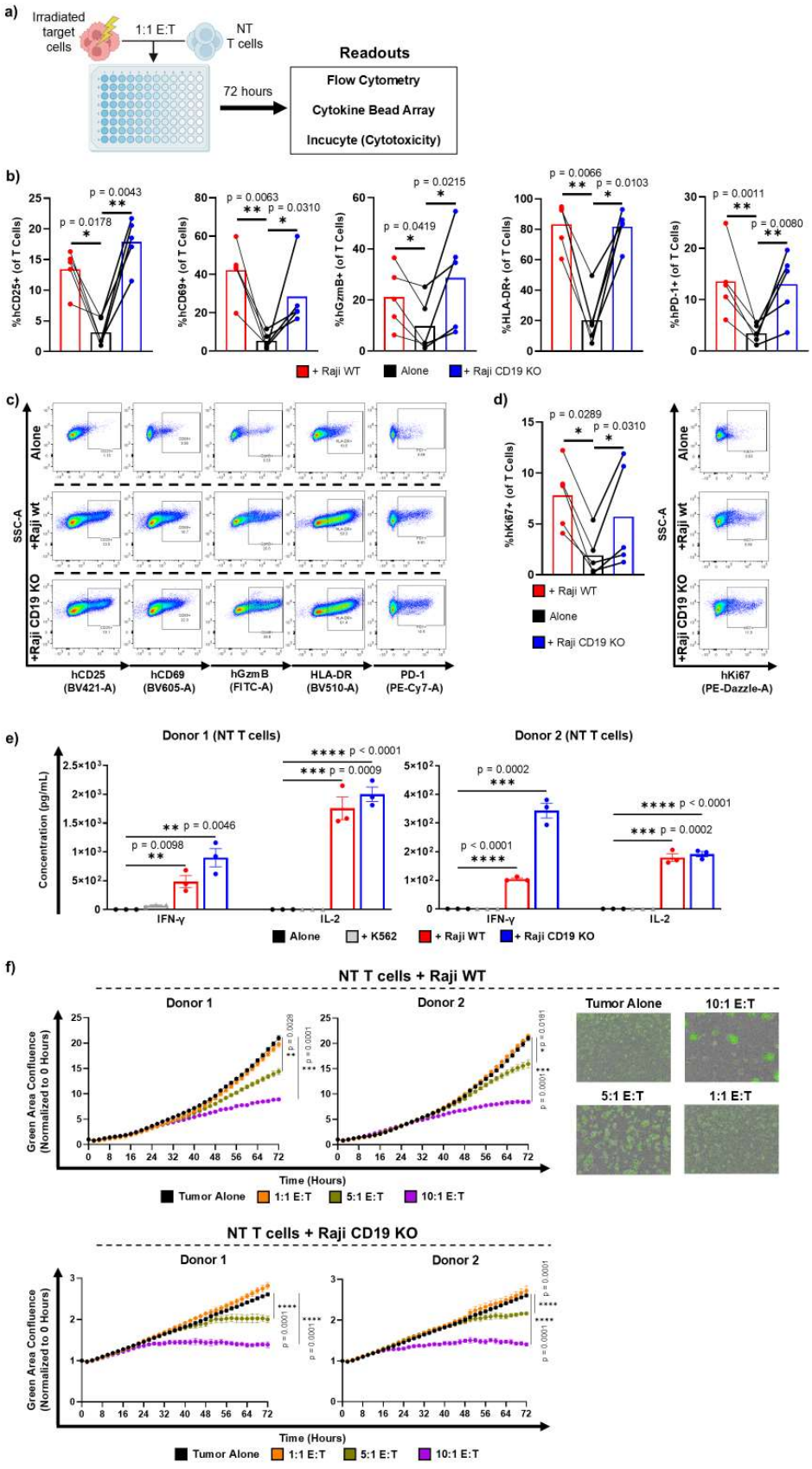
a)
Irradiated target cells
1:1 E:T
NT T cells
72 hours
Readouts
Flow Cytometry
Cytokine Bead Array
Incucyte (Cytotoxicity)
b)
%hCD25+ (of T Cells)
%hCD69+ (of T Cells)
%hGzmB+ (of T Cells)
%HLA-DR+ (of T Cells)
%hPD-1+ (of T Cells)
+ Raji WT
Alone
+ Raji CD19 KO
c)
Alone
+Raji wt
+Raji CD19 KO
SSC-A
hCD25 (BV421-A)
hCD69 (BV605-A)
hGzmB (FITC-A)
HLA-DR (BV510-A)
PD-1 (PE-Cy7-A)
d)
%hKi67+ (of T Cells)
hKi67 (PE-Dazzle-A)
e)
Donor 1 (NT T cells)
Donor 2 (NT T cells)
Concentration (pg/mL)
IFN-γ
IL-2
Alone
+ K562
+ Raji WT
+ Raji CD19 KO
f)
NT T cells + Raji WT
Donor 1
Donor 2
Green Area Confluence (Normalized to 0 Hours)
Time (Hours)
Tumor Alone
10:1 E:T
5:1 E:T
1:1 E:T
NT T cells + Raji CD19 KO

Figure 3: Human non-transduced (NT) T cells also mediate anti-tumor activity against Raji cells *in vitro*, exhibiting a phenotype consistent with TCR-driven alloreactivity

(a) Experimental schematic: Raji WT or CD19 KO cells were co-incubated with NT T cells.

(b, c) Expression of T cell activation markers hCD25, hCD69, hGzmB, HLA-DR, and hPD-1 on NT T cells by flow cytometry (b) and representational flow (c) after co-culture.

(d) Expression of T cell proliferation marker hKi67 on NT T cells after co-culture.

(e) Cytokine levels of hIFN-γ and hIL2 after co-culture.

(g) Raji WT and CD19 KO cells engineered with Nuclight Green were incubated with NT T cells in an Incucyte Live-Cell Analysis System with fluorescence measured over time.

Data in b and d involves NT T cells generated from 5 different donors (n=5 [except for hCD69 expression which is from 4 donors]) and in e-f contains NT T cells generated from 2 different donors run in technical triplicates. Statistical comparisons were performed using a two-tailed paired ratio (b, d) or Student's t test without Welch's correction (e), or a two-way ANOVA (f). Data are presented as mean ± standard error of the mean (SEM), with individual data points shown where applicable.

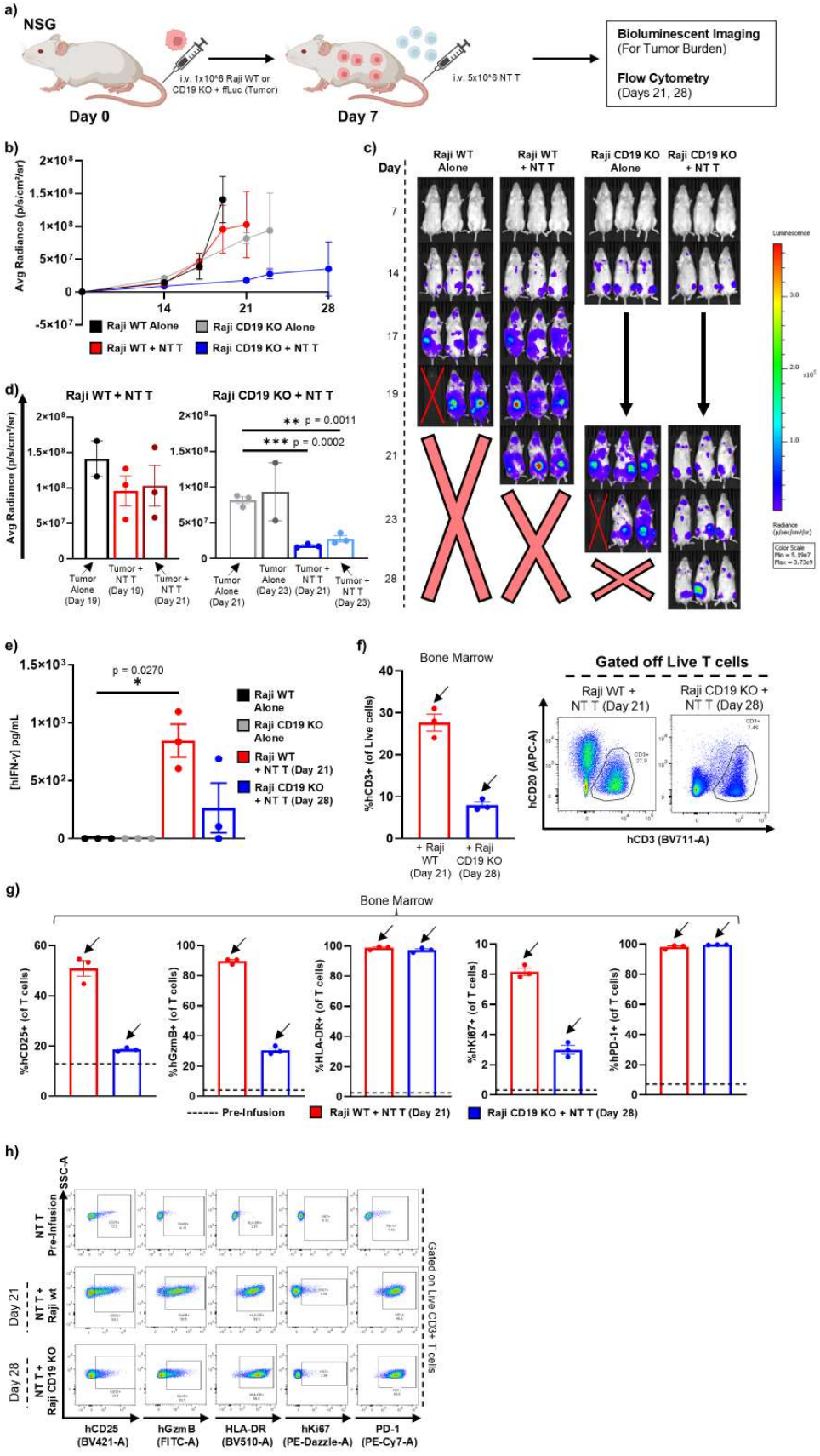
a)
NSG
i.v. 1x10^6 Raji WT or CD19 KO + ffLuc (Tumor)
Day 0
Day 7
i.v. 5x10^6 NT T
Bioluminescent Imaging
(For Tumor Burden)
Flow Cytometry
(Days 21, 28)
b)
Avg Radiance (p/s/cm²/sr)
Raji WT Alone
Raji CD19 KO Alone
Raji WT + NT T
Raji CD19 KO + NT T
c)
Day
Raji WT Alone
Raji WT + NT T
Raji CD19 KO Alone
Raji CD19 KO + NT T
Luminescence
Radiance (p/sec/cm²/sr)
Color Scale
d)
Raji WT + NT T
Raji CD19 KO + NT T
** p = 0.0011
*** p = 0.0002
Tumor Alone (Day 19)
Tumor + NT T (Day 19)
Tumor + NT T (Day 21)
Tumor Alone (Day 21)
Tumor Alone (Day 23)
Tumor + NT T (Day 21)
Tumor + NT T (Day 23)
e)
[hIFN-γ] pg/mL
p = 0.0270
Raji WT Alone
Raji CD19 KO Alone
Raji WT + NT T (Day 21)
Raji CD19 KO + NT T (Day 28)
f)
Bone Marrow
%hCD3+ (of Live cells)
+ Raji WT (Day 21)
+ Raji CD19 KO (Day 28)
Gated off Live T cells
Raji WT + NT T (Day 21)
Raji CD19 KO + NT T (Day 28)
hCD20 (APC-A)
hCD3 (BV711-A)
g)
Bone Marrow
%hCD25+ (of T cells)
%hGzmB+ (of T cells)
%hHLA-DR+ (of T cells)
%hKi67+ (of T cells)
%hPD-1+ (of T cells)
------ Pre-Infusion
Raji WT + NT T (Day 21)
Raji CD19 KO + NT T (Day 28)
h)
SSC-A
NT T Pre-Infusion
Day 21 NT T + Raji wt
Day 28 NT T + Raji CD19 KO
Gated on Live CD3+ T cells
hCD25 (BV421-A)
hGzmB (FITC-A)
HLA-DR (BV510-A)
hKi67 (PE-Dazzle-A)
PD-1 (PE-Cy7-A)

Figure 4: Human NT T cells also mediate anti-tumor activity against Raji cells *in vivo*

(a) Experimental schematic: Raji WT or CD19 KO tumor-bearing NSG mice were treated with human NT T cells.
(b-d) Tumor burden by bioluminescent imaging of Raji WT or CD19 KO tumor-bearing NSG mice treated with human NT T cells.
(e) Serum cytokine levels of hIFN-γ in Raji WT or CD19 KO tumor-bearing NSG mice treated with human NT T cells.
(f) Frequency of T cells by flow cytometry in bone marrow of Raji WT or CD19 KO tumor-bearing NSG mice treated with human NT T cells.
(g, h) Expression of T cell activation markers hCD25, hGzmB, HLA-DR, hPD-1 and the proliferation marker Ki67 by flow cytometry (g) and representational flow (h) on NT T cells in bone marrow of Raji WT or CD19 KO tumor-bearing NSG mice treated with human NT T cells.

Data in b-g is representative of 2 independent experiments (n=3 per each group). Statistical comparisons were performed using a two-tailed unpaired Student's t test without Welch's correction (d-e). Data are presented as mean ± standard error of the mean (SEM), with individual data points shown where applicable.

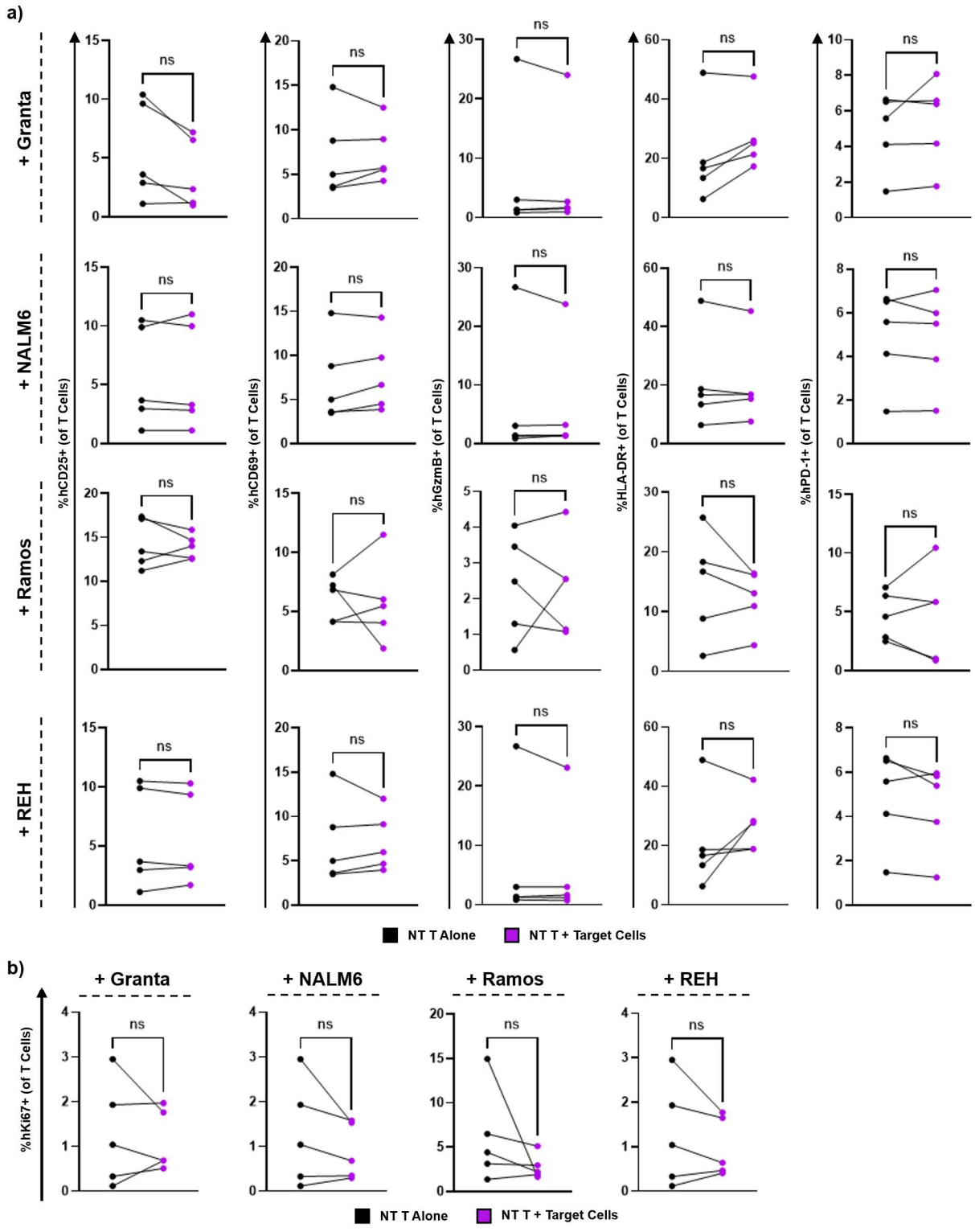
a)
+ Granta
+ NALM6
+ Ramos
+ REH
%hCD25+ (of T Cells)
%hCD69+ (of T Cells)
%hGzmB+ (of T Cells)
%HLA-DR+ (of T Cells)
%hPD-1+ (of T Cells)
ns
NT T Alone
NT T + Target Cells
b)
%hKi67+ (of T Cells)
+ Granta
+ NALM6
+ Ramos
+ REH
ns
NT T Alone
NT T + Target Cells

Figure 5: Other non-Raji lymphoma cell lines do not induce activation in T cells

(a) Expression of T cell activation markers hCD25, hCD69, hGzmB, HLA-DR, hPD-1 by flow cytometry on NT T cells after co-culture for 72 hours with non-Raji lymphoma target cells.
(b) Expression of T cell proliferation marker hKi67 by flow cytometry on NT T cells after co-culture for 72 hours with non-Raji lymphoma target cells.

Data in a-b is NT T cells generated from 5 different donors. Statistical comparisons were performed using a two-tailed ratio paired Student's t test. Data are presented as mean ± standard error of the mean (SEM), with individual data points shown where applicable.

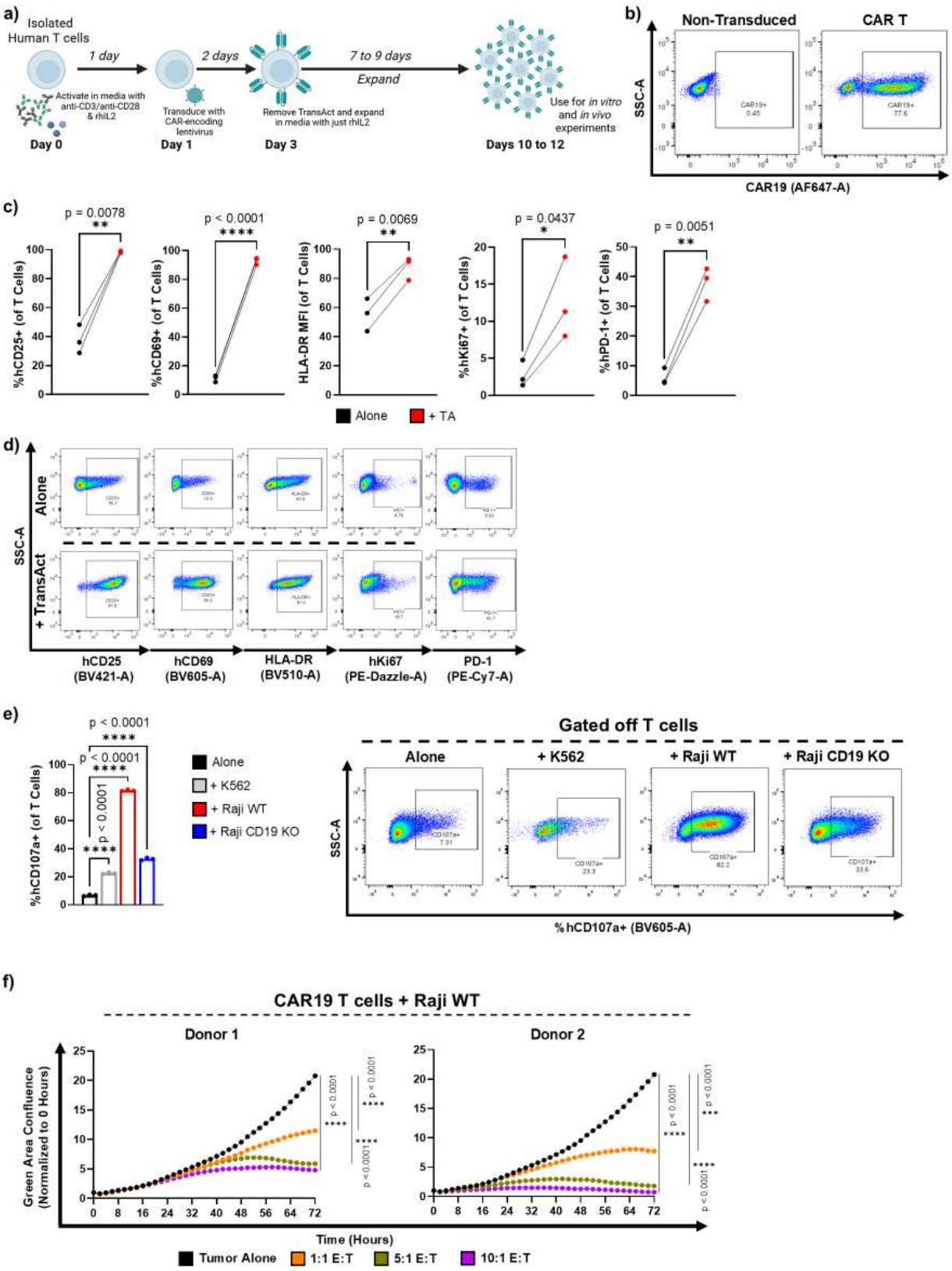
a)
Isolated Human T cells
1 day
2 days
7 to 9 days
Expand
Activate in media with anti-CD3/anti-CD28 & rhIL2
Transduce with CAR-encoding lentivirus
Remove TransAct and expand in media with just rhIL2
Use for in vitro and in vivo experiments
Day 0
Day 1
Day 3
Days 10 to 12
b)
Non-Transduced
CAR T
SSC-A
CAR19 (AF647-A)
c)
p = 0.0078
p < 0.0001
p = 0.0069
p = 0.0437
p = 0.0051
%hCD25+ (of T Cells)
%hCD69+ (of T Cells)
HLA-DR MFI (of T Cells)
%hKi67+ (of T Cells)
%hPD-1+ (of T Cells)
Alone
+ TA
d)
Alone
+ TransAct
SSC-A
hCD25 (BV421-A)
hCD69 (BV605-A)
HLA-DR (BV510-A)
hKi67 (PE-Dazzle-A)
PD-1 (PE-Cy7-A)
e)
p < 0.0001
%hCD107a+ (of T Cells)
Alone
+ K562
+ Raji WT
+ Raji CD19 KO
Gated off T cells
Alone
+ K562
+ Raji WT
+ Raji CD19 KO
SSC-A
%hCD107a+ (BV605-A)
f)
CAR19 T cells + Raji WT
Donor 1
Donor 2
Green Area Confluence (Normalized to 0 Hours)
Time (Hours)
Tumor Alone
1:1 E:T
5:1 E:T
10:1 E:T

Supplemental Figure 1: Additional human CAR19 T cell phenotypic data from *in vitro experiments*

(a) Experimental schematic: hCD19-targeted CAR T cells were generated then expanded for 10 to 12 days.
(b) Validation of CAR transduction efficiency by flow cytometry.
(c, d) Expression of T cell activation/proliferation markers hCD25, hCD69, HLA-DR, hKi67, and hPD-1 by flow cytometry (c) and representational flow (d) after co-culture with TransAct.
(e) Expression of T cell degranulation marker hCD107a after co-culture and representational flow.
(f) Raji WT cells engineered with Nuclight Green were incubated with CAR19 T cells in an Incucyte Live-Cell Analysis System with fluorescence measured over time.

Data in c involves CAR19 T cells generated from 3 different donors (n=3), in e involves CAR19 T cells generated from 2 different donors run in technical triplicates, and in f involves CAR19 T cells generated from 1 donor run in technical triplicates. Statistical comparisons were performed using a two-tailed paired (c) or Student's t test without Welch's correction (f), or a two-way ANOVA (e). Data are presented as mean ± standard error of the mean (SEM), with individual data points shown where applicable.

a)

	CAR19 T + Raji WT		CAR19 T + Raji CD19 KO	
	Mice Survived (by Day 50)	% Mice Survived (by Day 50)	Mice Survived (by Day 50)	% Mice Survived (by Day 50)
Donor 1	2/3	66.7	3/6	50
Donor 2	3/3	100	3/3	100
Donor 3	3/3	100	2/3	66.7
Donor 4	3/3	100	0/3	0

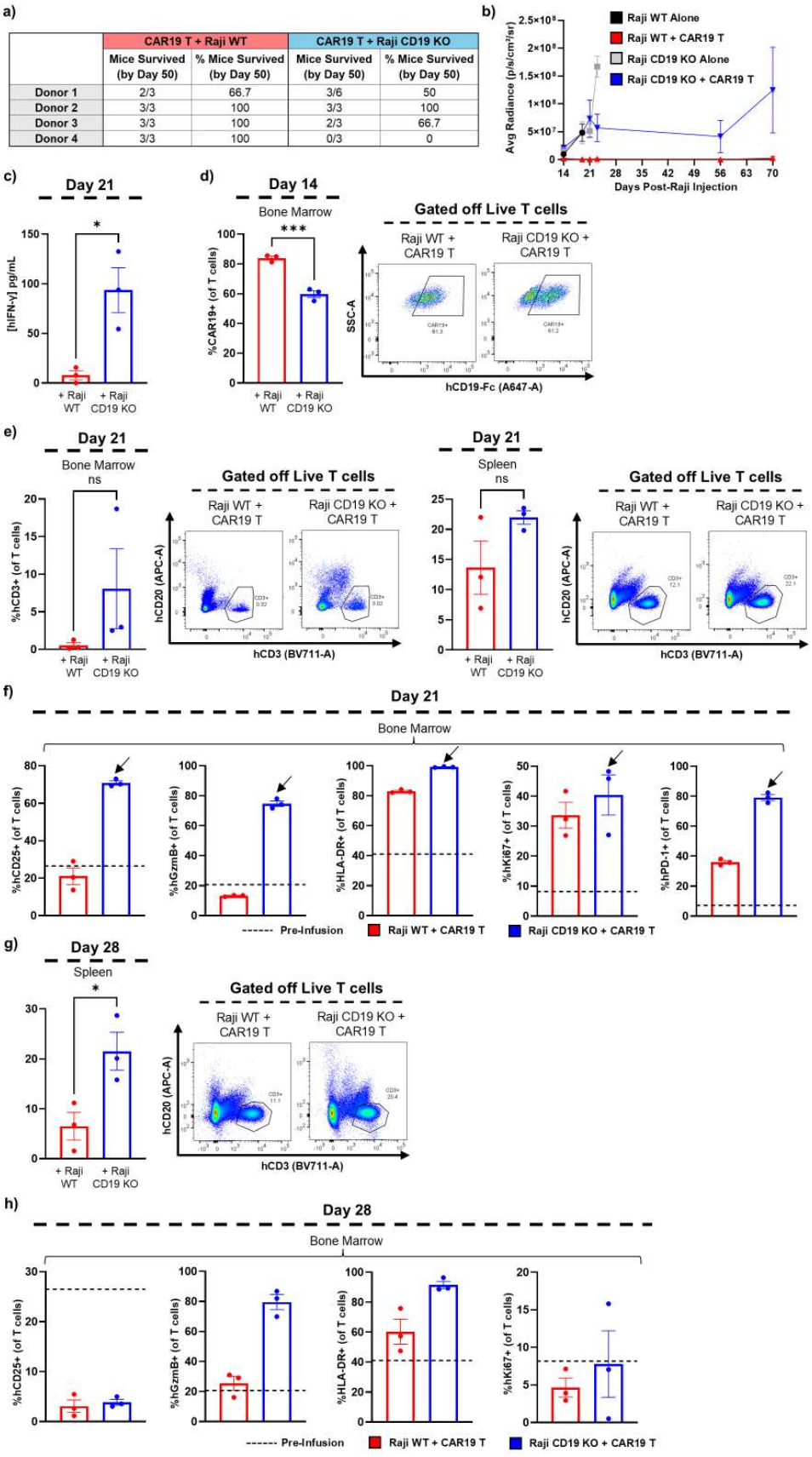

Supplementary Figure 2: Extra phenotype data from Raji WT or CD19 KO tumor-bearing NSG mice treated with human hCD19-targeted CAR T cells

(a) Comparison of survival in Raji WT or CD19 KO tumor-bearing NSG mice treated with human hCD19-targeted CAR T cells made from different donors.
(b) Full time course tumor burden by bioluminescent imaging of Raji WT or CD19 KO tumor-bearing NSG mice treated with human hCD19-targeted CAR T cells.
(c) Day 21: serum cytokine levels of hIFN-γ in Raji WT or CD19 KO tumor-bearing NSG mice treated with human hCD19-targeted CAR T cells.
(d) Day 14: CAR expression of T cell activation markers hCD25, hGzmB, HLA-DR, hKi67, hPD-1 by flow cytometry.
(e) Day 21: frequency of T cells by flow cytometry in bone marrow of Raji WT or CD19 KO tumor-bearing NSG mice treated with human hCD19-targeted CAR T cells in bone marrow and spleen.
(f) Day 21: expression of T cell activation markers hCD25, hGzmB, HLA-DR, hKi67, hPD-1 by flow cytometry.
(g) Day 28: frequency of T cells by flow cytometry in spleen of Raji WT or CD19 KO tumor-bearing NSG mice treated with human hCD19-targeted CAR T cells in spleen.
(h) Day 28: expression of T cell activation markers hCD25, hGzmB, HLA-DR, hKi67, hPD-1 by flow cytometry.

Data in c-h i is representative of 2 independent experiments (n=3 per each group). Statistical comparisons were performed using a two-tailed unpaired Student's t test without Welch's correction. Data are presented as mean ± standard error of the mean (SEM), with individual data points shown where applicable.

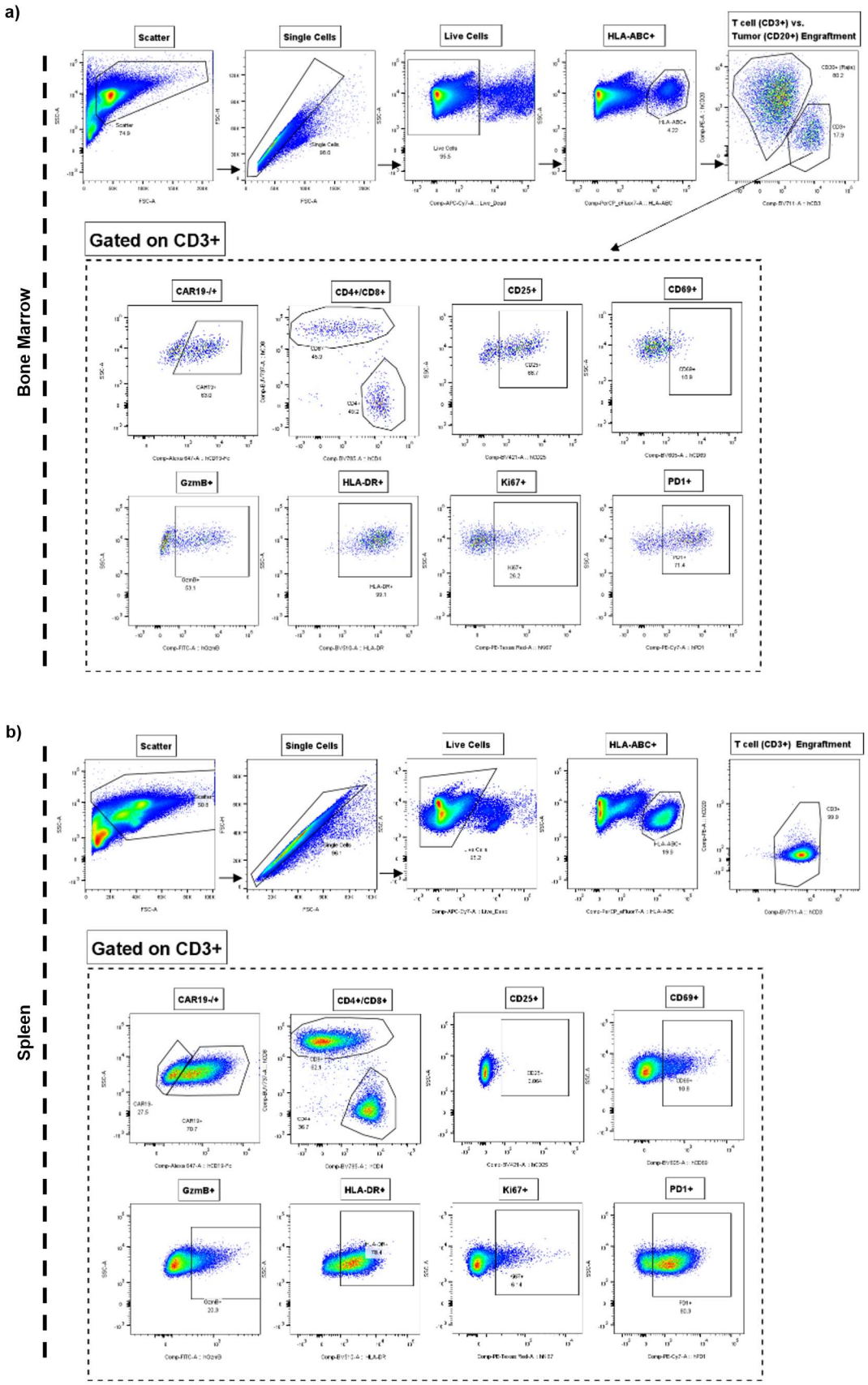
a)
Bone Marrow
Scatter
Single Cells
Live Cells
HLA-ABC+
T cell (CD3+) vs. Tumor (CD20+) Engraftment
Gated on CD3+
CAR19-/+
CD4+/CD8+
CD25+
CD69+
GzmB+
HLA-DR+
Ki67+
PD1+
b)
Spleen
Scatter
Single Cells
Live Cells
HLA-ABC+
T cell (CD3+) Engraftment
Gated on CD3+
CAR19-/+
CD4+/CD8+
CD25+
CD69+
GzmB+
HLA-DR+
Ki67+
PD1+

Supplementary Figure 3: Gating strategy of Raji WT or CD19 KO tumor-bearing NSG mice treated with human hCD19-targeted CAR T cells

(a, b) Gating strategy for phenotyping T cells from bone marrow (a) or spleen (b) of tumor-bearing mice.

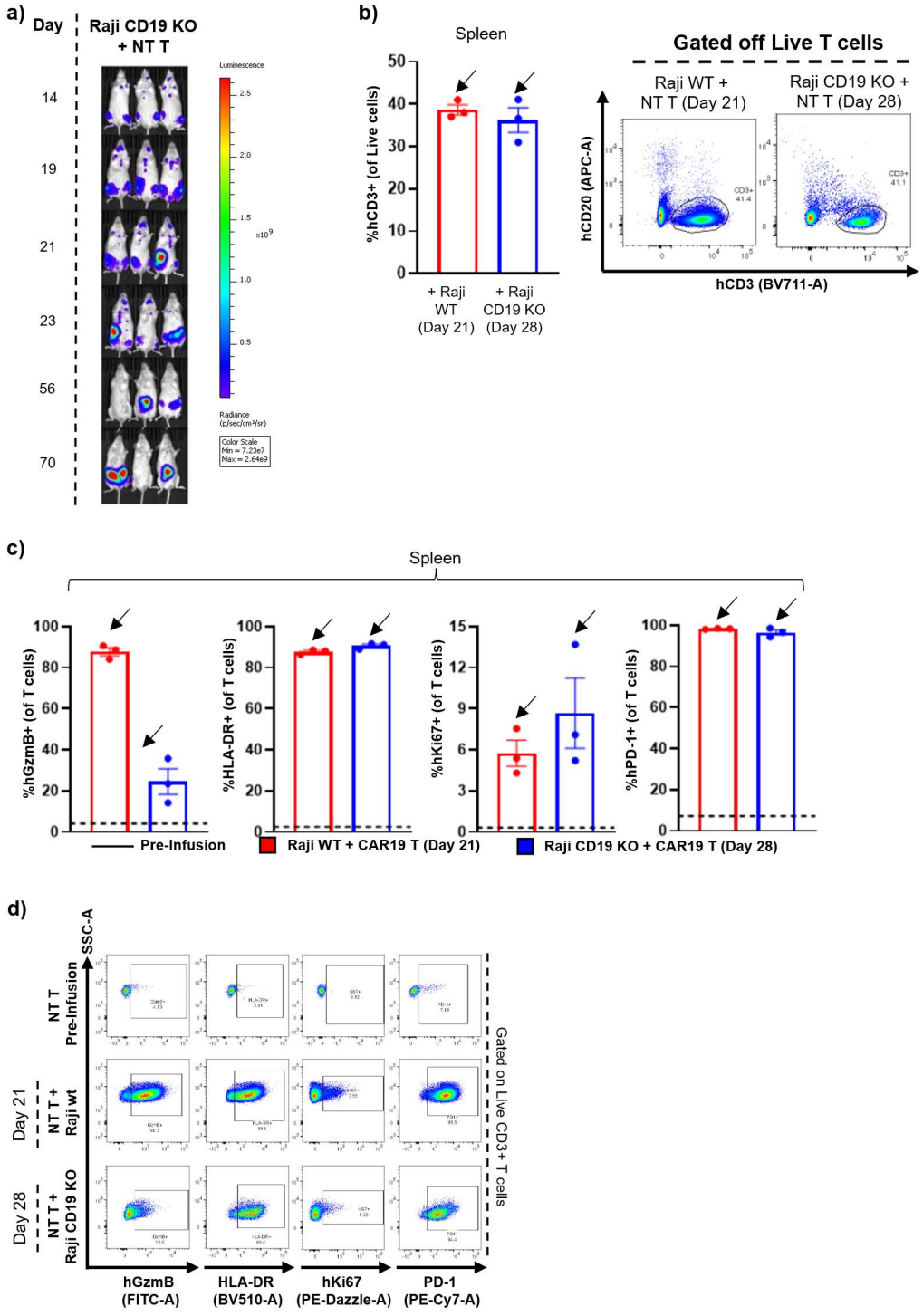
a)
Day
Raji CD19 KO
+ NT T
14
19
21
23
56
70
Luminescence
2.5
2.0
1.5
x10^9
1.0
0.5
Radiance
(p/sec/cm²/sr)
Color Scale
Min = 7.23e7
Max = 2.64e9
b)
Spleen
%hCD3+ (of Live cells)
50
40
30
20
10
0
+ Raji
WT
(Day 21)
+ Raji
CD19 KO
(Day 28)
Gated off Live T cells
Raji WT +
NT T (Day 21)
Raji CD19 KO +
NT T (Day 28)
hCD20 (APC-A)
hCD3 (BV711-A)
c)
Spleen
%hGzmB+ (of T cells)
%HLA-DR+ (of T cells)
%hKi67+ (of T cells)
%hPD-1+ (of T cells)
100
80
60
40
20
0
15
12
9
6
3
Pre-Infusion
Raji WT + CAR19 T (Day 21)
Raji CD19 KO + CAR19 T (Day 28)
d)
SSC-A
NT T
Pre-Infusion
Day 21
NT T +
Raji wt
Day 28
NT T +
Raji CD19 KO
Gated on Live CD3+ T cells
hGzmB
(FITC-A)
HLA-DR
(BV510-A)
hKi67
(PE-Dazzle-A)
PD-1
(PE-Cy7-A)

Supplementary Figure 4: Extra phenotype data from Raji WT or CD19 KO tumor-bearing NSG mice treated with human NT T cells

(a) Tumor burden by bioluminescent imaging of an additional study treating Raji WT or CD19 KO tumor-bearing NSG mice with human NT T cells from Donor 2.
(b) Frequency of T cells by flow cytometry in spleens of Raji WT or CD19 KO tumor-bearing NSG mice treated with human NT T cells.
(c, d) Expression of T cell activation markers hGzmB, HLA-DR, hKi67, hPD-1 by flow cytometry on NT T cells in spleens of tumor-bearing NSG mice treated with human NT T cells (c) and representational flow (d).

Data in b-d is representative of 2 independent experiments (n=3 per each group). Data are presented as mean ± standard error of the mean (SEM), with individual data points shown where applicable.

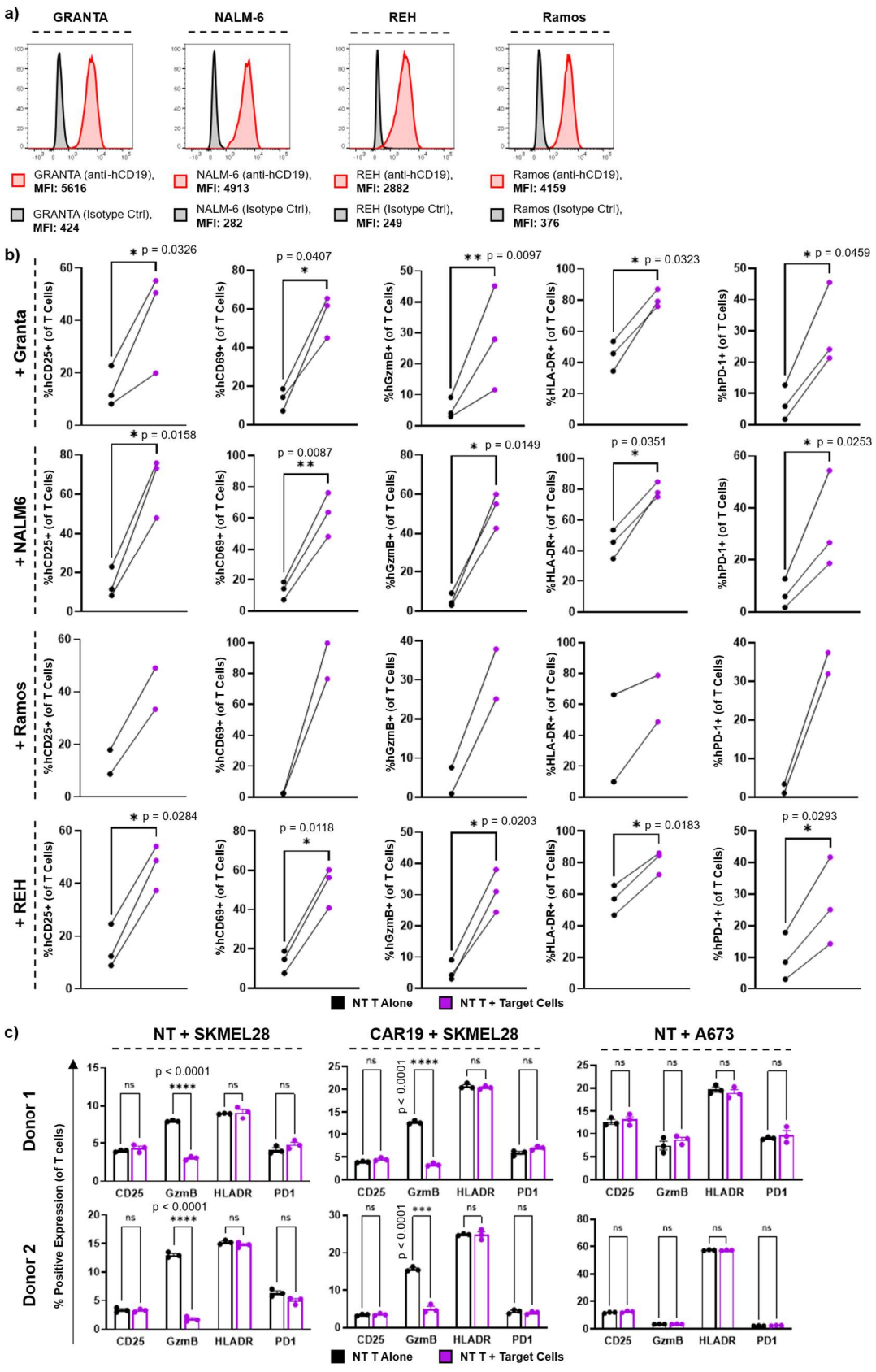
a)
GRANTA
NALM-6
REH
Ramos
GRANTA (anti-hCD19), MFI: 5616
NALM-6 (anti-hCD19), MFI: 4913
REH (anti-hCD19), MFI: 2882
Ramos (anti-hCD19), MFI: 4159
GRANTA (Isotype Ctrl), MFI: 424
NALM-6 (Isotype Ctrl), MFI: 282
REH (Isotype Ctrl), MFI: 249
Ramos (Isotype Ctrl), MFI: 376
b)
+ Granta
+ NALM6
+ Ramos
+ REH
%hCD25+ (of T Cells)
%hCD69+ (of T Cells)
%hGzmB+ (of T Cells)
%HLA-DR+ (of T Cells)
%hPD-1+ (of T Cells)
* p = 0.0326
p = 0.0407
** p = 0.0097
* p = 0.0323
* p = 0.0459
* p = 0.0158
p = 0.0087
* p = 0.0149
p = 0.0351
* p = 0.0253
* p = 0.0284
p = 0.0118
* p = 0.0203
* p = 0.0183
p = 0.0293
NT T Alone
NT T + Target Cells
c)
NT + SKMEL28
CAR19 + SKMEL28
NT + A673
Donor 1
Donor 2
% Positive Expression (of T cells)
p < 0.0001
p < 0.0001
p < 0.0001
p < 0.0001
ns
****
***
CD25
GzmB
HLADR
PD1
NT T Alone
NT T + Target Cells

Supplementary Figure 5: Other non-Raji cell lines extended phenotype with and without co-culture

(a) Expression of hCD19 on other non-Raji lymphoma cell lines.
(b) Expression of T cell activation markers hCD25, hCD69, hGzmB, HLA-DR, hPD-1 by flow cytometry on CAR19 T cells after co-culture for 72 hours with non-Raji lymphoma target cells.
(c) Expression of T cell activation markers hCD25, hGzmB, HLA-DR, hPD-1 by flow cytometry on NT and/or CAR19 T cells after co-culture for 72 hours with non-Raji solid tumor target cells.

Data in b is CAR19 T cells generated from 5 different donors and in c is NT or CAR19 T cells run in technical triplicates. Statistical comparisons were performed using either a two-tailed paired Student's t test (b) or unpaired Student's t test (c). Data are presented as mean ± standard error of the mean (SEM), with individual data points shown where applicable.

CHAPTER 4: Final Remarks

Conclusion

My dissertation investigated the molecular and cellular regulation of T cell biology pertaining to activation, persistence, and cytotoxicity, with a particular focus on how this impacts adoptive T cell therapies such as CAR T cells. While CAR T cell therapy has achieved remarkable clinical success, particularly in hematological malignancies, its therapeutic impact and persistence in systemic circulation remain inconsistent across patients. Furthermore, preclinical models often fail to fully recapitulate physiologically relevant conditions and tumor-intrinsic factors, potentially generating misleading efficacy data. My work presented here demonstrates how activation-induced cell death (AICD) can negatively impact conventional and CAR T cell persistence, and how translational discrepancies pertaining to false-positive efficacy data can arise from preclinical modeling limitations.

In Chapter 1, I summarized key discoveries in T cell signaling and described how this molecular foundation has been leveraged to engineer antigen-specific CAR T cells that function independently of MHC restriction. Furthermore, I reviewed the evolving CAR T cell development pipeline and discussed how CAR construct design, optimized manufacturing, and current and next-generation preclinical modeling systems can be integrated to generate more clinically relevant efficacy data and improve translational success.

In Chapter 2, I identified a role for PD-1 signaling in protecting both conventional and CAR T cells from AICD. These findings challenge the notion that checkpoint

inhibition is unilaterally beneficial in augmenting effector function instead suggesting there is a tradeoff between heightened activation and long-term persistence. This dual role for PD-1 provides not only novel insight into the role of PD-1 signaling in shaping T cell responses but has direct implications on how immune checkpoint inhibitors are administered in combination with adoptive T cell therapies in clinical settings.

In Chapter 3, I uncovered a key limitation in preclinical modeling by demonstrating that both non-transduced and CAR T cells can exhibit activation and cytotoxicity against antigen-negative Raji tumor cells. These findings show that certain tumor cell lines can trigger unintended T cell activation and cause tumor regression independent of CAR specificity. This underscores the importance of carefully vetting tumor cell lines for baseline reactivity to T cells prior to their use in preclinical modeling applications in order to avoid producing confounding efficacy data.

Collectively, the studies presented in this dissertation provide novel mechanistic insights into the regulation of T cell activation and survival while also critically assessing the preclinical systems used to model CAR T cell functionality. These findings deepen our understanding of how signaling pathways can regulate T cell responses and also how preclinical model selection may impact interpretations of potential therapeutic performance. Future studies should aim to optimize the molecular design of CAR T cells to enhance function and persistence and improve upon the preclinical models and methodologies used to evaluate them, in order to realize their full therapeutic potential across a broad range of cancers.